A THEORETICAL AND COMPUTATIONAL STUDY OF SOFT ADHESION MEDIATED BY SPECIFIC BINDERS

Dimitri KAURIN

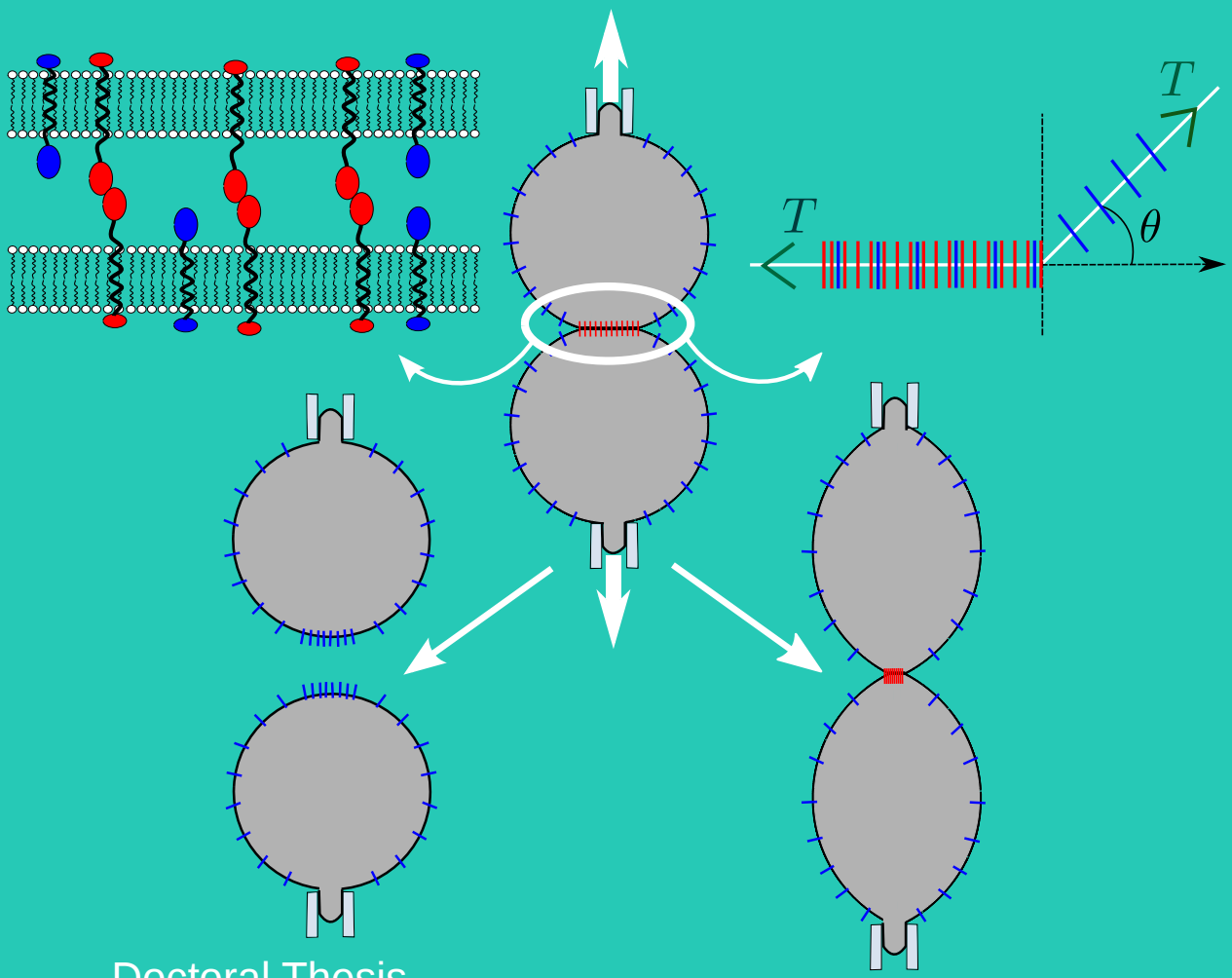

Doctoral Thesis
Barcelona, September 2018

UNIVERSITAT POLITÈCNICA DE CATALUNYA
BARCELONATECH

A theoretical and computational study of soft adhesion mediated by specific binders

Dimitri Kaurin

ADVERTIMENT La consulta d'aquesta tesi queda condicionada a l'acceptació de les següents condicions d'ús: La difusió d'aquesta tesi per mitjà del repositori institucional UPCommons (http://upcommons.upc.edu/tesis) i el repositori cooperatiu TDX (http://www.tdx.cat/) ha estat autoritzada pels titulars dels drets de propietat intel·lectual **únicament per a usos privats** emmarcats en activitats d'investigació i docència. No s'autoritza la seva reproducció amb finalitats de lucre ni la seva difusió i posada a disposició des d'un lloc aliè al servei UPCommons o TDX. No s'autoritza la presentació del seu contingut en una finestra o marc aliè a UPCommons (*framing*). Aquesta reserva de drets afecta tant al resum de presentació de la tesi com als seus continguts. En la utilització o cita de parts de la tesi és obligat indicar el nom de la persona autora.

ADVERTENCIA La consulta de esta tesis queda condicionada a la aceptación de las siguientes condiciones de uso: La difusión de esta tesis por medio del repositorio institucional UPCommons (http://upcommons.upc.edu/tesis) y el repositorio cooperativo TDR (http://www.tdx.cat/?locale-attribute=es) ha sido autorizada por los titulares de los derechos de propiedad intelectual **únicamente para usos privados enmarcados** en actividades de investigación y docencia. No se autoriza su reproducción con finalidades de lucro ni su difusión y puesta a disposición desde un sitio ajeno al servicio UPCommons No se autoriza la presentación de su contenido en una ventana o marco ajeno a UPCommons (*framing)*. Esta reserva de derechos afecta tanto al resumen de presentación de la tesis como a sus contenidos. En la utilización o cita de partes de la tesis es obligado indicar el nombre de la persona autora.

WARNING On having consulted this thesis you're accepting the following use conditions: Spreading this thesis by the institutional repository UPCommons (http://upcommons.upc.edu/tesis) and the cooperative repository TDX (http://www.tdx.cat/?locale-attribute=en) has been authorized by the titular of the intellectual property rights **only for private uses** placed in investigation and teaching activities. Reproduction with lucrative aims is not authorized neither its spreading nor availability from a site foreign to the UPCommons service. Introducing its content in a window or frame foreign to the UPCommons service is not authorized (framing). These rights affect to the presentation summary of the thesis as well as to its contents. In the using or citation of parts of the thesis it's obliged to indicate the name of the author.

A THEORETICAL AND COMPUTATIONAL STUDY OF SOFT ADHESION MEDIATED BY SPECIFIC BINDERS

Dimitri KAURIN

Doctoral Thesis
Advisor: Marino Arroyo
Barcelona. September 2018

Departament d'Enginyeria Civil i Ambiental
Programa de Doctorat de Matemàtica Aplicada

"We grow in direct proportion to the amount of chaos we can sustain and dissipate"
-Ilya Prigogine, Order Out of Chaos: Man's New Dialogue with Nature

Abstract

A theoretical and computational study of soft adhesion mediated by specific binders

Dimitri Kaurin

We examine a classical problem in soft-matter physics: the specific adhesion between deformable elastic objects, such as vesicles, mediated by mobile adhesion molecules. This problem is relevant to cell-cell adhesion. To understand this fundamental yet poorly understood problem, in Part I of the thesis we develop mechano-stochastic minimal models to examine the coupling between the stochastic nature of the binding/unbinding of the adhesion molecules, the mechanical environment and geometrical architecture of the adhesion patch. Building on previous works, we specifically investigate the stability of adhesion clusters under hydraulic interstitial pressure, relevant in various physiological cellular processes, and the role of surface tension at the boundary of the media bridged by the molecular bond cluster. Remarkably, we find that surface tension has a strong stabilizing effect because it increases the rebinding rate. We also discuss the influence of the mobility of these molecules. This first part lays the ground for the main contributions of the thesis in Part II. Here, we develop a continuum general approach of soft adhesion mediated by mobile binders. This approach relies on Onsager's variational principle. We then apply this modeling framework to study the unbinding of adhering vesicles. We consider a membrane with bending rigidity, subject to a fixed tension and a separation force by a loading device, with mobile adhesion molecules. These molecules store elastic energy when deformed, diffuse, and react by attaching with partners in a neighboring vesicle. The binding kinetics strongly depend on the distance to potential partners and the unbinding kinetics depends on the force experienced by the binders (slip bond behavior). The equilibrium picture for this problem has long been known but the dynamics have been barely explored. Based on our theoretical framework, we perform numerical calculations to explore previously anticipated qualitative scenarios.

In particular, we characterize a diffusion-dominated regime in which, under an applied force, adhesion patches shrink in size and become increasingly concentrated in bond until a new equilibrium is reached. More interestingly, in an intermediate regime, motion of bonds by diffusion and bond-breaking compete during the remodeling of adhesion patches under force. This process always leads to full dissociation, but the lifetime depends very strongly on force, defining a critical force that delimits the threshold separating stability and instability. We show how this threshold depends on the physico-chemical properties of adhesion molecules and on molecular crowding. Since these properties can be controlled by cells, e.g. through calcium signaling, our study portrays soft adhesion mediated by mobile binders as a highly tunable process allowing cells to strongly hold to each other or disengage to remodel. Finally, in a reaction-dominated limit, we identify a new unusual tear-out regime, in which an adhesion patch shrinks under force by progressive bond-breaking near its edge, but which is critically controlled by diffusion occurring in a small zone near the edge.

Acknowledgments

Firstly, I would like to express my sincere gratitude to my advisor Prof. Marino Arroyo for the continuous support of my Ph.D study and related research, for his patience, enthusiasm, motivation, and he is one of the smartest person I know. I hope I could be as lively and open-minded as Marino and to someday be able to address an audience as well as he can. His guidance helped me in all the time of research and writing of this thesis. I could not have imagined having a better advisor and mentor for my Ph.D study.

I would like to thank the LaCàN research center. I am truly indebted and thankful for the assistance of administrative staff, in particular Imma Rius, Anna Fabregas, Susana Algarra and the technical support of David Ortin and Ignasi Mallafre.

During this research work, I have collaborated with many colleagues for whom I have sincere regards. I am indebted to all my colleagues in LaCàN at Barcelona, and all my friends, who supported me during this period. It has been an honor to share many moments with them. The group has been a source of friendship as well as good advice and collaboration. I would like to acknowledge my gratitude to Alejandro Torres for all the insightful and interesting discussions we had around coffees during all these years.

And finally, I would like to thank the funding sources that have directly or indirectly supported my research. In particular, I would like to thank the support of the European Research Council (grants No. 240487 and 681434).

I want to thank my loving, supportive, patient and understanding girlfriend Elisavet, whose faithful support during the the final stages of this thesis is so appreciated. Finally, I cannot find words to express my gratitude to my family, for their love and unconditional support throughout my life. For my parents, who raised me with the love of questioning the world and supported me in all my pursuits. For my brother, for showing me what courage and abnegation are, you are an example for me and I'm so proud of you. I love you all dearly.

Contents

List of Figures

Chapter 1

Introduction

Cell-cell adhesion

Adhesion between animal cells is a fundamental mechanical function during development and physiology. Cells adhere to each other to form confluent tissues, which need to remain cohesive during extreme morphogenetic events [Guillot and Lecuit, 2013] or during the large deformations routinely experienced by cell monolayers in our lungs, guts or vascular system [Ethier and Simmons, 2007, Fung, 2013]. Failure to resist the mechanical forces at cell-cell contacts can lead to tissue fracture [Casares et al., 2015, Harris et al., 2012, Khalilgharibi et al., 2018], developmental failure and physiological disruptions such as pulmonary edema [Network, 2000, Suki and Hubmayr, 2014], see Fig. 1.1(a,b). Cell-cell adhesion is also crucial in immune or neural synapses [Qi et al., 2001, Dalva et al., 2007], or during cell sorting [Maître et al., 2012b, Steinberg and Takeichi, 1994]. Interestingly, cells also need to disengage from other cells during tissue remodeling, including massive changes in junctional network topology [Guillot and Lecuit, 2013], cell extrusion [Saw et al., 2017], wound healing [Brugués et al., 2014], see Fig. 1.1(c), or pressure-driven cell-cell separation during luminogenesis [Sigurbjörnsdóttir et al., 2014, Dasgupta et al., 2018].

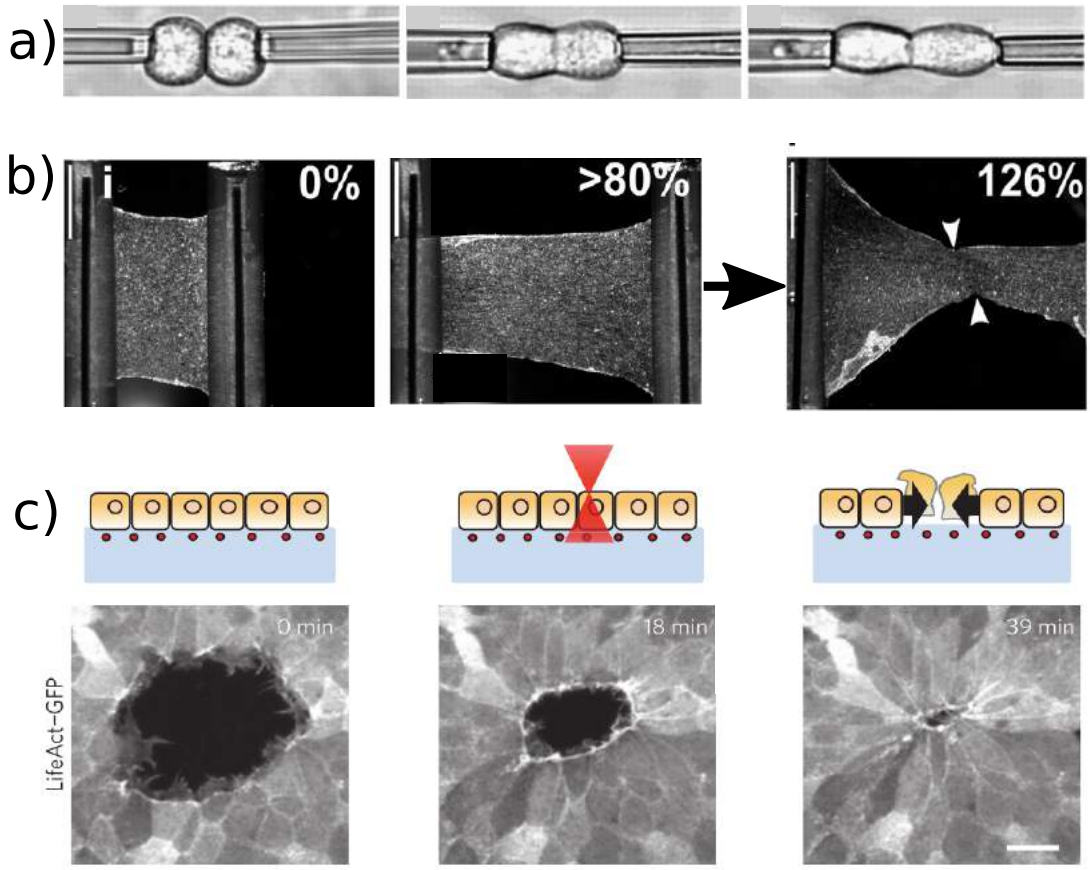

Figure 1.1: a) Two adhering cells pulled apart by a micropipette. The adhesion can sustain large cell strains. Reproduced from [Chu et al., 2004b]. b) Deformation of a monolayer under stretch. Images acquired by bright-field microscopy for a monolayer at 0 and 80% extension. A bigger stretch (126%) can lead to fracture. Reproduced from [Harris et al., 2012]. c) Schematic view of wound healing experiment by ablation of cells in a monolayer and series of fluorescent images (LifeAct) of the closing of the wound at different instants. Reproduced from [Brugués et al., 2014].

Thus, cell-cell adhesion needs to provide mechanical resilience and at the same time support remodeling. To deal with these conflicting requirements, cells avoid the unspecific mechanisms of adhesion acting between lipid membranes, including depletion [Kuhl et al., 1998, Evans et al., 1996], electrostatic [Bernard et al., 2000] or van der Waals forces [Chaffey, 2003] since these are difficult to tune and control. They also avoid specific adhesion by covalent bonds since breaking one such bond would require the energy released in the hydrolysis of 10s of ATP molecules. Instead, they resort to a mechanism of specific adhesion mediated by a set of transmembrane bridging molecules or cell adhesion molecules (CAMs) such as cadherins, which engage in homophilic or heterophilic binding [Takeichi, 1988], see Fig. 1.2(e). The low affinity of these binding molecules enables dynamical binding and unbinding, and hence enables remodeling of adhesion complexes. On the other hand, since these binders are laterally mobile in the fluid plasma membrane, they can aggregate and form clusters or plaques with high concentration of weak bonds, see Fig. 1.2(a,b,c), which collectively can sustain large stresses.

Thermodynamic theories of specific adhesion between membranes with mobile binders predict that, in equilibrium, adhesion patches should form with high and uniform concentration of adhesion molecules [Bell et al., 1984a]. Yet, CAMs have been shown to unevenly distribute in cell-cell junctions, forming puncta ranging from nano-clusters with 10s of molecules to micro-clusters with 100s of molecules [Tru]. Cis-interactions between CAMs, known to form upon formation of trans-bonds, are thermodynamic driving forces favoring aggregation. Interestingly, cis-interactions can be chemical or membrane-mediated and physical in nature [Fenz et al., 2017]. Besides the attractive interaction between CAMs, the competition between long-range repulsion by the repellent molecules (e.g. the glycocalyx) and short-range attraction by specific binders is another physical mechanism leading to phase-separation at cell-cell junctions with CAM-rich domains of tight adhesion [Albersdörfer et al., 1997, Bruinsma and Sackmann, 2001]. Yet, these physical mechanisms do not explain why these concentrated domains of tight adhesion do not coarsen into larger patches. Biological activity is thought to provide the

necessary active stirring to maintain an "emulsion" of small clusters at cell-cell interfaces, which should thus be viewed as out-of-equilibrium dynamical structures. The precise cellular mechanisms that lead to these adhesive clusters are not well-understood, but are thought to involve CAM recycling by endocytosis and the interaction with the actin cytoskeleton (corral effect, stirring, regulation of mobility and turnover) [Tru, Yap et al., 2015, Changede and Sheetz, 2017]. In fact, the association between adhesion molecules and the actin cytoskeleton through a group of adaptor molecules is another hallmark of cell-cell adhesion [Maître and Heisenberg, 2013]. By coupling the actin cortices of adjacent cells, adhesion molecules can transmit tension through a multi-cellular assembly [Maître et al., 2012b]. Cadherins only associate with the actin cytoskeleton upon formation of trans-bonds, see Fig. 1.2(d) . This association during maturation of cell-cell contacts reduces the mobility and turnover of adhesion molecules, stabilizing adhesion clusters. In turn, similarly to cell-matrix adhesions [Case and Waterman, 2015, Elosegui-Artola et al., 2016], cell-cell adhesion complexes form a mechano-sensing and mechano-transduction system that regulate the architecture of the actin cytoskeleton through mechanosensitive adaptor proteins, e.g. by vinculin recruitment mediated by $\alpha-$catenin under force [Engl et al., 2014a, Yap et al., 2017]. This mechanosensitive system includes catch and slip bonds, whose properties depend on the chemical [Pokutta et al., 1994, Nagar et al., 1996, Sotomayor and Schulten, 2008] and physical environment [Liu et al., 2015, Rakshit et al., 2012, Manibog et al., 2014, Huang et al., 2017, Cai et al., 2016]. In summary, cell-cell adhesion is a highly complex and tunable out-of-equilibrium process mediated by mobile binder molecules of low affinity, which assemble into clusters to provide mechanical strength and couple to the cytoskeleton to form a mechanosensitive system that transmits tension through tissues and multi-cellular aggregates.

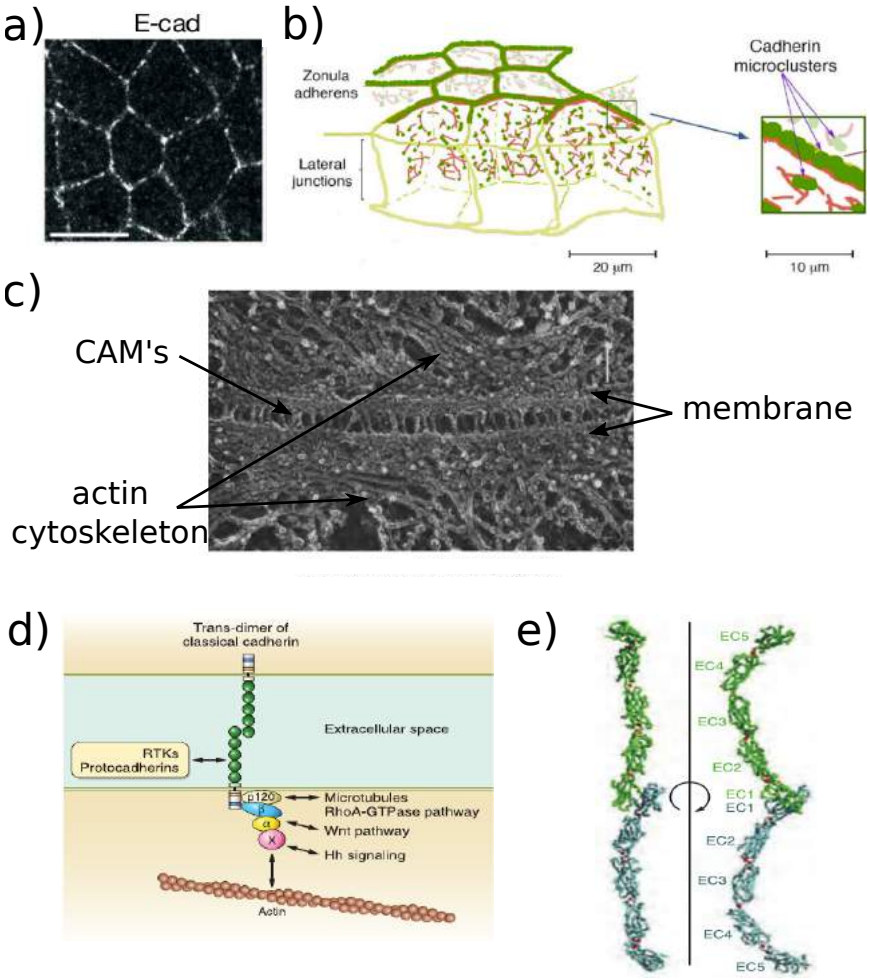

Figure 1.2: a) Florescence imaging of E-cadherins from a cell monolayer. The cadherins are clearly concentrated at the cell-cell interfaces and form microclusters. Reproduced from [Cavey et al., 2008]. b) Schematic representation of a cell monolayer and the distribution of cadherins forming microclusters. Reproduced from [Yap et al., 2015]. c) Deep-etch image of the bridging structure between two adjacent cells and the connected actin cytoskeleton visible on both sides of the membrane. Reproduced from [Hirokawa and Heuser, 1981]. d),e) Schematic representation of cell-cell adhesion with the different components involved: adhesion molecules (cadherins), adaptor molecules (α-catenin and β-catenin) and cytoskeleton (actin) and crystal structure of the ectodomain of C-cadherin. Reproduced from [Hirano and Takeichi, 2012].

A simplified problem: soft adhesion mediated by mobile binders

Since cell adhesion involves many agents and numerous couplings between chemistry, mechanics and biological signaling (involving different transmembranes molecules, adaptor molecules and their connection to actin cytoskeleton ...), modeling experiments on cell adhesion, see Fig. 1.3(a,b,c), raises numerous questions and complexity increases rapidly. Towards a better understanding of this problem, simpler models are necessary. As a simpler model for cell-cell adhesion, we consider here the adhesion of nearby fluid membranes containing membrane-anchored binder molecules, which can move laterally in the membrane and can react with a molecule in the neighboring membrane to form a bond, see Fig. 1.3(d,e). Because this simple model system recapitulates many features of cellular adhesion, its understanding is a pre-requisite before invoking models of mechano-transduction in cell-cell adhesions coupling binders and the cytoskeleton. Furthermore, because the actin cortex is also a viscous thin layer under tension over long time-scales due to turnover [Salbreux et al., 2012a] to which adhesion molecules or clusters are attached, the simplified model studied here could be relevant to cell-cell adhesion under specific regimes.

This simplified model system of soft adhesion mediated by mobile binders has been physically realized in a number of biomimetic systems over the past decade, in which lipid vesicles or supported bilayers have been functionalized with a variety of binder molecules including cadherins [Nam and Santore, 2007, Fenz and Sengupta, 2012, Sackmann and Smith, 2014, Liu and Fletcher, 2009, Schmid et al., 2016a, Fenz et al., 2017]. This system is also amenable to theoretical modeling, including equilibrium and non-equilibrium thermodynamical models where binders are described in terms of concentrations [Bell et al., 1984a, Zhu, 1991, de Gennes et al., 2003, Brochard-Wyart and de Gennes, 2002a, 2003], or stochastic models often examined through Monte Carlo simulations and where binders are discrete [Erdmann and Schwarz, 2004, Qian et al., 2008, Gao et al., 2011, Krobath et al., 2011, Bihr et al., 2012, 2015].

These experimental and theoretical works have shown that this simplified problem is in fact very rich and displays mechano-chemical feedbacks at multiple scales [Zhu, 2000]. On the one hand, the nanoscale interactions between adhesive molecules (formation of trans- bonds, or their lateral interactions) determines the architecture and adhesive tension of adhesion complexes at a mesoscale. On the other hand, the mechanics of the adhesion patch, and in particular the stress distribution and membrane separation at the interface, determines the microscopic binding/unbinding rates or the lateral bias for diffusion. Significant progress has been achieved over the last decades in understanding soft adhesion by mobile binders, such as cooperative effects mediated by membrane mechanics, which explain formation of domains in the presence of binders of different lengths [Krobath et al., 2011, Schmid et al., 2016a] or the effect of membrane fluctuations on the growth and structure of adhesion domains [Fenz et al., 2017]. Yet, the interplay between mechanics, binder motion and chemical kinetics conforms a rich landscape of scenarios [de Gennes et al., 2003, Brochard-Wyart and de Gennes, 2002a], which remains poorly understood.

Aims and structure of the thesis

In this thesis, we examine the behavior and stability of adhesion complexes under force using theoretical and computational models, with the goal of understanding the physical principles that allow cell adhesion to sustain significant stresses or remodel. This question has been addressed experimentally using cell doublet [Tozeren et al., 1989, Berk and Evans, 1991, Chu et al., 2004a, 2005, Maître et al., 2012b, Engl et al., 2014a] and vesicles adhered to supported bilayers [Smith et al., 2008a]. We address this problem with two complementary approaches, discrete stochastic modeling in Part I and continuous modeling in Part II.

In Part I, we develop discrete stochastic models of specific adhesion and we study the stability of a stressed adhesive junction as a function of

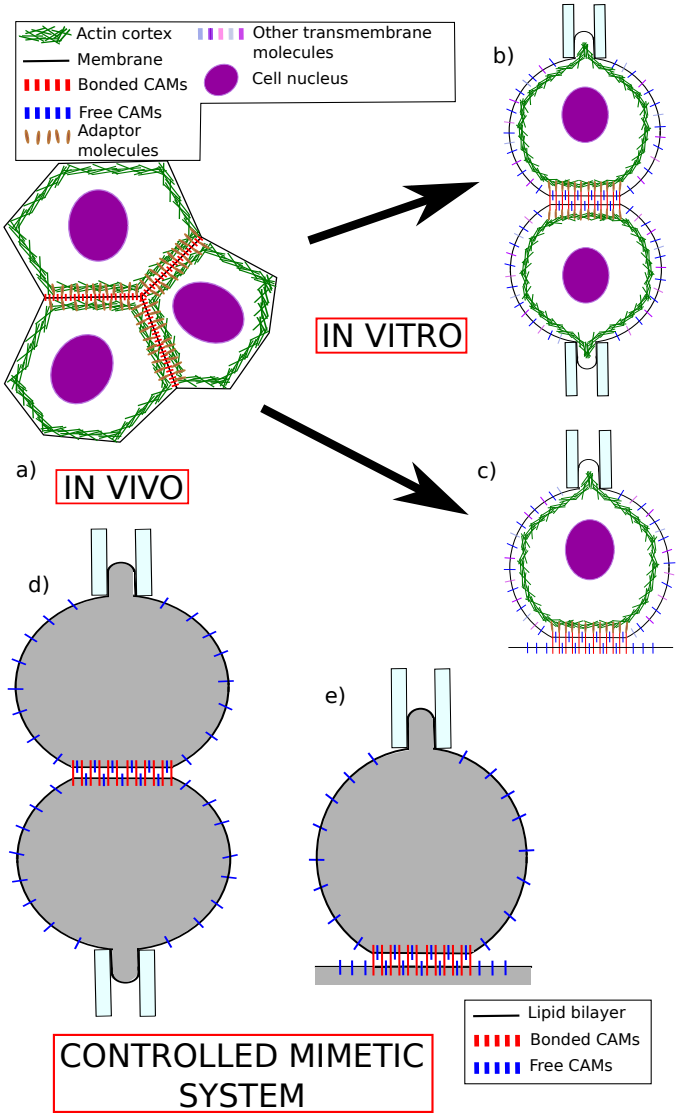

Figure 1.3: a) Schematic representation of cell-cell adhesion in a tissue. b) Schematic representation of an experiment of cell-cell decohesion controlled via micropipettes. c) Schematic representation of an in-vitro experiment of adhesion between a cell and a supported bilayer or a rigid substrate controlled via micropipettes. d) and e) Biomimetic analogs of b) and c) using lipid membranes with anchored binders.

the cluster architecture. These kind of models have examined the relation between the chemical kinetics of binding/unbinding and the mechanical environment of the bonds, including the effect of unequal force sharing [Qian et al., 2008, Gao et al., 2011], or membrane and fluctuation mediated cooperativity effects [Krobath et al., 2011, Bihr et al., 2012, 2015]. Here, we focus on the important but previously unexplored case of a junction loaded hydraulically, relevant to hydraulic fracturing and delamination of cells and epithelial monolayers [Casares et al., 2015, Kosmalska et al., 2015] or to luminogenesis [Dasgupta et al., 2018]. In this situation, bonds bridge a pressurized cavity (either by a stretch-induced poroelastic effect or because of active ionic pumping) and are connected by a tense membrane. These factors determine the nature of unequal bond sharing and suppress the effect of membrane fluctuations. Building on previous work, we develop a family of minimal models and characterize how membrane tension and bond mobility control the lifetime clusters and the optimal cluster size.

In Part II, we adopt a continuum perspective and develop a family of non-equilibrium models that couple the reaction kinetics of binders molecules, their diffusion, and adhesion mechanics. One of the main objectives of this part of the thesis is to understand the competition between different modes of junction remodeling under force, and more specifically the competition between a tear-out regime, in which adhesion patches shrink due to bond breaking, and a diffusion-dominated regime, in which adhesion patches shrink due to bond motion [de Gennes et al., 2003, Brochard-Wyart and de Gennes, 2002a]. The behavior of adhesion patches under force has been generally understood in terms of these extreme scenarios, with instances of tear-out [Berk and Evans, 1991, Casares et al., 2015] and of diffusion-dominated cell-cell separation [Tozeren et al., 1989]. The tear-out and diffusion-dominated responses upon force application have also been reported in biomimetic systems depending on the mobility of bonds [Smith et al., 2008a]. This and previous references also examined a different but related problem, in which a membrane with mobile binders adheres to a solid substrate decorated with receptors. In this widely studied situation, free binders are mobile but bonds

are not since they connect mobile binders to receptors fixed to a substrate. As a consequence, the growth of a patch involves reactions to form new bonds and diffusion to recruit free binders from the non-adhered part of the vesicle into the adhesion patch [Boulbitch et al., 2001, Freund and Lin, 2004, Shenoy and Freund, 2005], but the membrane-substrate separation necessarily proceeds by progressive bond breaking [Pierrat et al., 2004a, Cuvelier and Nassoy, 2004, Lin and Freund, 2007, Cheng et al., 2009, Alert and Casademunt, 2016]. In principle, the case studied here of mobile binders and mobile bonds is compatible with more complex scenarios involving the coexistence of bond breaking and motion, and in fact observations during cell doublet separation suggest mixed tear-out/diffusion regimes [Maître et al., 2012b]. However, despite previous theoretical [Zhu, 1991, de Gennes et al., 2003, Brochard-Wyart and de Gennes, 2002a] and experimental efforts [Smith et al., 2008a], the dynamics of adhesion patches formed by mobile bonds under forces have not been systematically examined. In Part II, we develop a theoretical framework to examine this problem, which observes the compliance and force-sensitivity of the molecular bonds and molecular crowding at the adhesive junction [Nam and Santore, 2007, Schmid et al., 2016a] to resolve coupled mechano-chemistry of soft adhesion mediated by mobile binders.

Part I

Part I: Mechano-Stochastic modeling of the dynamics of soft adhesion mediated by specific binders

Chapter 2

Introduction to Part I

A single molecular bond has a binding energy E_b of only some tens of $k_B T$. Looking at the bond's dissociation process as a thermally assisted escape over the potential energy barrier E_b, the low binding energy of the bonds leads to a short lifetime: in absence of applied force, the average lifetime of a molecular bond is in the order of a second. Applying an external force to the molecular bond will modify the energy landscape of the dissociation process and therefore will modify the process itself [Bell, 1978b]. Over the last decades, numerous studies have characterized the behavior of individual molecular bonds under external forces, both experimentally and theoretically [Evans, 2001, Evans and Ritchie, 1997, Zhu, 2000]. However, the collective association of bonds into molecular bonds cluster can exhibit far longer lifetimes even in the presence of an external force. Although a characterization of individual bonds has been well accepted, the collective behavior of molecular bond clusters is still poorly understood. How can multiple bonds acting together sustain longer to applied forces? What are the processes involved? Different approaches have been made over the last years to model molecular bond clusters, both deterministic and stochastic. Depending on the approach chosen, they provide some interesting insights into the different mechanisms, both mechanical and

kinetic, involved in soft adhesion.
In Part I of the thesis , we will first summarize pioneering works made to model the behavior of individual bonds and the collective behavior of molecular bond clusters. We will then propose different minimal 2D models aimed at identifying the processes controlling specific adhesion under force or under hydraulic pressure such as elasticity, surface tension or the mobility of adhesion molecules.

Chapter 3

Stochastic modeling of bond clusters

The understanding of cell adhesion requires a proper characterization of a single bond. Inspired from the properties of polymers, modeling molecular bonds as elastic-spring like structures gives a good approximation for the complex behavior of the bonds, and captures the effects of force and displacement on the bond dynamics. Recently the behaviour of single receptor-ligands bonds under force have been investigated extensively, both for integrins [Zhang et al., 2002, Li et al., 2003] , cadherins [Baumgartner et al., 2000] and selectins [Fritz et al., 1998, Evans et al., 2001] and the elastic-spring model has been confirmed by these various experiments. Using dynamic force microscopy with different experimental techniques, including atomic force microscopy [Florin et al., 1994, Lee et al., 1994], laser optical tweezers [Kellermayer et al., 1997] and the biomembrane force probe [Merkel et al., 1999], experiments have revealed that a single molecular bond has a low binding energy of only 10-25 $k_B T$. To provide context for our contributions in Part I and Part II, we first summarize previous works about modeling a single bond under force, and then about modeling the collective behavior of bond clusters.

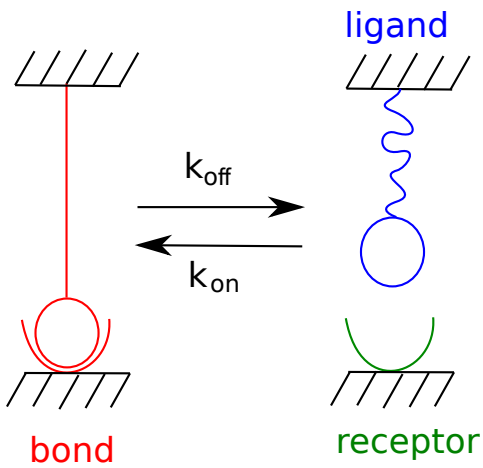

Figure 3.1: Schematic representation of bond breaking/formation as chemical reaction where k_{off} and k_{on} are the forward and reverse reaction rates.

3.1 Binding and unbinding of adhesion molecules as a chemical reaction

Unlike the non-specific adhesion due to Van Der Waals or electrostatic forces, the adhesion mediated by specific binders involves a chemical reaction. Using the framework of the elastic-spring model, we assume that receptors and ligands are elastic springs which interact via a reversible chemical process to form bond complexes, themselves having spring-like properties as shown in Fig. 3.1. These processes can be seen as chemical reactions, obeying the Eq. (3.1) where k_{on} and k_{off} are the forward and reverse reaction rates.

$$Receptor + Ligand \underset{k_{\text{off}}}{\overset{k_{\text{on}}}{\rightleftharpoons}} Bond \tag{3.1}$$

This chemical reaction is dependent on the mechanical and chemical environment surrounding the molecules, and particularly on the force applied to the bonds and the proximity of the binders. In the two following sections we detail how these rates depend on the mechanical environment.

Dependence of bond breaking on force

Experiments have shown that the unbinding of single bonds exhibit different force dependencies depending on their type or on the chemical environment. Many biological bonds exhibit slip-bond behavior, by which the bonds become weaker under an applied load, or catch-bond behavior, by which, counterintuitively, bonds strengthen under force. Some bond can even be insensitive to the applied load; such bonds are called ideal-bonds. For instance, depending on the chemical environment, E-cadherin homophilic bonds can switch between ideal-bond, slip-bond and a biphasic catch/slip-bond behavior [Rakshit et al., 2012].

Bell proposed, in a seminal theoretical paper [Bell, 1978a], a phenomenological model for the off rate of slip bonds extending the transition state theory for reactions in gases. It states that the off-rate of receptor-ligand interactions depends exponentially on the force on the linkage. One could think of an applied force tilting the energy landscape and accelerating the dissociation of the non-covalent receptor-ligand bond, see Fig. 3.2.

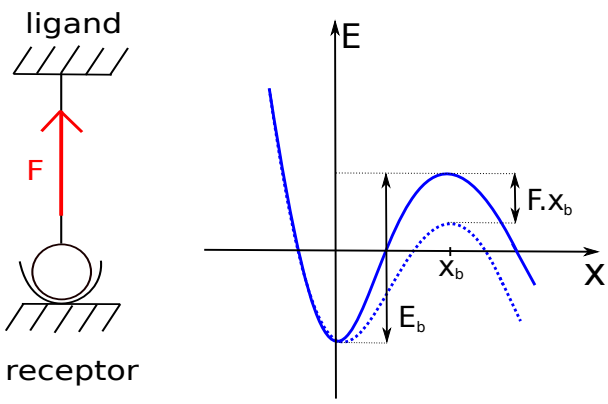

Figure 3.2: Schematic representation of the energy landscape for receptor-ligand interaction. The solid curve represents the energy landscape for an unstressed bond and the dotted line corresponds to the modified energy landscape in the presence of an applied force F.

According to Kramer's theory [Kramers, 1940], the spontaneous dissociation rate can be seen as a thermally activated escape over a transition barrier E_b:

$$k^0_{off} = \omega_0 e^{\frac{-E_b}{k_B T}}, \tag{3.2}$$

where ω_0 is the natural vibration frequency, in the order of 10^{-12} s^{-1}, E_b is the energy barrier required to break the bond, in the order of 10 to 25 $k_B T$, and $k_B T$ that sets the thermal energy.

According to Bell's model, when a force F is applied along the axis of the bond, the energy barrier is modified. To break the bond, the new barrier $\hat{E}_b(F)$ is $\hat{E}_b(F) = E_b - Fx_b$, with x_b the coordinate of the transition state along the axis of the bond. Thus, the new dissociation rate is:

$$k_{off}(F) = \omega_0 e^{\frac{\hat{E}_b(F)}{k_B T}} = \omega_0 e^{\frac{-E_b + Fx_b}{k_B T}} = k^0_{off} e^{\frac{Fx_b}{k_B T}} = k^0_{off} e^{\frac{F}{F_b}} \tag{3.3}$$

where k^0_{off} is the spontaneous dissociation rate in the absence of force, F the applied force and $F_b = \frac{kBT}{x_b}$ a force scale for bond strength (a typical scale in for E-cadherins being $F_b \simeq 4$ pN, for $x_b \simeq 1$ nm). This law is commonly called Bell's law in the literature.
This modeling of force dependence of the dissociation rate for slip bonds has been tested and verified experimentally for many different types of bonds. Some models [Evans and Ritchie, 1997] have been developed later, that take into account the dynamical loading and the limitations of such a simple model like the fact that all the features of the energy landscape are lumped in only one parameter, x_b. The importance of Bell's insight was to expose the significant role of mechanical forces in biological chemistry.

Inspired by Bell's and Evans [Evans et al., 2004] work, Pereverzev [Pereverzev et al., 2005a, 2011] introduced a similar model, the so-called two-pathway model, to explain the force dependence of the dissociation rate of catch bonds. It provides the simplest mathematical description of the catch-slip bond transitions but despite its simplicity has led to many useful analytical results and predictions [Pereverzev et al., 2005b, Pereverzev and Prezhdo, 2006].

Assuming that the minimum of the energy landscape corresponding to the bound state has two alternative pathways to escape corresponding to the catch and slip mechanisms of dissociation, this model states that the dissociation rate has the following form:

$$k_{off}(F) = k^0_{off-s} e^{\frac{F x^s_b}{k_B T}} + k^0_{off-c} e^{\frac{-F x^c_b}{k_B T}} = k^0_{off-s} e^{\frac{F}{F^s_b}} + k^0_{off-c} e^{\frac{-F}{F^c_b}} \tag{3.4}$$

with k^0_{off-s} and k^0_{off-c} the rate of dissociation for the slip and catch pathways at zero force, x^s_b and x^c_b the two distances from the minimum of the energy landscape to the two transition barriers. Finally F^s_b and F^c_b are the two force scales corresponding for both pathways. We plot in Fig. 3.3 the lifetime of slip and catch bonds for different values of the catch bond pathway force scale F^c_b. The lifetime of the slip bond decreases with the applied force while the catch bond lifetime reaches a maximum for a non-zero applied force. For higher forces, the catch bond exhibits a slip bond behavior.

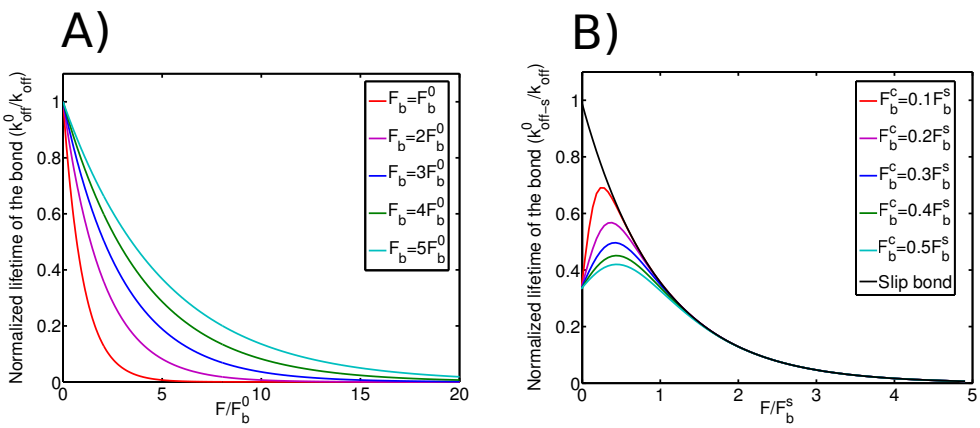

Figure 3.3: A) The normalized lifetime (k^0_{off}/k_{off}) of slip bonds. Here the emphasis is made on the influence of the force scale F_b. B) The normalized lifetime (k^0_{off-s}/k_{off}) of slip and catch bonds, where $k^0_{off-c} = 2k^0_{off-s}$. Here the emphasis is made on the influence of the catch bond pathway force scale F^c_b.

To sum up, the dissociation rate for the three prototypical types of bonds can be expressed as :

For ideal bonds: $k_{off}(F) = k^0_{off}$

For slip bonds: $k_{off}(F) = k^0_{off} e^{\frac{F}{F_b}}$

For catch bonds: $k_{off}(F) = k^0_{off} \left(e^{\frac{F}{F^s_b}} + A e^{\frac{-F}{F^c_b}} \right)$

Dependence of bond formation on separation

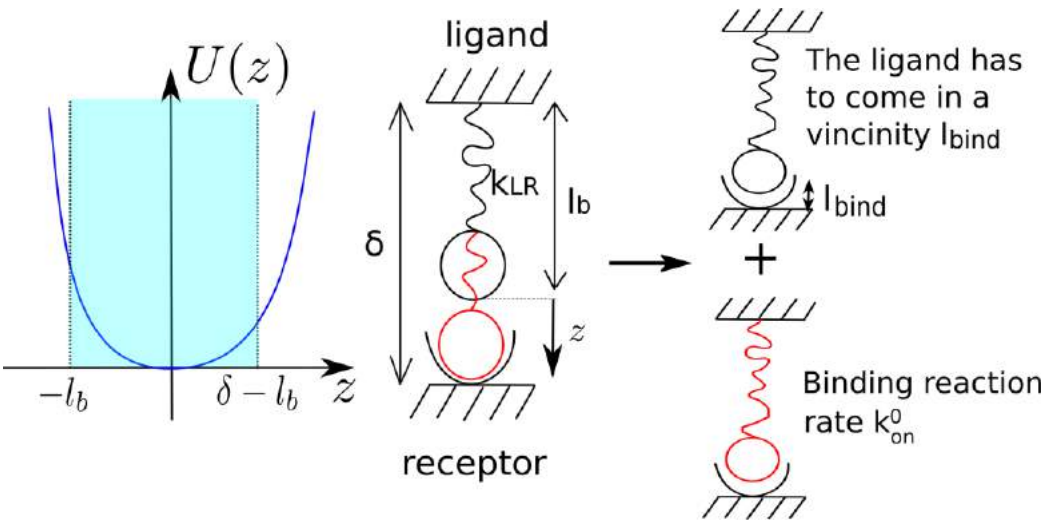

Figure 3.4: Schematic representation of the two steps necessary for the formation of the bond. In a first step, the ligand has to come in the vicinity of the receptor, within a distance l_{bind}. The distance z corresponds to the extension of the molecule from its rest position. The light blue domain corresponds to the accessible elongation for the binder. The second step is a chemical reaction in which the ligand and the receptor chemically react to form a bond with a constant rate k^0_{on}.

The reaction consisting of binding of two binders is actually a combination of two events [Bell et al., 1984b, Erdmann and Schwarz, 2006]. First, the ligand has to come close enough to the receptor and then react when they are in close range.
We keep the classical view of the ligand as attached to a spring of rest length l_b and stiffness k_{LR}. As it is stuck between the two surfaces, the ligand is allowed to move only in a zone delimited between $z = -l_b$ and $z = \delta - l_b$ in the potential $U(z)$, with z the extension of the molecule from its rest position and $U(z)$ such as:

$$U(z) = \frac{k_{LR} z^2}{2} \quad \text{for } z \in [-l_b, \delta - l_b] \tag{3.5}$$

As a classical result of statistical mechanics, the Maxwell Boltzmann statistics gives the probability density function $P(z)$ for the ligand to be in a position z:

$$P(z) = \frac{1}{Z} e^{\frac{-U(z)}{k_B T}} = \frac{1}{Z} e^{\frac{-k_{LR} z^2}{2 k_B T}}, \quad z \in [-l_b, \delta - l_b] \tag{3.6}$$

where Z is the partition function ensuring the normalization condition:

$$\int_{-l_b}^{\delta - l_b} P(z) dz = 1 \tag{3.7}$$

The normalization gives:

$$Z = \sqrt{\frac{\pi k_B T}{2 k_{LR}}} \left[\text{erf}\left((\delta - l_b) \sqrt{\frac{k_{LR}}{2 k_B T}} \right) + \text{erf}\left(l_b \sqrt{\frac{k_{LR}}{2 k_B T}} \right) \right], \tag{3.8}$$

with $erf : x \mapsto erf(x)$ the error function, also known as the Gauss error function. The probability for the ligand to come within a distance l_{bind} from the receptor, necessary for the binding reaction to happen, is:

$$p = \frac{l_{bind}}{Z} e^{\frac{-k_{LR} (\delta - l_b)^2}{2 k_B T}}. \tag{3.9}$$

With k_{on}^0 the reaction rate for binders separated by a distance $z < l_{bind}$, the rebinding rate can be written as:

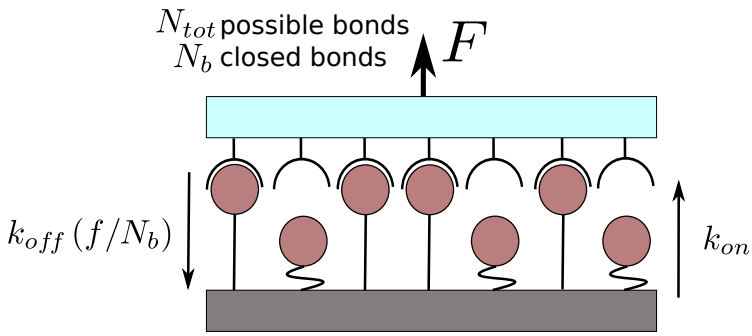

Figure 3.5: Schematic representation of an adhesion cluster under constant shared force F. N_{tot}, the total number of bonds, and N_b, the number of closed bonds.

$$k_{on} = k_{on}^0 p = k_{on}^0 \frac{l_{bind}}{Z} e^{\frac{-k_{LR}(\delta - l_b)^2}{2K_B T}}. \tag{3.10}$$

k_{on} is very difficult to determine experimentally, especially for adhesion mediated by a cluster of adhesion molecules [Chesla et al., 1998], when 3D bulk kinetics need to be reconciled with 2D kinetics [Hu et al., 2013]. As considered in previous theoretical works [Seifert, 2000, Erdmann and Schwarz, 2004] and in order to focus on the generic features of soft adhesion, we will consider k_{on}^0 force-independent for the rest of the thesis.

3.2 Discrete modeling of molecular bond clusters

Despite the steady progress in statistical description of a single molecular bond, their collective behavior is still poorly understood. Therefore, the physical description of single bond under force has to be extended to clusters of adhesion bonds under force. A pioneering theoretical framework for describing the collective behavior of molecular bonds was introduced by Bell [1978a].

Let us consider a simplified version of the model proposed by Bell, by considering a patch of N_{tot} couple receptor-ligands, forming bonds, that can be open or closed between two rigid media. A sketch of the model is given in Fig. 3.5. $N_b(t)$ bonds are closed at time t. A force F is applied to the patch and, because of the rigidity of both media, the force is equally shared among the N_b closed bonds. Thus each bond experiences a force $F_{bond} = F/N_b$. The binding and unbinding of bonds follows the chemical reaction $Receptor + Ligand \underset{k_{\text{off}}}{\overset{k_{\text{on}}}{\rightleftharpoons}} Bond$, with the unbinding rate given by Bell's law $k_{off}(F_{bond}) = k^0_{off}\exp(F_{bond}/F_b)$. For simplicity the binding rate is considered constant: $k_{on} = k^0_{on}$.
The evolution of the number of closed bonds N_b as a function of time is given by Eq. (3.11), expressing the balance of mass of closed bonds:

$$\frac{dN_b}{dt} = k_{on}(N_{tot} - N_b) - k_{off}(F/(N_b F_b))N_b \tag{3.11}$$

Let's consider the following non dimensional quantities:

$$\tau = k^0_{off}t, \quad F/F_b = f \quad \text{and} \quad \gamma = k_{on}/k^0_{off}$$

The equation 3.11 becomes:

$$\frac{dN_b}{d\tau} = \gamma(N_{tot} - N_b) - \exp\frac{f}{N_b}N_b \tag{3.12}$$

The exponential dependence on the force of the last term of the equation makes the stability of its solutions very dependent on the applied force. Studying this equation, Bell showed that it exists a critical force f_{cr} such as for $f < f_{cr}$ the Eq (3.12) has a stable solution and for $f > f_{cr}$ it does not accept stable solution. f_{cr} is given by:

$$f_{cr} = N_{tot}\text{plog}\left(\frac{\gamma}{e}\right) \quad \text{with plog(a) solution of } xe^x = a. \tag{3.13}$$

Thus, for an applied force f such as $f < f_{cr}$, the cluster is stable and stabilizes at a non-zero value of N_b, and for $f > f_{cr}$, the cluster is unstable and the number of bonds ultimately reaches $N_b = 0$. Moreover, the critical force is

increasing linearly with the size of the cluster: the bigger is the cluster, the bigger is the critical force necessary to unbind the whole cluster.

For equal loading shared between the bonds and constant rebinding rate, this deterministic approach of equilibrium properties of adhesion clusters is a first good approximate model to consider the competition between bond breaking and rebinding and provides an easy way to introduce the concept of critical forces.

Nevertheless, the deterministic approach does not allow us to explore the stochastic nature of cluster decohesion: indeed, according to single-molecule mechanics, a given bond may be closed at one instant and break at another as a result of thermally activated escape from the biding potential well.
A stochastic approach could let us explore stochastic trajectories for cluster evolution (from a state where all the bonds are closed until the total decohesion of the cluster), and access useful statistical information.

A stochastic version of Bell's model for bond clusters has been developed, but only studied in the limit of large systems, and for specific parameters values [Cozens-Roberts et al., 1990]. It has also been introduced for the case of absence of rebinding [Bell, 1978a] or to evaluate specific experiments. Focusing on the generic features of the stochastic dynamics of a cluster under shared constant loading and constant rebinding, [Erdmann and Schwarz, 2004] developed a stochastic version of Bell's model.

The system is also a patch of N_{tot} couple receptor-ligands (forming bonds) that can be open or closed. $N_b(t)$ bonds are closed at time t. A force F is applied to the patch and it is equally share among the N_b closed bonds. Thus each bonds experience a force $F_{bond} = F/N_b$. Now each bond undergoes stochastic dissociation, with a reaction rate $k_{off}(F)$ following Bell's law, and formation, with a constant reaction rate k^0_{on}.
The bonds are indistinguishable and, as a stochastic system, the evolution of the system is now given by its probability $p_i(t)$ to have i bonds closed at time

t. With the non-dimensional quantities $\tau = k^0_{off}t$, $F/F_b = f$, $\gamma = k_{on}/k^0_{off}$, we can derive the following one-step master equation for $p_i(t)$:

$$\frac{dp_i}{d\tau} = r_{i+1}p_{i+1} + g_{i-1}p_{i-1} - (r_i + g_i)p_i, \tag{3.14}$$

where $p_i(\tau)$ is the probability that i bonds are closed at time τ. r_i and g_i are the reverse rate of transition from i to $i-1$ closed bonds and the forward rate of transition from i to $i+1$ closed bonds:

$$r_i = ie^{\frac{f}{i}} \tag{3.15}$$

$$g_i = \gamma(N_t - i) \tag{3.16}$$

This equation has to respect some boundary conditions. For instance, the number of closed bonds is bounded by the total number of bonds: $N_b \leq N_{tot}$. Thus $g_{N_{tot}} = 0$, which is called a reflecting boundary. On the opposite, $N_b \geq 0$ and we consider rebinding impossible when all bonds are closed because of elastic recoil. Thus we have, $r_0 = 0$ and $g_0 = 0$, which is an absorbing boundary.

This one-step master equation is easy to write but solving it is quite difficult except for very simple cases. To illustrate this, let us look a two important quantities: the mean number of closed bonds $N_b(\tau)$ and its variance $\sigma_{N_b}(\tau)$:

$$N_b(\tau) =< i >= \sum_{i=1}^{N_{tot}} ip_i(\tau) \tag{3.17}$$

$$\sigma^2_{N_b} =< i^2 > - < i >^2= \sum_{i=1}^{N_{tot}} i^2p_i(\tau) - N_b^2 \tag{3.18}$$

Substituting both equations in the one-step master equation Eq. (3.14), we obtain:

$$\frac{dN_b}{d\tau} = \sum_{i=1}^{N_{tot}} i\frac{dp_i}{d\tau} =< g(i) > - < r(i) > \tag{3.19}$$

$$\frac{d\sigma^2_{N_b}}{d\tau} =< g(i) + r(i) > +2 < (i- < i >)[g(i) - r(i)] > . \tag{3.20}$$

If r_i and g_i were both linear functions in i, then Eq. (3.19) would become the classic deterministic equation Eq. (3.12) studied by Bell. But for $F \neq 0$, $r(i)$ is non-linear in i and therefore we cannot write $< r(i) >= r(< i >)$. As an approximation, we can expand $r(i)$ as a Taylor series around N, but this leads to a complex hierarchy of relations between lower moments. We see that the same problem will arise for higher moments like the variance, see Eq. (3.20). Finally such approach cannot describe the effect of the absorbing boundary for $i = 0$ which is compulsory to study physically relevant cases. To summarize, an analytical approach to solve the master equation is difficult.

In order to overcome these limitations, Erdmann and Schwarz [2004] used a Monte Carlo algorithm called the "first reaction method" Gillespie algorithm [Gillespie, 1976, 1977], to perform a stochastic analysis of the one-step master equation Eq. (3.14). This method offers a valuable insight into the typical nature of unbinding trajectories and is able to treat the problem with an absorbing boundary. Considering a constant average force per bond, they found that the cluster lifetime increases monotonically with the cluster size: bond clustering increases by orders of magnitude the long-term stability of clusters. Nevertheless, experiments show that in-vivo adhesion clusters size is usually limited to around few microns [Zaidel-Bar, 2004] in the case of focal adhesions. What is preventing the bonds to cluster on a bigger scale to achieve longer lifetimes?

One of the main hypothesis made here is the equal load sharing between the bonds but in biological systems, the general one can expect non-uniform force distribution. In case of non-uniformity of force distribution the off-rate r_i given in equation is modified as follows:

$$r_i = \sum_{j=1}^{i} e^{f_j}, \tag{3.21}$$

with f_j the force felt by the bond $1 < j < i$ among the i closed bonds.

Because of the convexity of the function $\exp(x)$ we can write the so-called Jensen inequality that states that for a convex function f(x), with $x_1, x_2, ..., x_i$ in its domain and real positive weights $a_1, a_2, ..., a_i$, we have

$$f\left(\frac{\sum_{j=1}^{i} a_j x_j}{\sum_{j=1}^{i} a_j}\right) \leq \frac{\sum_{j=1}^{i} a_j f(x_j)}{\sum_{j=1}^{i} a_j}. \tag{3.22}$$

Invoking this inequality, we can make the following statement about the dissociation rate

$$r_i = \sum_{j=1}^{i} e^{f_j} \geq ie^{(\frac{\sum_{j=1}^{i} f_j}{i})} = ie^{\frac{f}{i}}. \tag{3.23}$$

Thus, any force distribution different from the equally shared force case is increasing the total dissociation rate and thus leads to less stable clusters. The assumption $r_i = ie^{\frac{\sum_{j=1}^{i} f_j}{i}} = ie^{\frac{f}{i}}$, for equally shared force, tends to overestimate the lifetime of the cluster, and thus the overall distribution of forces over the cluster is thought to control the stability of molecular bond clusters.
In order to investigate such a problem, Qian et al. [2008] developed a model including mechanics into the stochastic problem previously studied and a method to estimate the force distribution over the cluster via a parameter accounting for the mechanical context of the bond cluster [Qian et al., 2009, Gao et al., 2011].

Their theoretical model consists of a periodic array of clusters of molecular bonds, of size $2a$, which are distributed over a length of $2c$. The arrays of bond clusters bridge an elastic medium, with Young modulus E and a Poisson ratio ν, and a rigid medium and is subjected to an applied tensile stress σ. For a given bond configuration and solving an elasticity problem, they are able to compute the distribution of forces over the cluster. Each bond undergoes stochastic dissociation (with a reaction rate k_{off}) and formation (with a reaction rate

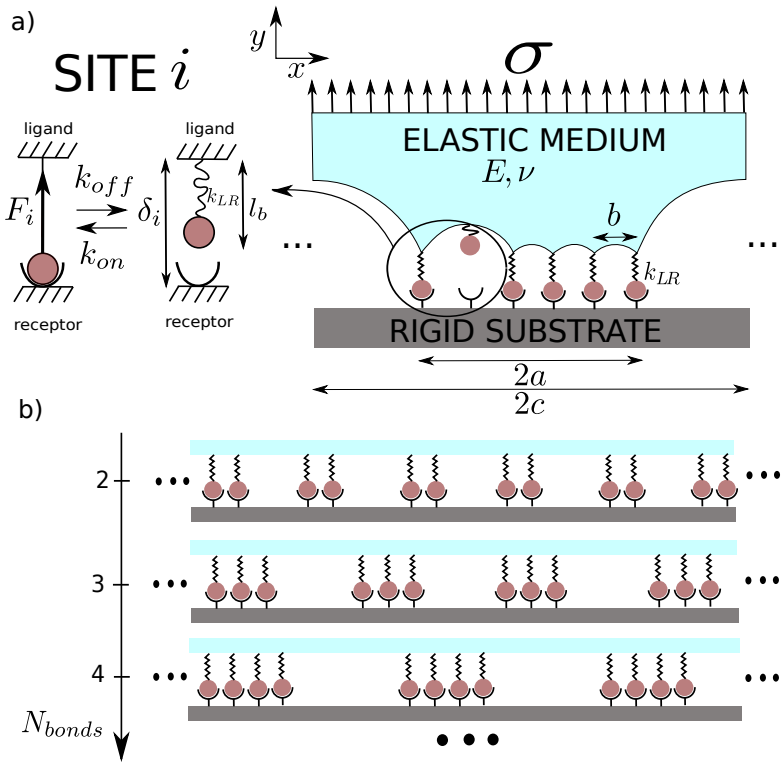

Figure 3.6: a) Schematic illustration of an idealized theoretical model of periodic adhesion between an elastic body and a rigid medium. The elastic medium is subjected to a tensile stress σ. Size of the system: $2c$. Size of the cluster : $2a$. The system is such that $c = 2a$. Bond's spacing is b. E and ν are the Young modulus and the Poisson's ratio of the elastic medium. The bonds have a stiffness k_{LR}. b) Illustration of the relation between the size of the crack and the size of the patch. With this set-up, the average density of bonds is kept constant and independent of the number of bonds N_{bonds}.

k_{on}). To study the influence of the cluster size N_{bonds}, the system is such that $c = 2a$, thus, the density of bond ρ is kept constant and $\rho = \frac{1}{2b}$. A sketch of the model can be seen in Fig. 3.6b). In order to characterize the mechanics of the adhesive contacts, they identified a dimensionless parameter α given by $\bar{\alpha}(a, b, E, \nu, k_{LR}) = \frac{a}{b^2} k_{LR}(1 - \nu^2)/E$. It controls how the interfacial stress is distributed over the adhesion domain. Looking at Fig. 3.7, we can see that

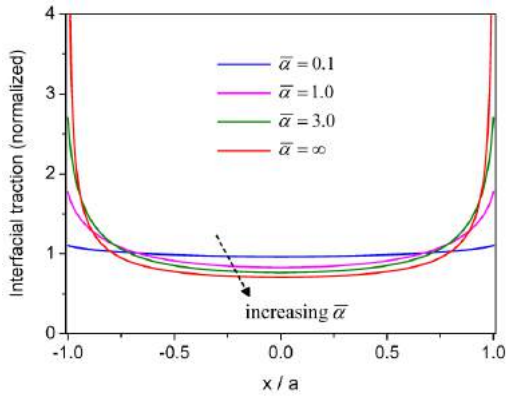

Figure 3.7: Distribution of interfacial stress over the cluster for different $\bar{\alpha}$, results reproduced from [Qian et al., 2008]. Low $\bar{\alpha}$ leads to uniform load distribution and high $\bar{\alpha}$ leads to crack-like failure distribution.

for low α, the applied tensile stress is equally shared among bonds and the system is similar to the one studied by Erdmann and Schwarz [2004]. On the other side, for a large α, the stress is concentrated on the edges, the bonds in this zone will bear a much large stress, and thus crack-like failure is expected at the adhesion edge. For intermediate values of α, the stress is maximum at the edges and minimum in the center of the patch.

This idealized stochastic-elasticity model unifies the statistical description of single bonds behavior at small scales with an elastic description of the adhesive contact at large scales. Using a Monte Carlo scheme, the Gillespie first reaction method, they are able to solve the coupled stochastic-elasticity equations and study the stability and the strength of molecular bond clusters joining two elastic bodies.

The results of the numerical simulations suggest that, for any given load, there exists a window of cluster size, for which the cluster exhibits a lifetime relatively larger than that of a single molecule with no force.
Furthermore, bond clusters are longer-lived at intermediate cluster sizes. Thus, under some assumptions, they could provide a model that reproduces the finite size clusters observed in the experiments. Despite the very idealized

framework proposed, this model provides a very elegant and efficient way to study the chemo-mechanical problem of soft adhesion mediated by specific binders, and will serve as a basis for further modeling presented in this first part of the thesis. This minimalistic mechano-stochastic approach has been extended in various ways over the recent years [Qian et al., 2009, Gao et al., 2011]. It has also been extended to 3-D environment accounting for membrane-mediated interaction and fluctuations, leading to cooperativity effects, to study the segregation of bonds of different sizes at adhesion patches [Krobath et al., 2011, Schmid et al., 2016b], or the dynamics and structure of adhesion patches [Smith et al., 2008b].

Chapter 4

Mechano-stochastic modeling

We saw in the previous chapter, that the mechanical environment and the structure of the clusters play a role in the stability of molecular bond clusters. Gao and coworkers idealized the cellular mechanical environment as an elastic half plane. Moreover, this and other groups considered that force was transmitted to the bonds by a tensile stress σ on this elastic medium. While the cytoskeleton can indeed behave like an elastic medium, binders are more closely associated to the membrane, which is often under tension. Furthermore, the cortex itself can be seen as a thin membrane under tension [Salbreux et al., 2012b]. We develop, in this chapter, an idealized 2D model coupling mechanics and stochastic reaction dynamics, which allows us to include the effect of surface tension, in addition to elasticity, to determine the force distribution over the bonds in a cluster. In addition, we consider the possibility that bonds are loaded through hydraulic pressure ΔP in the interstitial space bridged by bonds, as motivated in the Introduction. In this case, the membrane can be expected to be tense, and hence membrane fluctuations suppressed.

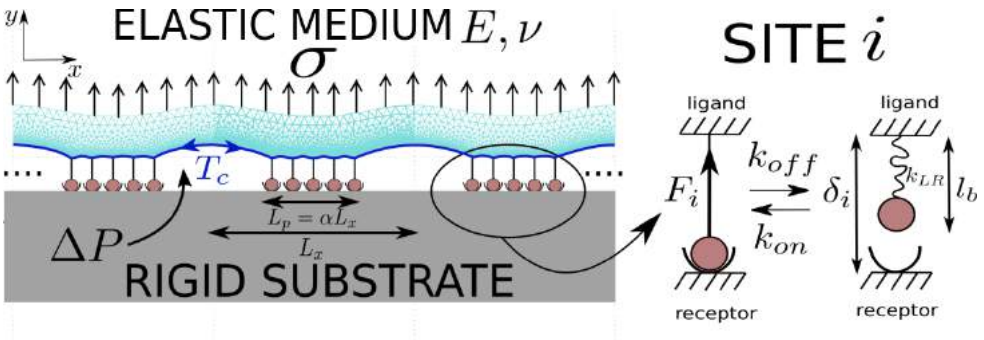

Figure 4.1: Scheme of the model for molecular bond clusters embedded on an elastic medium. The blue line on the bottom of the elastic medium is subject to the tension T_c and tends to oppose to its elongation. The elastic medium is subjected to a tensile stress σ or the interstitial space to an overpressure ΔP.

The model considered in this chapter is summarized in Fig. 4.1. We will introduce the different features of the model step by step to understand their role in stability of bond clusters.

4.1 Model

We consider a periodic array of size L_x of adhesion patches of size L_p made of closed bonds with a uniform spacing b, which establishes an adhesion between an elastic medium, with a Young's modulus E and a Poisson's ration ν, and a rigid substrate. The system is subjected to either a tensile stress σ or an interstitial overpressure ΔP. The interface is tense with a surface tension contribution T_c to the interface bounding the bottom part of the elastic medium. The effect of this tension is opposed to an increase of size of the bottom surface, see Fig. 4.1. In the present 2D setting, T_c is a line tension, which could represent membrane or cortical tension

The system is parameterized such that the density of bonds does not depend on the size of the patch. For simplicity, we set the size of the crack equal to the size of the patch. Thus, due to the periodicity of the problem, we will

focus on a system of size L_x with one cluster of size $L_p = \alpha L_x$, with $\alpha = 1/2$, made of $N_{bonds} = \frac{L_x}{2b} + 1$ bonds. Because of the constant average bond density independent of cluster size, we can state that for a given surface tension T_c and a given tensile stress σ or a given overpressure ΔP, the average force applied on closed bonds is constant whatever the size of the cluster is. Only the distribution of forces depends on the size of the system. Thus, this simple set-up allows us to examine the stability of the adhesion complex depending on its architecture at constant average bond density.
Each bond undergoes stochastic dissociation, with a reaction rate k_{off}, and formation, with a reaction rate k_{on}, which will depend on the force applied to the bond and on the separation distance between the two surfaces as discussed in subsection 3.1.

Mechanical modeling

To account for the elasticity of the system in a simple way, we consider a slice of linearly elastic material with vertical thickness $d = b$ as a plane strain problem. The molecular bonds are uniformly distributed within the adhesion domain at fixed spacing b. We neglect unspecific adhesion and, thus, adhesion is only mediated by the binders. We consider that only the vertical component of the force applied to the bond modifies the kinetics of unbinding.
In order to solve the mechanics, the elastic medium is discretized using a non-uniform 2D Finite element triangular mesh made with 8298 triangular elements, refined at the adhesion site. The lateral sides are subjected to periodic boundary conditions. The binders coincide with nodes at the bottom side of the material. According to its state, open or closed, the bond is free or fixed. When the bond is closed, the displacement of the corresponding node is fixed, and when the bond is open, the corresponding node is free. The elements on the bottom side of the elastic medium are subjected to a line tension T_c. We number the bonds from the left to the right from 1 to N_{bonds}.

The mechanics of the problem is then obtained through the minimization of the energy including the elastic energy E_E, the energy due to the overpressure E_P, the surface tension energy E_T and the potential of the loads E_L. For a global displacement $\mathbf{U}$ of the nodes of the mesh, K the stiffness matrix of the system, L_{bottom} the length of the bottom interface of the elastic medium, A_{bottom} the area between the two surfaces and $\mathbf{F}$ the vector of tensile forces due to the tensile stress σ, the energy E_{tot} of the system is:

$$E_{tot} = E_E + E_P + E_T + E_L = \frac{1}{2}\mathbf{U}^\top K\mathbf{U} - \Delta P A_{bottom} + T_c L_{bottom} - \mathbf{U}^\top \mathbf{F} \quad (4.1)$$

With the proper boundary conditions for periodicity and given set of bonds, minimization of the energy E_{tot} allows us to compute the vertical component of the force F_i felt by closed bond number i and the separation distance δ_j for a open bond number j. In this way we can compute the corresponding rates of dissociation and formation for each closed or open bonds in the cluster.

Stochastic modeling

The dissociation rate k_{off} follow the classical Bell's law

$$k_{off} = k^0_{off} e^{F_i/F_b}, \quad (4.2)$$

with F_b the force scale, typically in the pN range, k_0 the spontaneous dissociation rate in the absence of force, typically from a fraction of second to hundreds of seconds and F_i the vertical component of the force felt by the bond i
We can write the breaking rate, for a closed bond i subject to a force F_i, in a dimensionless form as

$$r_i = \frac{k_{off}}{k^0_{off}} = e^{Fi/F_b} = e^{f_i}, \quad (4.3)$$

with $f_i = \frac{F_i}{F_b}$ the normalized force acting on the bond.

And for the formation rate, we use the definition detailed in Fig. 3.4 that gives the non-dimensionalized formation rate for an open bond i at a distance δ_i from the opposite surface:

$$g_i = \frac{k_{on}}{k^0_{off}} = 2\gamma\sqrt{\frac{\beta}{\pi}}\frac{\exp(-\beta(\Delta_i - L_b)^2)}{\mathrm{erf}\left[(\Delta_i - L_b)\sqrt{\beta}\right] + \mathrm{erf}\left[L_b\sqrt{\beta}\right]}, \tag{4.4}$$

with $\Delta_i = \frac{\delta_i}{b}$ the surface separation normalized by the bond spacing b, $L_b = \frac{l_b}{b}$ the rest length of the bond after the same normalization, $\gamma = n\frac{k^0_{on}}{k^0_{off}}\frac{l_{bind}}{b}$ and $\beta = \frac{k_{LR}b^2}{2k_BT}$.

Numerical method: Gillespie algorithm

Considering our problem, where each molecular bond, opened or closed, has a different rate, solving the master equation is very difficult. Different methods have been proposed to study chemical reactions [Long et al., 1999, Tees et al., 1993], but to solve the master equation with spatially dependent rates, we will use in the following sections the "first reaction method" developed by Gillespie [Gillespie, 1976, 1977].

In order to do so, we consider each molecular bond i as an independent reaction site. We label the site of reaction by the bond number $i = 1, ..., N_{tot}$ and the corresponding rate a_i with $a_i = r_i = r(F_i)$ for closed bonds and $a_i = g_i = g(\delta_i)$ for opened bonds.

Following the first reaction method, we want to determine the site i where the first reaction happens and the time τ at which it will happen according to the probability distribution $P(i, \tau) = a_i e^{-a_{tot}\tau}$ with $a_{tot} = \sum_i^{N_{tot}} a_i$. Then, we generate a series of independent random numbers $\xi_\nu, \nu = 1, ..., N_{tot}$ uniformly distributed over [0,1] and compute the series $\tau_\nu = \dfrac{-\ln \xi_\nu}{a_\nu}$.

Then, the next event will happen after a time $\tau_i = \min_\nu(\tau_\nu)$ at the corresponding site i. If $a_i = r_i$ the corresponding bond will break and if $a_i = r_i$ the corresponding open bond will rebind. See Fig. 4.2 for a graphical description.

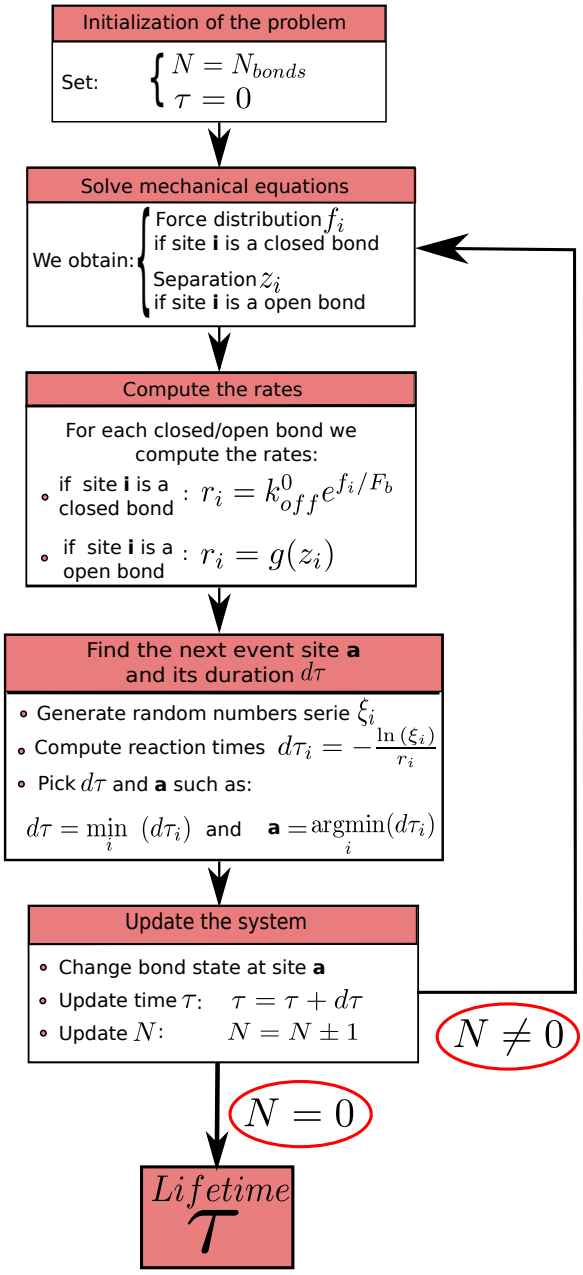

Figure 4.2: The flow chart of a Gillespie Monte Carlo scheme coupling stochastic descriptions of molecular bonds and elastic descriptions of cell-substrate adhesion.

Numerical parameters

For the following examples we choose numerical parameters in accordance with [Qian et al., 2008] in order to be able to compare results. A table below summarizes the numerical parameters.

Numerical parameters

- $b = 3.2 \cdot 10^{-8}$ m
- $l_b = 1.1 \cdot 10^{-8}$ m
- $\gamma = 1 - 100$
- $k_{LR} = 2.5 \cdot 10^{-4}$ N·m^{-1}
- $F_b = 4$ pN
- $N_{bonds} = 3 - 65$

4.2 Bond clusters attached to an elastic medium

Bond clusters under applied tensile stress σ

We start by studying the case of a uniform tensile stress σ applied on the surface of the elastic medium, thus ignoring surface tension and hydraulic pressure, in a problem previously studied by Gao and coworkers, it is natural to expect that the cluster will be more fragile as the applied tensile stress increases since the bonds are force sensitive. A sketch of the problem is given in Fig. 4.1, with $T_c = 0$ N·m^1 and $\Delta P = 0$ Pa. The mechanics of the problem is obtained through the minimization of the energy $E_{tot} = E_E + E_L$.
First, we will look at the influence of the tensile stress and the size of the cluster on the force profile and the separation distance between the two media, as the rates depend on these two variables.

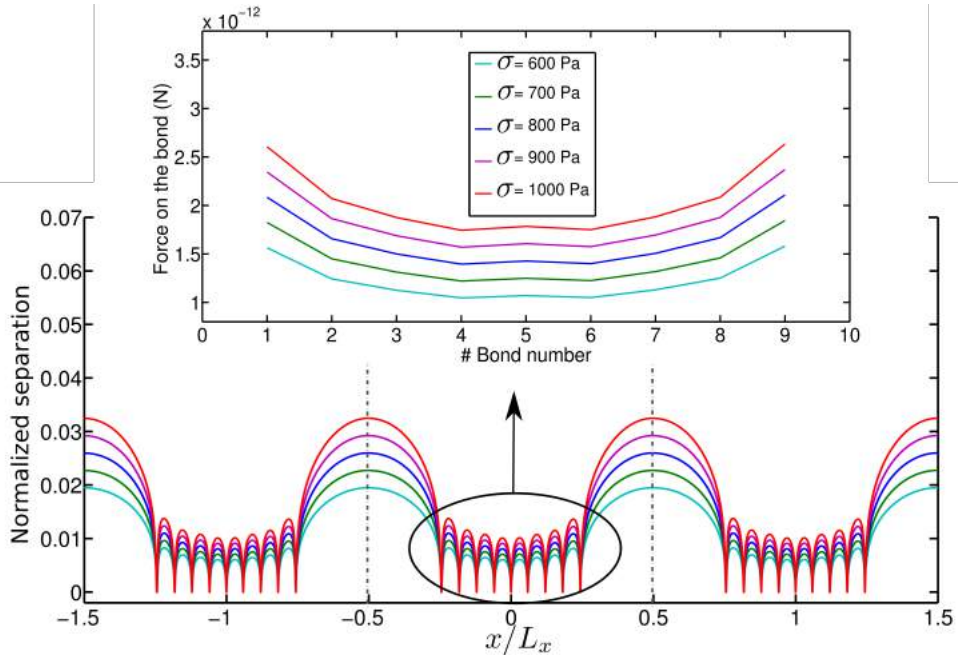

Figure 4.3: Force $F(N)$ on the bond and normalized separation y/L_x for different values of the applied tensile stress $\sigma(Pa)$. $E = 10$ kPa. $N_{bonds} = 9$. Force and displacements are linear with σ.

To illustrate the influence of the tensile stress σ on the mechanics, we plot in Fig. 4.3, for a cluster of 9 bonds initially closed, the distribution of forces over the cluster and the surface separation profile. We can see that, on the one hand, increasing the tensile stress σ will increase the separation between the two surfaces in the cracks making rebinding more difficult and, on the other hand, increasing the tensile stress σ increases the transmitted forces distribution over the cluster, which will make bonds more fragile. Its then expected that the cluster will also be more fragile.

It is also interesting to look at the influence of the cluster size. Fig. 4.4 shows the force distribution over the cluster for different value of the cluster size. We see that, as N_{bonds} increases, the force distribution transits from a uniform

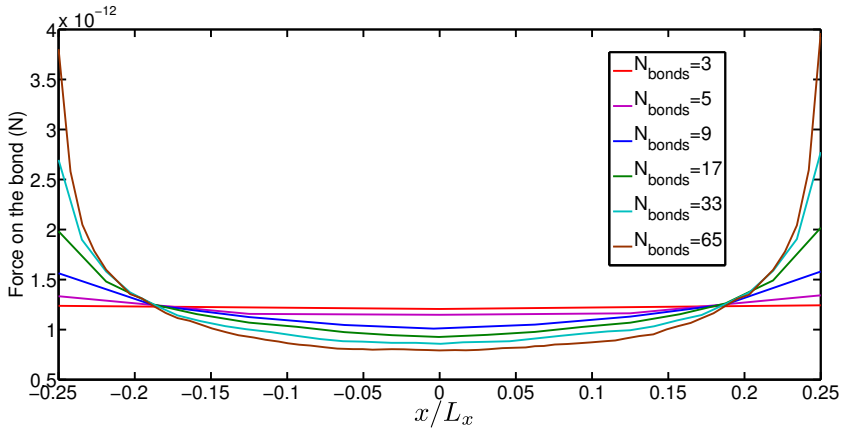

Figure 4.4: Force distribution $F(N)$ as a function of the cluster size N_{bonds}. L_x increases linearly with N_{bonds}. E = 10 kPa. σ = 500 Pa.

distribution to a crack-like distribution. Thus, the cluster size controls the overall force distribution and then the stability of the cluster.

These two remarks are illustrated in Fig. 4.6 and Fig. 4.5. Fig. 4.6 shows that the lifetime of the cluster decreases with the tensile stress σ. Fig. 4.5 shows that the size of the clusters, which scales as the size of the cracks, influences the ability of the cluster to resist to tensile stresses. Small clusters tend to live short due to the small number of bonds supporting the applied force and thus are very sensitive to thermal fluctuations. Large clusters, on the other hand, tend to live short and exhibit dramatic dissociations: for large clusters the cracks are so big that the force at the crack tip make the bonds more susceptible to break, and these bonds never rebind, as the separation also increases with the size of the cracks.

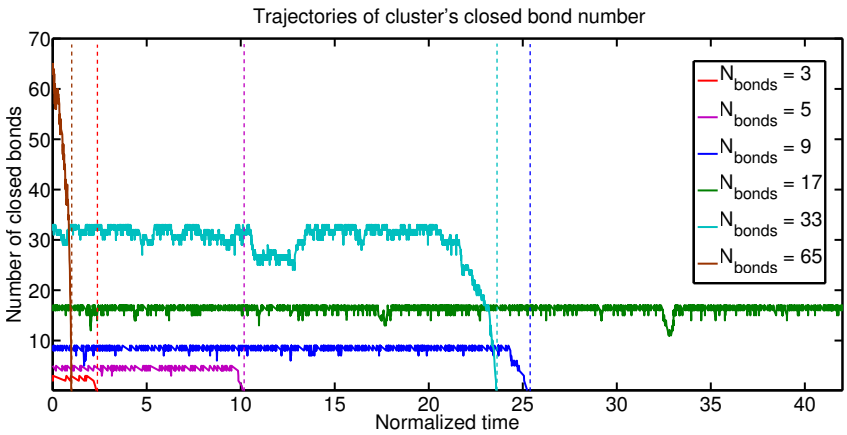

Figure 4.5: Simulation trajectories of a molecular bond clusters obtained for different initial number of closed bonds N_{bonds}. The tensile stress is constant with σ = 500 Pa. The rebinding rate factor γ is set as: $\gamma = 1$. E = 10 kPa.

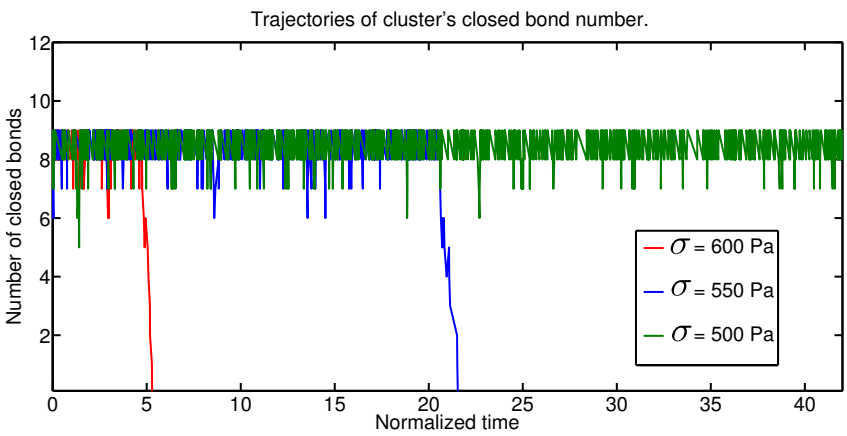

Figure 4.6: Simulation trajectories of a molecular bond cluster with N_{bonds}=9 closed bonds obtained for different applied tensile stresses. The rebinding rate factor γ is set as: $\gamma = 1$. E = 10 kPa.

These results only give a partial view of the process since the relevant information here would be the average of lifetimes for a large number of simulations. Nevertheless, such trajectories illustrate the random-like behavior of binding and unbinding.
In Fig. 4.5, we can see that reducing the tensile stress σ tends to stabilize the cluster and leads to a longer lifetime. We plot in Fig. 4.7 the average lifetime, obtained by averaging over 500 trajectories, as a function of the applied tensile stress σ. We observe that the lifetime of a cluster of given size increases as we decrease the applied tensile stress σ. It reaches asymptotically infinity below a critical value. Following the work by Qian et al. [2009] this critical value σ_c of the stress, for which the lifetime of the cluster approaches infinity, will be called the strength of the cluster. Here, we consider that the lifetime approaches infinity when the normalized average lifetime $\tau_\infty = k^0_{off} t_\infty$ is larger than 100, meaning that the lifetime of the cluster is 100 times longer that the average lifetime of an unstressed individual bond ($t_{individual}(F = 0) = 1/k^0_{off}$). The strength depends on the way we define τ_∞, but the curve for the lifetime has a very large slope near the critical stress. Then, a change in the definition of τ_∞ will have a little effect on the value of the strength of the cluster. As an indication of the consistency of the model with previous works, we reproduce in Fig. 4.8, the results presented by Qian et al. [2008], where there exists a window of enhanced stability at intermediate cluster sizes.

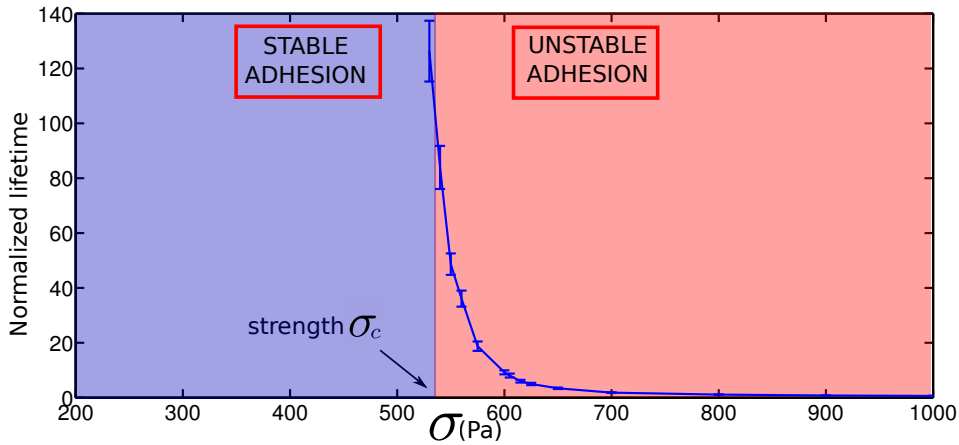

Figure 4.7: Average lifetime of a cluster of $N_{bonds} = 9$ closed bonds as a function of the applied tensile stress σ. The strength is defined as the critical value σ_c of the force for which the average lifetime of the cluster approaches infinity. $E = 10$ kPa. Lifetime and error bars are obtained from 500 trajectories.

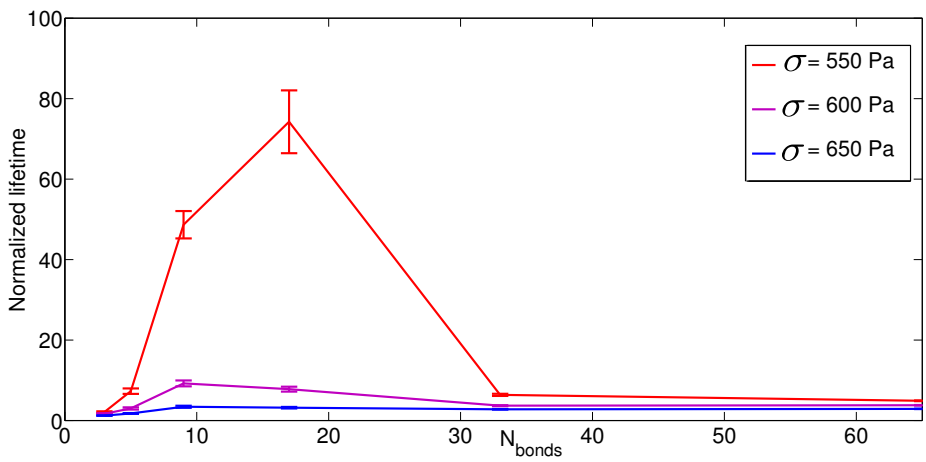

Figure 4.8: Normalized lifetime of clusters as a function of N_{bonds} for different tensile stresses σ. $E = 10$ kPa. Lifetime and error bars are obtained from 500 trajectories.

Bond clusters under applied hydraulic pressure ΔP

Justified by previous works [Casares et al., 2015], we adapt this framework to study the effect of an overpressure inside the crack. The system considered is given in Fig. 4.1, with with $T_c = 0$ N·m^1 and $\sigma = 0$ Pa. The mechanics of the problem is obtained through the minimization of the energy $E_{tot} = E_E + E_P$. As shown in various works, membrane fluctuations are thought to play an important role in cell adhesion. Pressurization of the crack would reduce drastically membrane fluctuations and would ensure that, for the considered problem, only the interplay between mechanics and reaction would drive the evolution of the system. With the proper boundary conditions for the periodicity and the bonds, minimizing the energy E_{tot} allows us to compute the force F_i felt by closed bond i and the separation distance δ_j for open bond j. This way we can compute the corresponding rates of dissociation and formation for each closed or open bonds in the cluster.

We see in Fig. 4.9, that the effect of an over-pressure and that of a tensile stress on the cell-cell separation and force felt by the bonds are very similar: a high over-pressure tends to separate the surfaces and increases the force felt by the bonds, making them more fragile. This observation is confirmed by further calculations. Thus the behavior of molecular bonds subject to tensile stress or over-pressure will show similar features.

4.3 Influence of surface tension

In order to study the influence of the surface tension on the stability of adhesion clusters, we update the model in section 4.2 by adding a surface tension contribution T_c to the interface bounding the bottom part of the elastic medium. The effect of this tension is opposed to an increase of size of the bottom surface, see Fig. 4.1. In the present 2D setting, T_c is a line tension, which could represent membrane or cortical tension. The mechanics of the problem is then obtained through the minimization of the energy $E_{tot} = E_E + E_T + E_L$. The line tension term introduces non-linearity in the model. With the proper

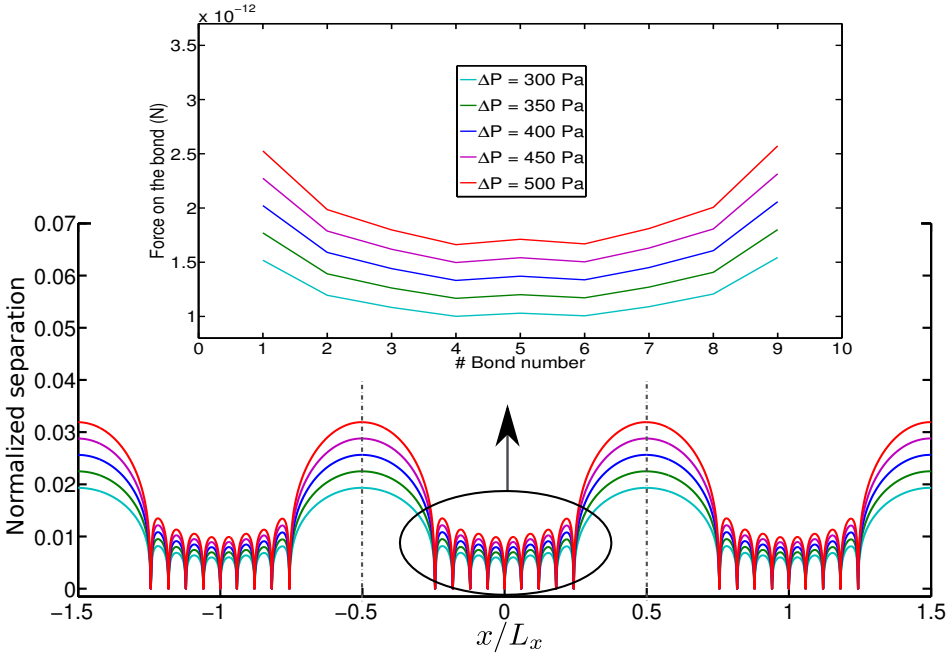

Figure 4.9: Force $F_y(N)$ on the bond and normalized separation y/L_x for different values of the overpressure ΔP (Pa). $N_{bonds} = 9$. $E = 10$ kPa. Force and displacement are linear with ΔP.

boundary conditions for the periodicity and the bonds, minimizing the energy E_{tot} allows us to compute the force felt by closed bonds and the separation distance for an open bond to compute the corresponding rates of dissociation and formation for each closed or open bonds in the cluster. The numerical stochastic algorithm is kept the same.

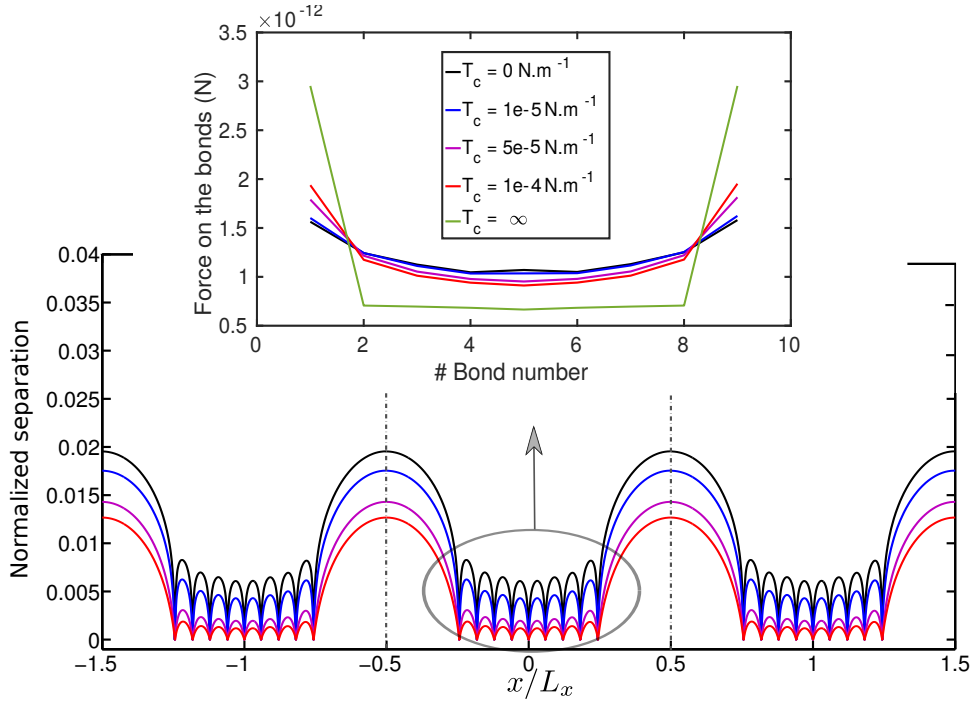

Figure 4.10: Force F_y(N) on the bond and normalized separation y/L_x for different values of the cortical tension T_c. Applied tensile stress σ = 600 Pa. E = 10 kPa.

Influence on the mechanics

Fig. 4.10 examines the influence of the surface tension T_c on the surface separation distance and on the force applied to the bonds: increasing the tension will tend to close the crack, making rebinding easier for broken bonds, and change the distribution of forces in the patch, increasing the force felt by the bonds at the edges of the crack, making them more fragile. Thus cortical tension is another way to control bond clusters dynamics, which we examine more closely in the following. The effect of the surface tension seems stronger on the normalized separation than on the overall force distribution.

We can see in the figure that T_c modulates the force distribution from a elasticity dominated system (black curve) to a surface tension dominated system (green curve). We consider values for T_c in an intermediate regime where tension and elasticity compete and play a significant role.

Influence on lifetime of the cluster

A shown in Fig. 4.11, from the point of view of the intrinsic strength of the cluster of a given size N_{bonds}, increasing the cortical tension T_c increases the strength of the cluster. This dependence of the strength σ_c on the cortical tension T_c could provide to the system a way to switch from stability to instability and thus allow the system to strengthen or to adapt and remodel. An illustration of this idea is given in Fig. 4.11: for a given stress $\sigma^0 > \sigma_c^0$ the cluster is unstable when $T_c = 0$. Increasing the surface tension to $T_c = 10^{-5}$ N·m^1 will displace the strength from σ_c^0 to σ_c^1 and we have $\sigma^0 < \sigma_c^1$ for which the cluster is stable.

Fig. 4.12 examines the effect of T_c on the lifetime of bond clusters of different size for a high applied stress, for which the cluster is very fragile. This figure shows the very strong effect of T_c on the lifetime: doubling T_c from $6 \cdot 10^{-5}$ to $12 \cdot 10^{-5}$ N·m^1 increases the maximum lifetime by an order of magnitude. The closing of the cracks due to surface tension combined with the strong dependence of the rebinding rate with normalized separation δ (as $\sim \exp(-(\delta/a)^2)$, with a a constant, see Eq. (3.10)) has a stronger effect on stability than the modification of the force distribution related to the breaking rate (as $\sim \exp(F/F_b)$, with F_b a constant, see Eq. (3.3)). Actually, this latter effect weakens the bonds at the crack tip. Thus, stability arises mainly from the change in shape due to an increase in surface tension.

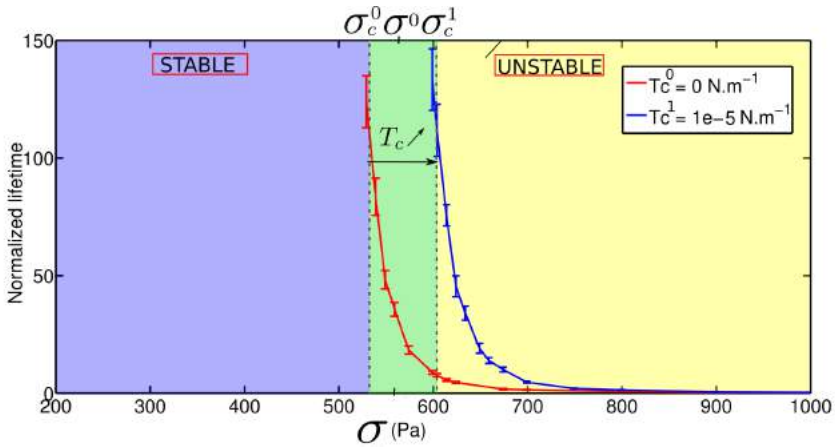

Figure 4.11: Average lifetime of a cluster of $N_{bonds} = 9$ closed bonds as a function of the applied stress for $T_c = T_c^0 = 0$ and $T_c = T_c^1 \neq 0$. The strength is defined as the critical value of the stress σ for which the average lifetime of the cluster approaches infinity and is given for both values of T_c as σ_c^0 and σ_c^1. The blue zone corresponds to stability for clusters under T_c^0 and T_c^1 and the yellow zone corresponds to instability for both tensions. In the green zone, clusters are unstable under T_c^0 and stable under T_c^1. We have $\sigma_c^0 < \sigma^0 < \sigma_c^1$. $E = 10$ kPa. Lifetime and error bars are obtained from 500 trajectories.

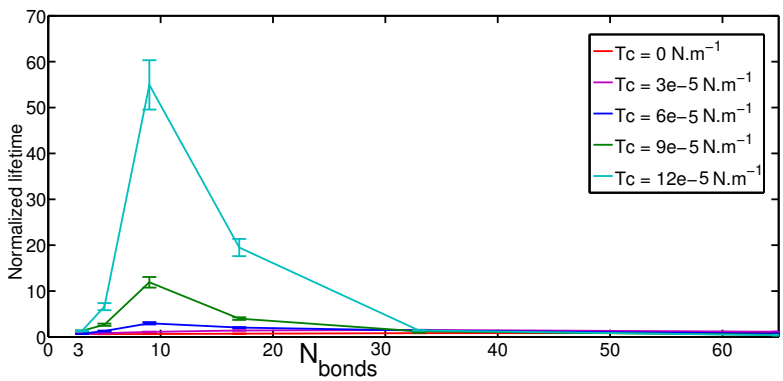

Figure 4.12: Average lifetime of clusters as a function of N_{bonds} for different tension Tc. $\sigma = 1000$ Pa and $E = 10$ kPa. Lifetime and error bars are obtained from 500 trajectories.

Chapter 5

Capillary-stochastic modeling

We now propose a simpler model at the limit of vanishing elasticity using Laplace law to model the mechanics of the cell surface.

5.1 Model

The previous models suggest that the mechanical effect on an array of bond clusters of an over-pressure and of a tensile stress on the mechanics of the adhesion cluster are equivalent. The models presented above considered the mechanics of the medium on which the molecular bond cluster is embedded as elastic with a surface tension. As stated in the introduction, this modeling choice is pertinent for some systems such as vesicles filled with a gel.
This model, however, is not relevant in other situations. For instance, in adhered lipid vesicles under hydraulic stress, the force on the bonds is determined by the membrane mechanics without the presence of an elastic medium. For animal cells with a well-defined actin cortex, bonds can be assumed to be attached to a thin and tense interface, made of the membrane and the underlying cortex, and therefore, membrane mechanics would determine forces and separations between opposite open bonds. In either of these

situations, membrane mechanics can be modeled using capillarity, according to which the surface tension and the inner pressure are related through the Laplace's law. In the capillary limit, the bending rigidity κ of the membrane is neglected. This approximation is correct at scales larger than $\ell_{\kappa T} = \sqrt{\kappa/T_c}$. Here that requires this $\ell_{\kappa T} < b$, with $b = 32$ nm, the minimum spacing between bonds, and $\ell_{\kappa T} \ll L_x$, with L_x, the size of the system. For tense membranes, $T_c = 10^{-3}$ N·m^1 and $\kappa = 10^{-20}$ N·m we have $\ell_{\kappa T} = 3$ nm $< b \ll L_x$. We can conclude that, for such parameters, the capillary hypothesis is justified, and the mechanics of the membrane can be computed using Laplace's law. Thus, in order to provide a framework to study the behavior of molecular bond clusters on tense membranes under hydraulic stress, we will derive a simpler capillary model for which the mechanics are ruled by surface tension and pressure through the Laplace law. The model considered here is based on the same set-up detailed in previous sections with molecular bond clusters adopting the same structure and following the exact same kinetics. An illustration of the model is given in Fig. 5.1

5.2 Parameterization of the problem

Between two fixed bonds, the shape of the curve is given by Laplace's law: it is an arc of circle with a radius of curvature R given by

$$R = \frac{T_c}{P}. \tag{5.1}$$

Thus we can consider the whole membrane as a combination of the arcs formed between each closed bonds. To reconstruct the full shape and force distribution, it is necessary, using a proper parameterization, to compute the length of each arc, the area below the arcs and the force acting on each bonds. The parameterization of the arc is given in Fig. 5.2. Simple geometric considerations give the length L of the membrane, the area A below the arc and the vertical F_y and lateral forces F_x on the bonds as stated on the same figure. The overall mechanics can thus be obtained by considering the shape

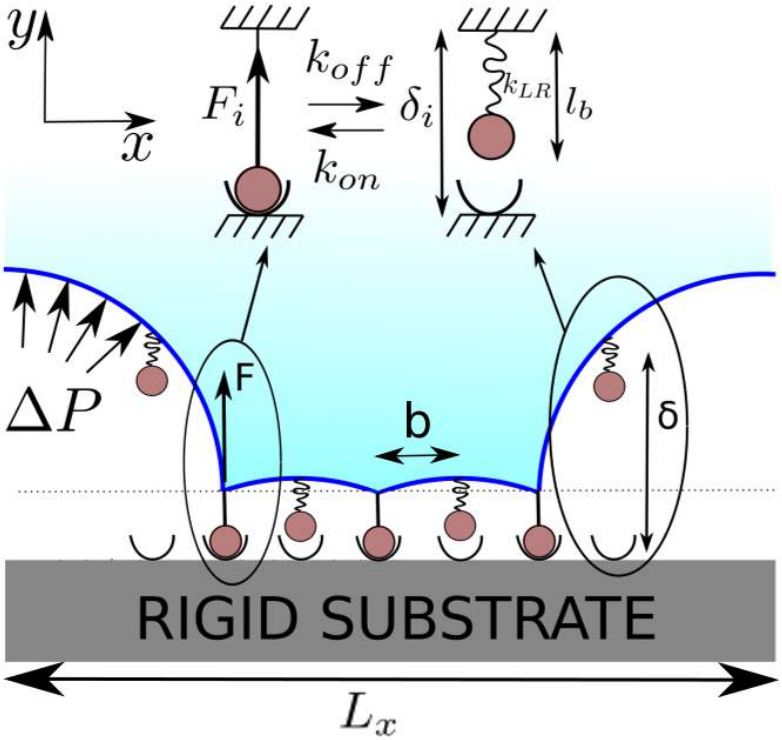

Figure 5.1: Scheme of the model. The structure of the cluster is kept the same that the one detailed on fig 4.1. The blue line is a purely capillary membrane. The bonds follow the exact same reaction than in previous sections.

of the vesicle as a combination of arcs. To obtain the forces on the closed bonds we sum the contribution of the two adjacent arcs. This way we obtain, at low computational cost, all the data necessary to perform the algorithm described in section 4.1. Thus, we obtain a very cheap and efficient procedure to compute the shape and the force distribution on the bonds, which greatly reduces the computational cost as compared to the previous method using Finite elements or the method using Green functions provided by Qian et al. [2008].

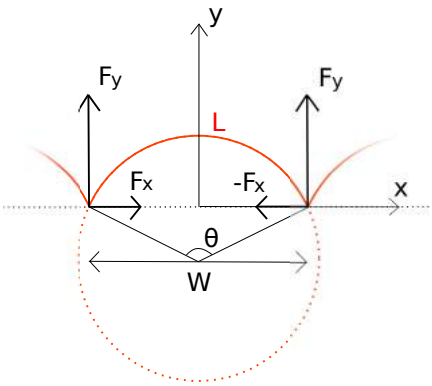

$$\frac{W}{2R} = sin\,\frac{\theta}{2} \implies \theta = 2\arcsin\frac{W}{2R} \tag{1}$$

$$L = R\theta \tag{2}$$

$$A = \frac{R^2}{2}(\theta - \sin\theta) \tag{3}$$

$$F_y = T_c\, sin\,\frac{\theta}{2} \tag{4}$$

$$F_x = T_c\, cos\,\frac{\theta}{2} \tag{5}$$

Figure 5.2: Parameterization of the problem. The red line represents the shape of the membrane between two bonds separated by a spacing W. R is the radius of curvature given by Laplace law. The lateral and vertical projection of the resultant forces on the bonds due to the tension T_c are F_x and F_y

5.3 Results

Mechanics

Looking at the influence of the overpressure ΔP and the cortical tension T_c the force distribution over the system and the profile of separation between the rigid substrate and the membrane, we can make the following observations summarized in Fig. 5.3.

First, we recover important features of the previous models. The force transmitted to the bonds is mostly borne by the bonds on the edge of the crack, while the distribution of forces inside the patch is uniform and much lower. Secondly, we see that increasing the overpressure ΔP tends to increase the height of the cracks and the overall forces transmitted to the bonds (see Fig. 5.3(b)) while an increase of the cortical tension T_c would leave the distribution unchanged (see Fig. 5.3(a)). Finally, we recover another important feature of the previous models: increasing the cortical tension tends to reduce the opening gap of cracks.

Thus, with this minimalistic and very efficient capillary-stochastic model, we recover the main features driving the unbinding of the clusters: non uniformity of transmitted forces and a competition between the closing and opening of the cracks.

Energy release rate

In analogy with fracture mechanics, another way to characterize the system as a material is to look at the energy release during crack propagation, the thermodynamic driving force of the system.
In order to do so, we will consider the following system: starting from a state where all bond are closed, we will break the bonds one by one until full separation to simulate the propagation of the crack. For each state we will compute the total energy of the system. Thus, we will be able to compute the rate of change of energy in the system during the propagation of the crack.
In Fig. 5.4, we plot the energy release rate for different values of the cortical tension. We can see that increasing the cortical tension tends to reduce the total energy release rate of the system. Keeping the analogy with fracture mechanics we can say that the cortical tension has a toughening effect as it reduces the driving force for crack propagation.

Lifetime

To characterize the effect of the cortical tension T_c on the stability of the clusters we adapt the Fig. 4.7, giving the strength of a given cluster, to the capillary-stochastic model. We use a new criterion to define the strength of the cluster: the strength ΔP_c is such as the normalized lifetime $\tau(\Delta P)$ is such as $k^0_{off}\tau(\Delta P_c) = 400$. The results are given in Fig. 5.5. This better assessment of the lifetime and the better statistics in this figure are possible thanks to the high computational efficiency of this model. The capillary-stochastic model reproduces the same behavior with the force that we reported for an applied force: there exist a critical pressure ΔP_c for which an overpressure $\Delta P < \Delta P_c$

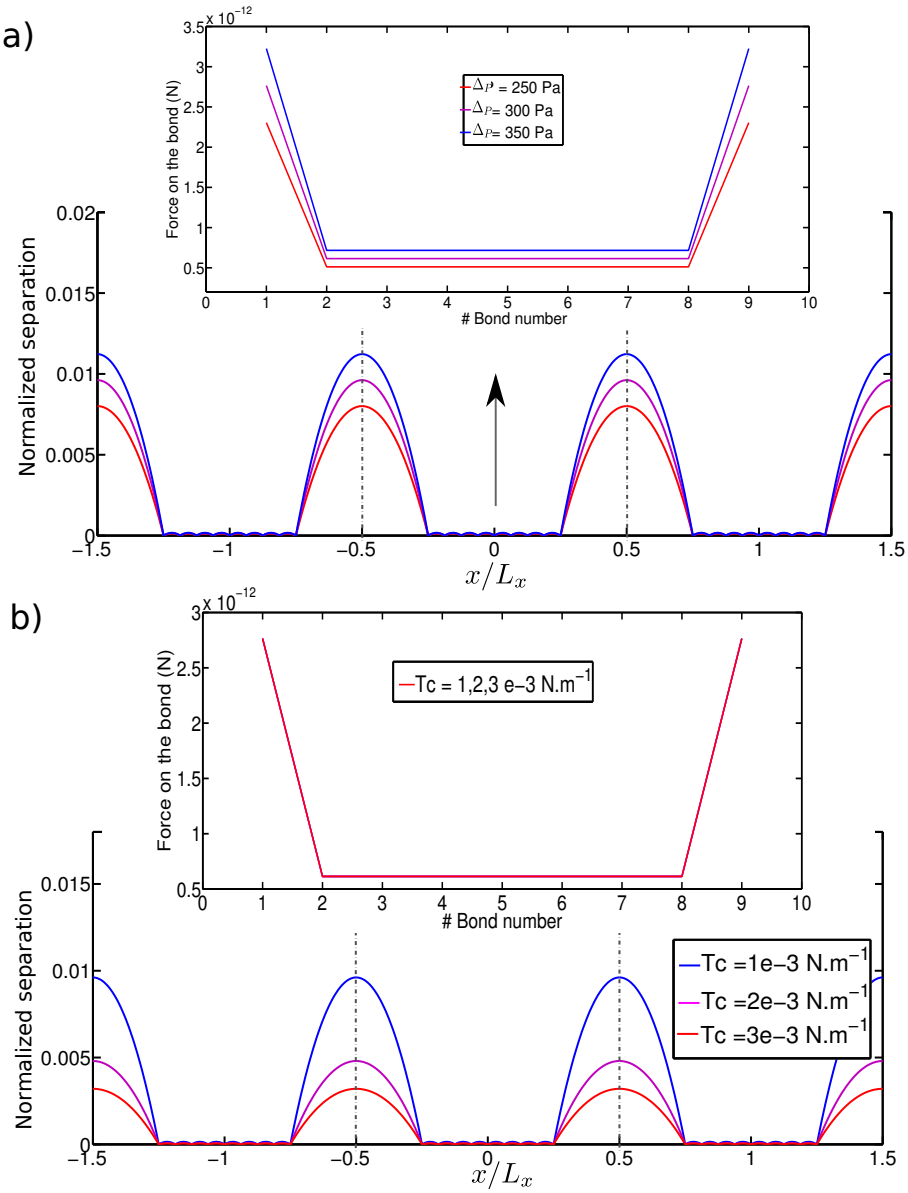

Figure 5.3: a) Force $F_y(N)$ on the bond and normalized separation y/L_x for different values of the overpressure ΔP. $Tc = 10^{-3}$ N·m^1. b) Force $F_y(N)$ on the bond and normalized separation y/L_x for different values of the cortical tension T_c. $\Delta P = 300$ Pa.

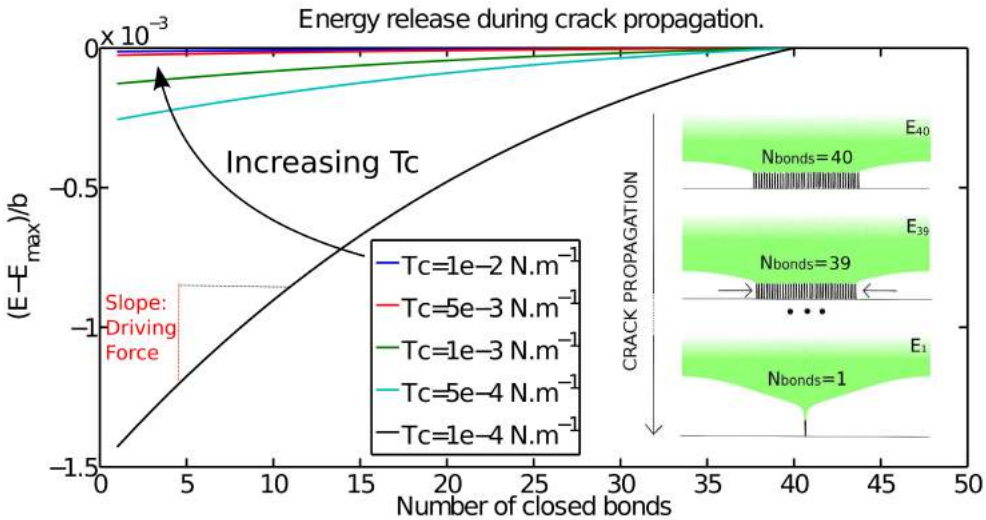

Figure 5.4: Energy release during crack propagation for different values of the cortical tension T_c. An illustration of the crack propagation is given in the right corner of the figure.

will leave the cluster stable and an overpressure $\Delta P > \Delta P_c$ will lead to total decohesion of the cluster. We see that the value of ΔP_c is dependent on the cortical tension T_c: the bigger the cortical tension, the bigger the critical stress. Thus, at a given cluster size and overpressure, increasing the tension will increase the stability. Similarly to the previous chapters in section 4.3, modulating cortical tension could provide a way for the system to switch between stability and instability and thus allow strengthening or remodeling. Concerning the dependence of the lifetime of the cluster on the cluster size, the results are given in Fig. 5.6. If we consider a cortical tension $T_c = 3 \cdot 10^{-3}$ N·m^1, we can see that the capillary-stochastic model captures the dependence we found with the elastic-stochastic model discussed in the previous chapter. There exists a window of cluster size for which clusters are stable under a given force and a small increase in surface tension leads to a large increase in lifetime. A series of kymographs illustrating the difference of behavior of

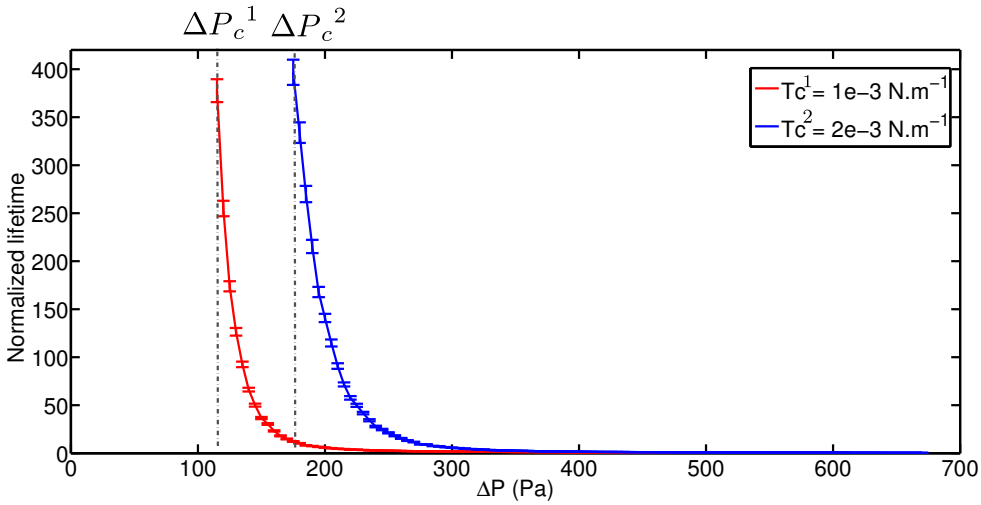

Figure 5.5: Average lifetime of a cluster of $N_{bonds} = 9$ closed bonds as function of overpressure ΔP for $T_c = T_c^1 = 10^{-3}$ N·m^1 and $T_c = T_c^2 = 2 \cdot 10^{-3}$ N·m^1. The strength is defined as the critical value of the overpressure for which the average lifetime of the cluster approaches infinity and is given for both values of T_c as $\Delta P_c{}^1$ and $\Delta P_c{}^2$. ΔP =300 Pa. Lifetime and error bars are obtained from 2000 trajectories

clusters depending on their size are given in Fig. 5.7. They clearly show the dependence of the lifetime on the cluster size and the different features of the failure mode, with a crack propagation mechanism for large clusters. Going back to Fig. 5.6, we observe that increasing the surface tension increases the width of the window: large unstable clusters can become stable by increasing the tension. The strong dependence of the maximum lifetime on tension is illustrated in the inset in Fig. 5.6: the maximum of the lifetime increases rapidly with surface tension. This strong dependence is expected since the rebinding rate strongly depends on the normalized separation, see Eq. (3.10) and the comments given on section 4.3.

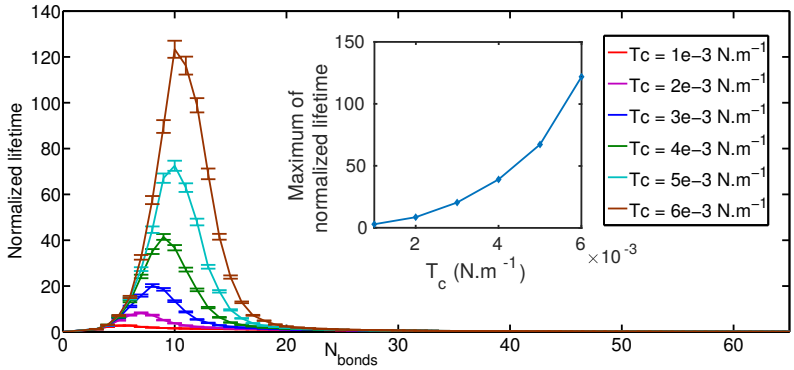

Figure 5.6: Average lifetime of clusters as a function of N_{bonds} for different tension Tc. ΔP = 300 Pa. Lifetime and error bars are obtained from 2000 trajectories. (inset): Maximum of the normalized lifetime as a function of the surface tension.

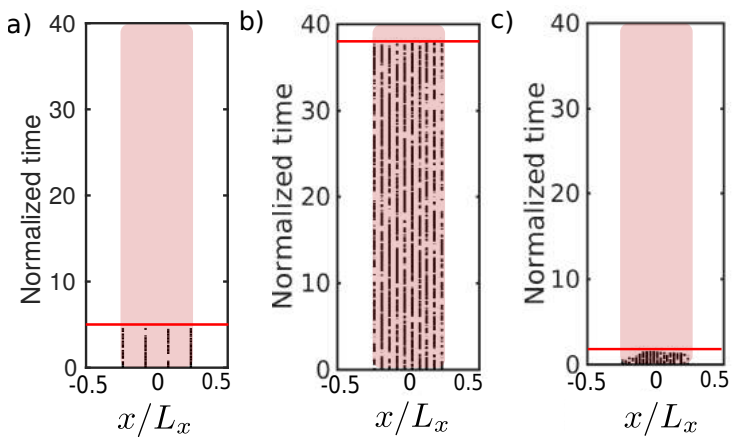

Figure 5.7: Kymographs describing trajectories of closed bonds for different cluster size N_{bonds}. The black lines represent closed bonds. The pink line domain represents the extension of the initial patch of closed bonds. The red line represents the instant at which the cluster fails. ΔP = 300 Pa and $T_c = 3 \cdot 10^{-3}$ N·m^{-1}. a) N_{bonds} = 4. b) N_{bonds} = 10. c) N_{bonds} = 20.

5.4 Mobile molecular bonds

Up to now, we have considered fixed bonds and fixed binders. We want to consider now the possibility of lateral diffusion of bonds and binders during the separation.
During the time corresponding to a reaction the bonds diffuse according to a normal distribution around their initial position. The extent of their diffusion is parametrized by the constant diffusion D. The bonds are attached to the two membranes so we expect $D_{bonds} = \frac{D_{binders}}{2}$. A sketch of the problem is given in Fig. 5.8.

Modeling diffusion

Every molecule, bound or unbound, is diffusing according to Brownian motion dynamics. In 1D diffusion along x, any adhesion molecule, with a diffusion constant D, at x_0 at $t = 0$ has a probability $p(x, t)$ of being at x after a time t is given by the Fokker-Planck equation in the absence of external forces:

$$\frac{\partial p}{\partial t} = D\frac{\partial^2 p}{\partial x^2} \tag{5.2}$$

A solution of the equation is given by the following probability distribution function $p(x, t)$:

$$p(x,t) = \frac{1}{\sqrt{4\pi D dt}} e^{-\frac{(x-x_0)^2}{4Dt}} = \frac{1}{\sqrt{2\pi\sigma(t)^2}} e^{-\frac{(x-m(t))^2}{2\sigma(t)^2}}, \tag{5.3}$$

with $m(t) = x_0$ the mean of the distribution and $\sigma(t) = \sqrt{2Dt}$ its standard deviation.

In order to model the diffusion of the adhesion molecules on the membrane, we perform a Monte Carlo algorithm simulating Brownian motion. This Monte Carlo scheme will be implemented in the Gillespie algorithm. The

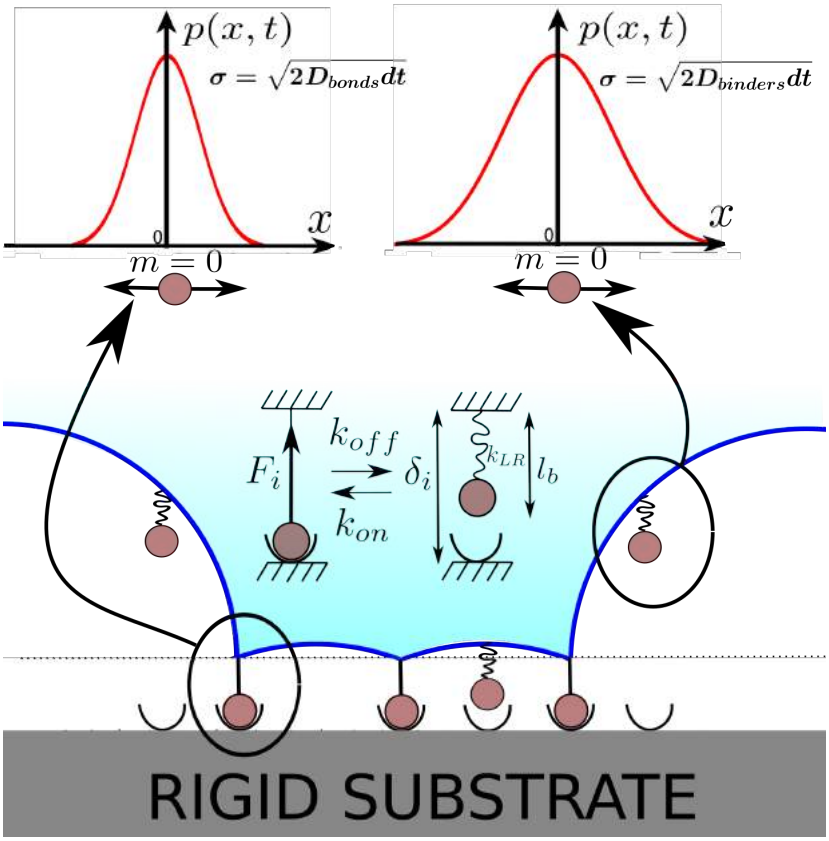

Figure 5.8: Schematic representation of the diffusion of the bonds/binders and the corresponding probability distribution for the movements.

general scheme of the reaction/diffusion algorithm is described in Fig. 5.9.

For each event predicted by the Gillepsie algorithm, a time τ is assigned, corresponding to the duration of the first reaction. The random walk is performed for each molecule, binders and bonds, during this time τ, as following:

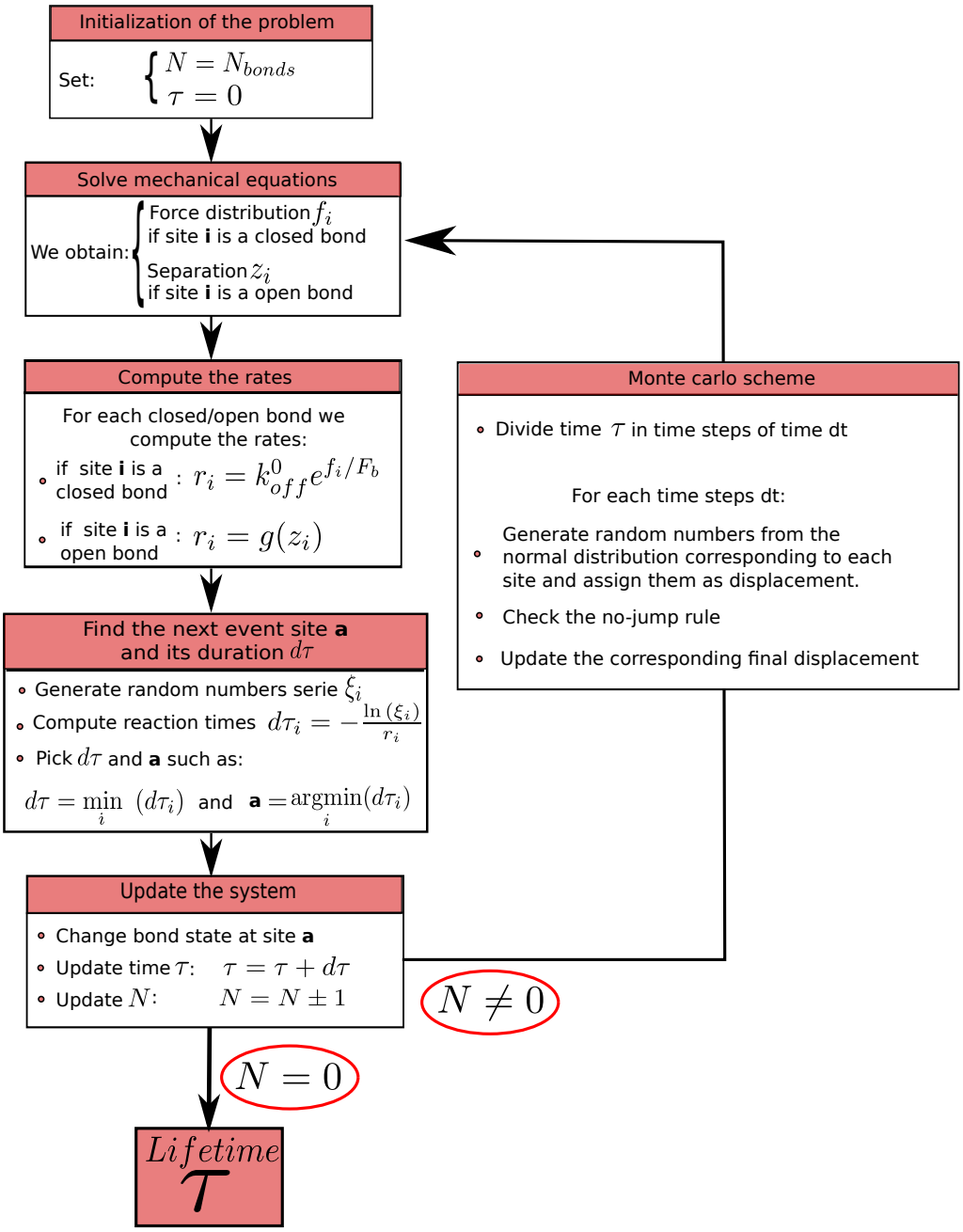

Figure 5.9: General scheme of the reaction/diffusion algorithm.

- Given this time τ, the duration is divided into intervals of duration $dt << \tau$.

- For each time steps dt, we perform a random walk procedure. We assign a random displacement dx_i according to a normal distribution of mean m and standard deviation σ such as $m = 0$ and $\sigma = \sqrt{2D_i dt}$, with $D_i = D_{bonds}$ for bonds and $D_i = D_{binders}$ for binders. The bonds move on a lattice with a spacing of $\bar{b} = b/10$.

- The movement of the adhesion molecules obeys some rules: the molecule assigned to τ is fixed during the procedure and the others cannot jump over each other or get too close to each other (steric crowding).

- When all the movements are assigned for each dt, we update all the positions of the bonds in the Gillespie algorithm and determine the next time τ. The whole procedure ends when all the bonds are open.

Influence on the lifetime

We now look at the influence of the mobility of the bonds on the dependence of the lifetime of the cluster with the size of the cluster. The results are given in Fig. 5.10. We observe that increasing the diffusivity D_{bonds} of the molecules on the membrane increases the size of the window of stability: the faster the diffusion, the bigger is the range of cluster size that are stable under the applied overpressure. Moreover the lifetime of large cracks is also increased by the the mobility of the bonds. This can be interpreted as follows: if the kinetics are unchanged, bonds with faster diffusion can more easily move into the crack faces and close them, reducing the forces exerted on the edges and thus

increasing the overall lifetime of larges clusters. The fragility of large clusters is determined by the crack-like force concentration at the crack's tip. Indeed considering a time $\tau = 1/k^0_{off} = 1$ s corresponding to the average lifetime of an unloaded bond, the standard deviation $\sigma(t) = \sqrt{2Dt}$ is such as $\sigma(\tau) \sim N_{tot} b$ for the values of D_{bonds} considered in this section: for this kind of set-up, a crack can easily be closed during the average time of binding/unbinding thanks to the diffusion of the binders. This observation is illustrated in Fig. 5.11, where trajectories are presented as kymographs. We see that for fixed bonds, the cluster evolves towards decohesion by increasing the two existing cracks. When the bonds are mobile, the bonds and binders are able to cross the cracks and close them, thus increasing the overall lifetime of the clusters. Increasing mobility enhances this effect: for faster diffusion (see Fig. 5.11c), after a small duration, the initial cracks have disappeared and the patch of bonds have spread and the effect of the overpressure is shared over the whole periodic box. In the Appendix A, we discuss the influence of the bias on the mobility of the bonds due to the lateral forces exerted by the membrane on the bonds, which may limit the spreading of bonds over the whole periodic box.

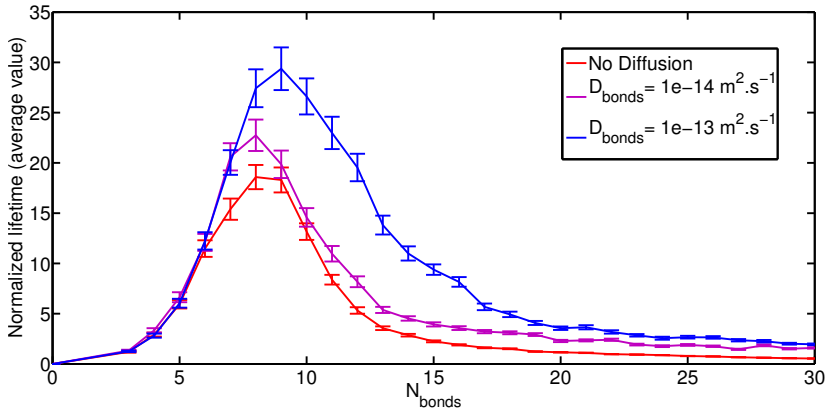

Figure 5.10: Average lifetime of clusters as a function of N_{bonds} for different diffusion constant D_{bonds}. ΔP = 300 Pa and $T_c = 3 \cdot 10^{-3}$ N.m^{-1}. The case of immobile bonds (red curve) is given as a comparison. Lifetime and error bars are obtained from 2000 trajectories.

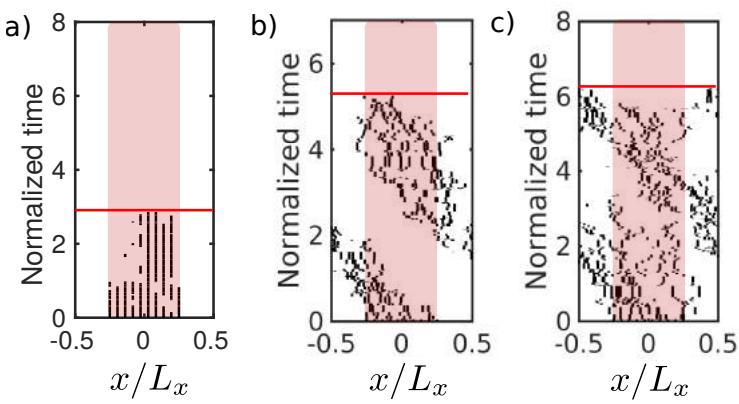

Figure 5.11: Kymographs describing trajectories of clusters for different diffusion constant D_{bonds}. The black lines represent closed bonds. The pink domain represents the extension of the initial patch of closed bonds. The red line represents the instant at which the cluster fails. N_{bonds}=10, ΔP = 300 Pa and $T_c = 3 \cdot 10^{-3}$ N·m^{-1}. a) D_{bonds} = 0 m^2·s^{-1}. b) D_{bonds} = 10^{-14} m^2·s^{-1}. c) D_{bonds} = $5 \cdot 10^{-14}$ m^2·s^{-1}.

Chapter 6

Conclusion to Part I

We have examined the effect of geometrical and mechanical architecture on the stability of molecular bond clusters embedded on an elastic medium at fixed average density. We have first developed an elasto-stochastic model using finite elements to solve the mechanics of the elastic medium and the Gillespie algorithm to solve the stochastic master equation ruling the evolution of the number of bond, reproducing previous results on similar system [Qian et al., 2008]: for a given applied tensile stress and elasticity of the elastic medium, there exists a window of cluster sizes for which the bond clusters is stable. At a given cluster size, there exists a critical stress σ_c which defines the stability of the clusters. This critical stress is called the strength of the cluster.

Using the same model, we have studied the effect of an overpressure between the two surface and found similar results for the stability of the cluster, either pulling the medium apart with a tensile stress or pressurizing the interstitial space.

We have examined the effect of a surface tension T_c on the mechanics of the problem. We found that increasing T_c modulates the overall force distribution on the closed bonds, concentrates the force at the crack tip, thus increasing fragility of the bonds at the tip, and closes the space inside the crack, thus

favoring rebinding. We identified the closing of the crack as the major factor for the strong increase in lifetime. As a consequence, the lifetime of the cluster strongly increases with surface tension. Moreover, for a given cluster size, we found that the strength depends on the surface tension. Given the very strong sensitivity of lifetime on surface tension, this mechanism could provide a way for adhesion to switch between instability and stability by modulating surface tension.

We have proposed a simplified and very efficient capillary-stochastic model, in which the the mechanics are dominated by surface tension. In such a system, the shape is given simply by Laplace's law, which greatly simplifies the computation. This model was able to reproduce the same features detailed previously. Using this framework we studied the influence of surface tension on energy release during crack propagation. In analogy with fracture mechanics, we found that the surface tension has a toughening effect as it reduces the driving force for crack propagation. Modifying the Gillespie algorithm, we extended our model to mobile bonds and binders. We found that mobility of bonds and binders increases the stability of clusters of all sizes as it allows bonds and binders to close cracks and thus reduces the force borne by bonds at the crack tip.

Part II

Part II: Continuum modeling of the dynamics of soft adhesion mediated by mobile binders

Chapter 7

Introduction to Part II

Soft adhesion mediated by mobile binders is a multi-scale problem coupling adhesion mechanics at a macro-scale and reaction kinetics at a micro-scale. Part I of the thesis has focused on stochastic minimalistic models examining how bond cluster architecture and mechanical environment affect the stability of adhesion patches. This modeling approach provides insight about micro and mesoscopic phenomena, but it is very difficult to access sufficiently large length scales and larger time scales to model non-equilibrium phenomena such as unbinding occurring at a vesicle/ cell scale.

In this Part II of the thesis, we propose another approach to the problem based on continuum modeling. We consider adhesion between two vesicles mediated by reacting adhesion molecules that can bind or unbind according to reaction rates coupled with the mechanics. We focus on the unbinding of the vesicles due to a force applied on the vesicle with a loading device, e.g. a micropipette. A sketch of the problem is given in Fig. 7.1. This is a prototypical dissipative problem in soft matter physics mixing elasticity and capillarity of the fluid membrane with diffusion of mobile and reacting chemical species, and all these ingredients being tightly coupled and relevant to biology. The equilibrium of this problem has been extensively studied [Bell et al., 1984a]

and classical results are given in Fig. 7.1. Essentially, in equilibrium, the concentration of free binders in the entire vesicle and that of bonds in the adhesion patch are uniform and need to obey the balance of molecular number, a chemical equilibrium condition, and force balance at the contact point between mechanical tension on the membrane and the osmotic tension of the bonds, which are confined to the adhesion patch whose boundary can be viewed as a semi-permeable boundary that free binders but not bonds can cross. Force balance at the contact point couples the chemical and mechanical aspect of the problem. This problem is notoriously subtle , and dynamics have only been barely explored [Brochard-Wyart and de Gennes, 2002b, de Gennes et al., 2003]. In principle, different behaviors can be proposed for extreme regimes, as it is summarized in Fig. 7.1. For the regime dominated by unbinding kinetics of bonds, we expect a tear-out decohesion [Berk and Evans, 1991, Casares et al., 2015]. On the opposite, a regime where diffusion dominates will lead to an increase in the concentration of bonds in a shrinking adhesion patch [Tozeren et al., 1989].

To formulate a consistent model coupling all these different physics we will need a systematic approach. Based on the Onsager's variational principle, we will detail a general framework allowing us to generate the governing equation of the problem we want to study by making energetic considerations on the free energy and the dissipation of the problem.

Chapter 8 gives an overview of Onsager's principle using simple examples oriented towards our problem. Chapter 9 develops the application of this principle to study the chemo-mechanical problem of soft adhesion mediated by mobile binders for cases of unbinding or growth and maturation. General hypotheses will be discussed and the last chapters will detail the consequences on the dynamics when theses hypotheses do not hold. Towards this objective, Chapter 10 discusses the influence of the compliance of the bonds on the dynamics while Chapter 11 discusses the modeling of slip bonds and the influence of the nature of the bonds on the dynamics. Finally, Chapter 12 considers molecular crowding on the membrane.

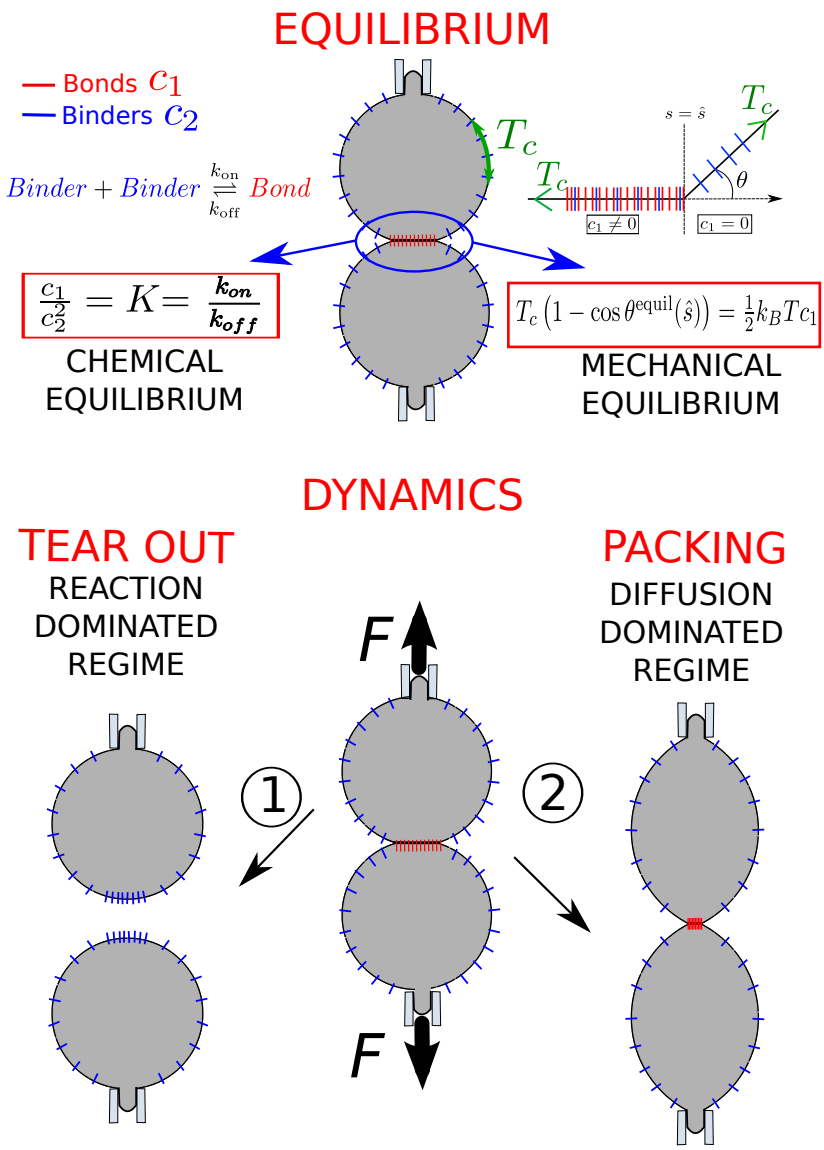

Figure 7.1: Symmetric vesicle doublet whose tension is controlled by a micropipette, which can also apply a force on the adhesion patch. (top) Summary of the classical equilibrium picture, where the concentration of bonds in the patch and of the free binders in the entire vesicle need to satisfy chemical and mechanical equilibrium conditions. (bottom) Alternative out-of-equilibrium scenarios of the unbinding of the doublet under an applied force.

Chapter 8

Onsager's variational principle

8.1 Introduction

Our main objective is to introduce an emerging variational modeling framework for the dissipative dynamics of soft-matter and biological systems, which provides a systematic and transparent approach to generate complex models coupling multiple physics. This approach used under different names in different contexts and recently formalized [Doi, 2011, Peletier, 2013] states that the dynamics result from the interplay between energetic driving forces and dissipative drag forces, each of them deriving from potentials that are the sum of individual contributions for each physical mechanism. Models coupling different physics can be assembled by just adding more terms to the energy and dissipation potentials, and encoding in them the interactions between the different physical mechanisms. In this way, this framework provides a flexible and thermodynamically consistent method to generate complex models. Unlike Onsager's relations, this approach is not limited by linearity and is able to deal with mechanical and chemical nonlinearity, arising for instance from molecular crowding.

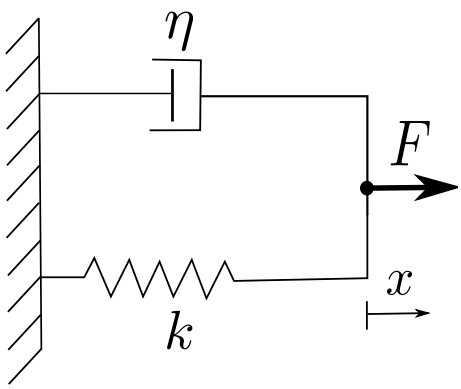

Figure 8.1: Sketch of the elementary model. A spring with stiffness k is in parallel with a dashpot with a drag coefficient μ and a force F is applied. The system is characterized by its displacement x from its equilibrium position.

The goal of the Chapter is to convey Onsager's variational principle through examples. More specifically, the emphasis is made on simple models exhibiting coupling between diffusion, reaction and mechanics. We will conclude with a general statement of the variational principle that will provide the framework for the modeling of vesicle unbinding in subsequent chapters. For a more extensive introduction to Onsager's variational principle in soft matter physics, see [Doi, 2012, Arroyo et al., 2018]. The interested reader may also find recent applications of the variational principle to lipid membranes elsewhere [Arroyo and DeSimone, 2009, Rahimi and Arroyo, 2012, Fournier, 2015].

8.2 Elementary examples

Competition between energy release and dissipation

The first example is a very simple model to illustrate that the dynamics of dissipative dynamics arises from a competition between energy release and dissipation. Let us consider a spring with stiffness k coupled with a dashpot with a drag coefficient η under the action of a force F. The sketch of the model is given in Fig. 8.1. This very simple system will allow us to understand some

of the most essential ideas underlying the Onsager's variational principle.
In the present system, the variable characterizing the state of the system is the elongation x of the spring and this elongation generates a conservative force $F_{cons} = -kx$. But because of the dashpot in parallel, the system also experiences a viscous force $F_{visc} = -\eta v = -\eta \dot{x}$.
If the drag is considered large enough, the inertia of the system can be neglected and we can write the following balance of forces:

$$F_{cons} + F_{visc} + F = 0, \tag{8.1}$$

leading to the differential equation governing the system:

$$\eta \dot{x} + kx = F. \tag{8.2}$$

But let us look at this equation from another perspective: both F_{cons} and F derive from a potential (elastic energy stored in the spring and the potential energy of the external force F). We can express this potential $\mathcal{F}$, which can be seen as the free energy of the system, as follows:

$$F_{cons} + F = -\frac{\partial \mathcal{F}}{\partial x} \text{ with } \mathcal{F}(x) = \frac{kx^2}{2} - Fx. \tag{8.3}$$

In the same way, the viscous force F_{visc} can be expressed as deriving from a potential. This potential $\mathcal{D}$, which depends on v, is often referred to as the dissipation potential and it obeys:

$$F_{visc} = -\frac{\partial \mathcal{D}}{\partial x} \text{ with } \mathcal{D}(x) = \frac{\eta v^2}{2}. \tag{8.4}$$

We can express the rate of change of the free energy $\mathcal{F}$ as follows:

$$\frac{d\mathcal{F}}{dt} = (kx - F)v = (kx - F)\dot{x}. \tag{8.5}$$

The rate of change $\frac{d\mathcal{F}}{dt}$ is a function of x and v. Let us now define the so-called Rayleighian as:

$$\mathcal{R}(x, v) = \dot{\mathcal{F}}(x, v) + \mathcal{D}(v) = (kx - F)v + \frac{\eta v^2}{2}. \tag{8.6}$$

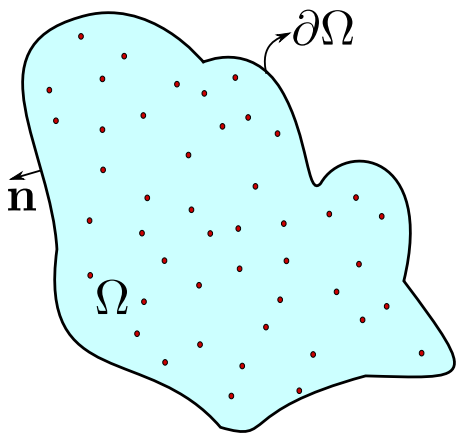

Figure 8.2: Elementary model for diffusion. The bulk domain Ω represent a quiescent fluid and $\partial\Omega$ its impermeable container. The dilute specie is labeled with red dots.

It is now obvious that the governing equation of the system derives from the minimization of the Rayleighian $\frac{\partial \mathcal{R}}{\partial v} = 0$. Noting that since $\eta > 0$, the Rayleighian is convex in v and thus, the governing equation follows from the variational principle

$$v = \underset{w}{\operatorname{argmin}}\, \mathcal{R}(x, w). \tag{8.7}$$

In contrast with the classical principle of minimum potential energy the minimization is here performed over the rate of change of the system v. This variational principle establishes a competition between dissipation and energy release. The examples below show that this principle is broadly applicable to systems in which dissipation dominates over inertia and for which the dissipation forces derive from a potential $\mathcal{D}$.

Diffusion of particles in a bulk

In order to apply this principle to our problem of interest, we consider now a classical problem, the diffusion of solute particles in a quiescent fluid. For

this, let us consider Ω, a region of space occupied by a quiescent fluid with a dilute distribution of non-interacting solute molecules and delimited by an impermeable container. The state of the system is defined by the continuous field on Ω , $c(\mathbf{x}, t)$, the molar concentration of solute molecules at instant t. A sketch of the problem is given in Fig. 8.2. Such a problem is governed by the diffusion equation

$$\frac{\partial c}{\partial t} = D\Delta c, \tag{8.8}$$

and its appropriate boundary conditions. Here D is the diffusion constant and Δ is the Laplacian. Furthermore, the Stokes-Einstein equation provides a microscopic expression for the diffusion coefficient as

$$D = \frac{k_B T}{f}, \tag{8.9}$$

where k_B is the Boltzmann constant, T is the absolute temperature and f is the hydrodynamic drag coefficient, that is the proportionality coefficient between the drag force experienced by a solute molecule and the speed at which it is moving relative to the fluid.

Let us now apply the Onsager's variational principle to this problem.

In such a system the main driving force is the minimization of the entropic free energy (or the maximization of the mixing entropy, that is to say the tendency for the dilute molecules to homogenize their concentrations). For a dilute solution, the free energy can be expressed as:

$$\mathcal{F}[c] = RT \int_\Omega c(\log c - 1) dV + \int_\Omega c\mu_0 dV, \tag{8.10}$$

where μ_0 is the standard chemical potential and R the universal gas constant. Noting that the boundary is impermeable, the rate of change of the free energy at an instant t is given by the Reynolds transport formula

$$\frac{d}{dt}\mathcal{F}[c(,t)] = \int_\Omega (\mu_0 + RT \log c)\frac{\partial c}{\partial t} dV = \int_\Omega \mu(c)\frac{\partial c}{\partial t} dV, \tag{8.11}$$

with

$$\mu(c) = \frac{\delta \mathcal{F}}{\delta c} = \mu_0 + RT \log c, \tag{8.12}$$

the chemical potential at concentration c. This quantity measures the free energy cost of adding one mole of solute molecules per unit of volume at a given concentration c. Thus gradients in μ will drive the migration of molecules to reduce the free energy.

Now, let us consider the dissipation in the system. If a solute molecule is moving at a velocity $\mathbf{w}$ compared to the quiescent fluid, it experiences a drag force $\mathbf{F} = -f\mathbf{w}$ with f the previously defined hydrodynamic drag coefficient. The corresponding dissipation potential is $\frac{f|\mathbf{w}|^2}{2}$. So, if we keep assuming the solution to be diluted, that is to say that the presence of other molecules does not affect the solute molecules, we can write the total dissipation potential $\mathcal{D}$ as the sum of the dissipation potentials of the $N_a c$ solute molecules in the system, with N_a the Avogadro's constant:

$$\mathcal{D}[\mathbf{w}] = \int_\Omega \frac{N_a f}{2} c|\mathbf{w}|^2 dV. \tag{8.13}$$

The field $\mathbf{w}$ is called process variable. We can note that, for this system, in contrast to the previous example of the spring and dashpot, the rate of change of the energy does not depend only $\partial_t c$ but rather on the field $\mathbf{w}$. Thus, the Rayleighian $\mathcal{R}(x, v) = \dot{\mathcal{F}}(x, v) + \mathcal{D}(v)$ depends on two different ways to characterize changes in the state of the system: $\partial_t c$ and $\mathbf{w}$. What variable should we minimize $\mathcal{R}$ with respect to? To overcome this issue, we invoke the continuity equation of local conservation of mass,

$$\partial_t c + \nabla \cdot (c\mathbf{w}) = 0, \tag{8.14}$$

which following [Peletier, 2013], we call process operator. Plugging this equation in Eq. (8.11), and performing a integration by parts, we can express the rate of change of the free energy as:

$$\frac{d}{dt}(\mathcal{F}[c(,t)]) = -\int_\Omega \mu(c)\nabla \cdot (c\mathbf{w}) dV \tag{8.15}$$

$$= -\int_{\partial\Omega} \mu(c) c\mathbf{w} \cdot \mathbf{n} dS + \int_\Omega c\nabla\mu(c) \cdot \mathbf{w} dV. \tag{8.16}$$

Since we assume the container to be impermeable, we have $\mathbf{w} \cdot \mathbf{n} = 0$ over $\partial\Omega$. Thus the Rayleighian of the system can be expressed as follows:

$$\mathcal{R}[c, \mathbf{w}] = \int_\Omega c\nabla\mu(c).\mathbf{w}dV + \int_\Omega \frac{N_a f}{2} c|\mathbf{w}|^2 dV. \tag{8.17}$$

Minimizing this functional with respect to the field $\mathbf{w}$ we obtain the following condition:

$$\int_\Omega RT\nabla c.\delta\mathbf{w}dV + fN_a \int_\Omega c\mathbf{w}.\delta\mathbf{w}dV = 0, \tag{8.18}$$

which should hold for any admissible variation $\delta\mathbf{w}$. Thus we can express the molar diffusive flux of solute molecules as:

$$\mathbf{j}_D = c\mathbf{w} = -\frac{RT}{fN_a}\nabla c = -\frac{k_B T}{f}\nabla c, \tag{8.19}$$

which is the Fick's law of diffusion. Plugging this equation in Eq. (8.14), we recover the diffusion equation:

$$\frac{\partial c}{\partial t} = \frac{k_B T}{f}\Delta c \text{ in } \Omega. \tag{8.20}$$

Thus, the Onsager's variational principle is able to derive the diffusion equation, and the Stokes-Einstein equation, from physically motivated considerations on the free energy and the dissipation in the system.

Diffusion-reaction problem: chemical reaction as an energetic-dissipative process

In order to apply the Onsager's variational principle to our coupled problem we provide a last example describing a problem coupling diffusion of reacting species in a quiescent fluid delimited by a container impermeable to both species. See [Mielke, 2011, 2012] for more general energetic-dissipative formulation of chemical reactions satisfying the law of mass action. Let us denote Ω the region of space delimiting the fluid, X_1 and X_2 the two species, with

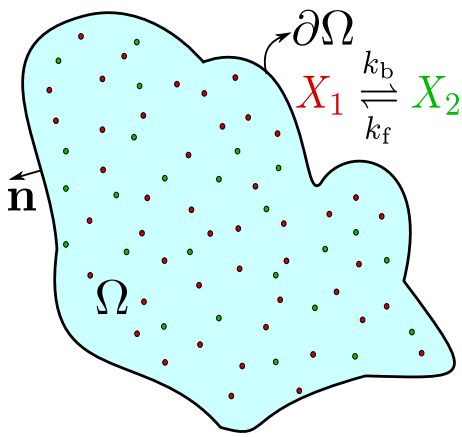

Figure 8.3: Elementary model for diffusion-reaction. The bulk domain Ω represents a quiescent fluid and $\partial\Omega$, its impermeable container. The two dilute species X_1 and X_2 are labeled with red and green dots and they react through the reaction $X_1 \underset{k_b}{\overset{k_f}{\rightleftharpoons}} X_2$.

c_1 and c_2 the corresponding molar concentrations, transforming through the following simple reaction:

$$X_1 \underset{k_b}{\overset{k_f}{\rightleftharpoons}} X_2. \tag{8.21}$$

A sketch of the model is given in Fig.8.3. We assume that the reaction follows the law of mass action, that is to say that the net forward rate is

$$r = k_f c_1 - k_b c_2. \tag{8.22}$$

Then the dynamics can be modeled through the linear set of reaction-diffusion equation in Ω:

$$\partial t c_1 = D_1 \Delta c_1 - r = D_1 \Delta c_1 - k_f c_1 + k_b c_2, \tag{8.23}$$

$$\partial t c_2 = D_2 \Delta c_2 + r = D_2 \Delta c_2 + k_f c_1 - k_b c_2, \tag{8.24}$$

with the corresponding initial and boundary conditions. D_1 and D_2 and the diffusion constants of the two reacting species. At the equilibrium, we have

$r = 0$ and thus ${c_2}^{eq}/{c_1}^{eq} = k_\mathrm{f}/k_\mathrm{b} = K$, where K is the so-called equilibrium constant of the reaction (8.21). The state of the system is defined by $Z = (c_1, c_2)$. Let us now see how we can derive the same equations using considerations on the free energy and the dissipation in the system using the Onsager's variational principle. For a dilute solution, the free energy is expressed as

$$\mathcal{F}(Z) = RT \int_\Omega c_1(\log c_1 - 1)dV + \int_\Omega c_1 \mu_{0,1}, dV \tag{8.25}$$

$$+ RT \int_\Omega c_2(\log c_2 - 1)dV + \int_\Omega c_2 \mu_{0,2}, dV, \tag{8.26}$$

where $\mu_{0,1}$ and $\mu_{0,2}$ are the standard chemical potentials of both species.
As a reaction-diffusion problem, the concentration can evolve due to the diffusive velocities $\mathbf{w}_1$ and $\mathbf{w}_1$ of both species but also due to the chemical reaction which is quantified by the net forward rate r. So the new set of process variables is now $W = \{\mathbf{w}_1, \mathbf{w}_2, r\}$. Accounting for chemical reactions, the process operator is then given by the equations

$$\begin{aligned} \partial_t c_1 + \nabla \cdot (c_1 \boldsymbol{w}_1) + r &= 0, \\ \partial_t c_2 + \nabla \cdot (c_2 \boldsymbol{w}_2) - r &= 0, \end{aligned} \tag{8.27}$$

encoding balance of mass for the dissolved species. The conditions $0 = \boldsymbol{w}_i \cdot \boldsymbol{n}$ in $\partial\Omega$, reflecting the fact that $\partial\Omega$ is impermeable, can also be viewed as part of the process operator. Following the same procedure than in the previous section and using the process operators, we can write the rate of change of the free energy as

$$\dot{\mathcal{F}}(Z; W) = -\int_\Omega \mu_1 \nabla \cdot (c_1 \mathbf{w}_1) dV - \int_\Omega \mu_2 \nabla \cdot (c_2 \mathbf{w}_1) dV \tag{8.28}$$

$$+ \int_\Omega (\mu_2 - \mu_1) r dV, \tag{8.29}$$

with the chemical potentials defined as:

$$\mu_i(c_i) = \mu_{0,i} + RT \log c_i \text{ for } i = 1, 2. \tag{8.30}$$

Integrating by parts and using the impermeability of $\partial\Omega$, we obtain

$$\dot{\mathcal{F}}(Z;W) = RT\int_\Omega \nabla c_1 \cdot \mathbf{w}_1 dV + RT\int_\Omega \nabla c_2 \cdot \mathbf{w}_2 dV \tag{8.31}$$

$$+ \int_\Omega (\mu_2 - \mu_1) r dV. \tag{8.32}$$

Let us have a look now at equilibrium, that is to say the state that minimizes the free energy. The stationarity conditions with respect to $\mathbf{w}_1$ and $\mathbf{w}_2$ give that the concentrations are uniform over Ω and the condition with respect to r implies that $\mu_1 = \mu_2$ and $K = {c_2}^{eq}/{c_1}^{eq} = k_\mathrm{f}/k_\mathrm{b} = \exp\frac{-\Delta\mu_0}{RT}$ with $\Delta\mu_0 = \mu_{0,2} - \mu_{0,1}$. Thus K is a purely thermodynamic quantity.

Let us now go back to the dynamics. How does the system dissipate energy? We can argue physically that energy is dissipated through the drag of molecules during diffusion and through reactions, when the system is brought to a potential saddle point along the reaction coordinate and then inelastically relaxes to a neighboring metastable state. Thanks to Mielke [2011] we can to write a dissipation potential for the reaction as a quadratic function in r (all the dissipation potentials considered until now are so) :

$$\mathcal{D}_{reaction}(Z;r) = \int_\Omega \frac{1}{\bar{k}} r^2 dV \tag{8.33}$$

with $\bar{k} > 0$ unspecified for the moment. Thus the total dissipation potential $\mathcal{D}$ is :

$$\mathcal{D}(Z;W) = \int_\Omega \frac{N_a f_1}{2} c_1 |\mathbf{w}_1|^2 dV \int_\Omega \frac{N_a f_2}{2} c_1 |\mathbf{w}_1|^2 dV + \int_\Omega \frac{1}{\bar{k}} r^2 dV, \tag{8.34}$$

where f_i are the molecular drag coefficients of the two species. Forming the Rayleighian $\mathcal{R} = \dot{\mathcal{F}} + \mathcal{D}$ and minimizing it with respect to $\mathbf{w}_i$, we recover Fick's law for each species:

$$c_i \mathbf{w}_i = \frac{k_B T}{f_i} \nabla c_i \text{ in } \Omega, \tag{8.35}$$

and the minimization with respect to r leads to:

$$r = \bar{k}(\mu_1 - \mu_2). \tag{8.36}$$

Comparing Eq. (8.36) and Eq. (8.22), let us consider the following choice for $\bar{k}$:

$$\bar{k}(c_1, c_2) = k\frac{c_1 - e^{\Delta\mu_0/RT}c_2}{\mu_1 - \mu_2} \tag{8.37}$$

$$= \frac{ke^{-\mu_{0,1}/RT}}{RT}\frac{e^{\mu_1/RT} - e^{\mu_2/RT}}{\mu_1/RT - \mu_2/RT}, \tag{8.38}$$

where $k > 0$ is independent of the concentrations. From Eq. (8.37) we can see that $\bar{k} > 0$ for any choice of concentrations due to the convexity of the exponential function. Plugging the first equation in Eq. (8.36), we obtain the classic expression of the net forward rate:

$$r = \underbrace{k}_{k_f} c_1 - \underbrace{ke^{\Delta\mu_0/(RT)}}_{k_b} c_2, \tag{8.39}$$

and we note that we also recover Arrhenius law. Finally plugging Eq. (8.35) in the process equations 8.27 and using the last equation we recover the system of coupled reaction-diffusion equations 8.23 and 8.24 using the Onsager's variational principle. This derivation has shown that both reaction and diffusion are driven by the same chemical energy, which decreases during the dynamics. This free energy contains an entropic contribution, but also an enthalpic one given by the difference of reference chemical potentials between the reacting species $\Delta\mu_0$. Furthermore, we have understood that the forward and backward rates contain not only kinetic information but also thermodynamic information in the sense that their ratio depends on $\Delta\mu_0$. Onsager's principle has allowed us to untangle the kinetic and thermodynamic components of the reaction's dynamics.

Thus, this example further exemplifies two benefits of Onsager's principle: (1) it provides a systematic method to derive models for dissipative systems from a library of building blocks, and (2) it highlights the energetic-dissipative structure of such systems, providing physical insight into the model parameters.

8.3 General statement

Consistent with the previous examples and observations, we can write Onsager's variational principle in an abstract form [Peletier, 2013, Arroyo et al., 2018], which we will use later for the derivation of the equations of our model for vesicle unbinding but can also be used for other problems exhibiting analogous chemo-mechanical couplings. The procedure goes as follows:

ONSAGER'S VARIATIONAL PRINCIPLE

For a non-inertial dissipative chemo-mechanical system, given:

1. A set of state variables Z describing the system,
2. A set of process variables W describing how the system changes and the related process operator $\mathcal{P}$ such as $\dot{Z} = \mathcal{P}(Z)W$,
3. A free energy functional $\mathcal{F}(Z)$,
4. A dissipation potential $\mathcal{D}(Z;W)$,
5. An externally supplied power $P(Z;W)$.

The governing equations are obtained by minimizing the so-called Raleighian $\mathcal{R}(Z;W)$ with respect to the process variables W:

$$\boxed{W = \underset{V}{\operatorname{argmin}}\, \mathcal{R}(Z;V) = \underset{V}{\operatorname{argmin}}\, D\mathcal{F}(Z).\mathcal{P}(Z)V + \mathcal{D}(Z;V) + P(Z;V)} \tag{8.40}$$

If the process variables satisfy the constraint expressed as

$$\mathcal{C}(Z)V = 0, \tag{8.41}$$

the constrained dynamics can be equivalently characterized as stationary saddle points of the Lagrangian

$$\mathcal{L}(Z; W, \Lambda) = \mathcal{R}(Z; W) + \Lambda \cdot \mathcal{C}(Z), \tag{8.42}$$

where Λ are the Lagrange multipliers. Minimizing the Lagrangian to obtain W and using the process operators $\mathcal{P}$, we obtain the governing equations. The dissipative dynamics of such a system exhibits an interesting characteristic. To illustrate this property, let us examine stationarity of a homogeneous system such that the power supply is $P(Z; W) = 0$.
The stationarity condition $\delta_W \mathcal{L} = 0$ leads to $\mathcal{C}(Z)W = 0$.
The stationarity condition $\delta_Z \mathcal{L} = 0$ gives the following equation

$$D_Z\mathcal{F}(Z).\mathcal{P}(Z) + D_W\mathcal{D}(Z; W) + \Lambda.\mathcal{C}(Z) = 0 \tag{8.43}$$

Multiplying the last equation by W, and making the assumption $\mathcal{D}(\mathcal{Z}; W)$ quadratic in W, like all the dissipation potentials detailed in this chapter, we obtain:

$$\begin{aligned} D_Z\mathcal{F}(Z).\mathcal{P}(Z)W &= \dot{\mathcal{F}} \\ &= -D_W\mathcal{D}(Z; W)W - 0 \\ &= -2\mathcal{D}(Z; W) \leq 0 \end{aligned} \tag{8.44}$$

This shows that Onsager's principle complies with the second law of thermodynamics by construction and that $\mathcal{F}$ is a Lyapunov function of the dynamics, as long as $\mathcal{D}$ is chosen quadratic in W. In fact, to show this result we only need $\mathcal{D}$ to be convex, see [Arroyo et al., 2018].

Chapter 9

Theoretical model for soft adhesion mediated by mobile binders

9.1 Set-up of the problem and hypotheses

Physically and from a continuum perspective, the system can be understood as a membrane with bending rigidity κ, subject to a fixed tension T_c by a loading device such as a micropipette, with mobile adhesion molecules. A sketch of the model is given in Fig. 9.1. These molecules can attach with partners in a neighboring vesicle (we consider for simplicity a symmetric system, both along the horizontal and vertical axes. These molecules are compliant and can stretch due to external forces. Their stiffness is k_0. The binding kinetics strongly depends on the distance to potential partners in the neighboring membrane. The unbinding kinetics depends on the force experienced by the binders, see Chapter 3. The bound and unbound molecules are treated as concentrations and we assume that the binder and the bonds do

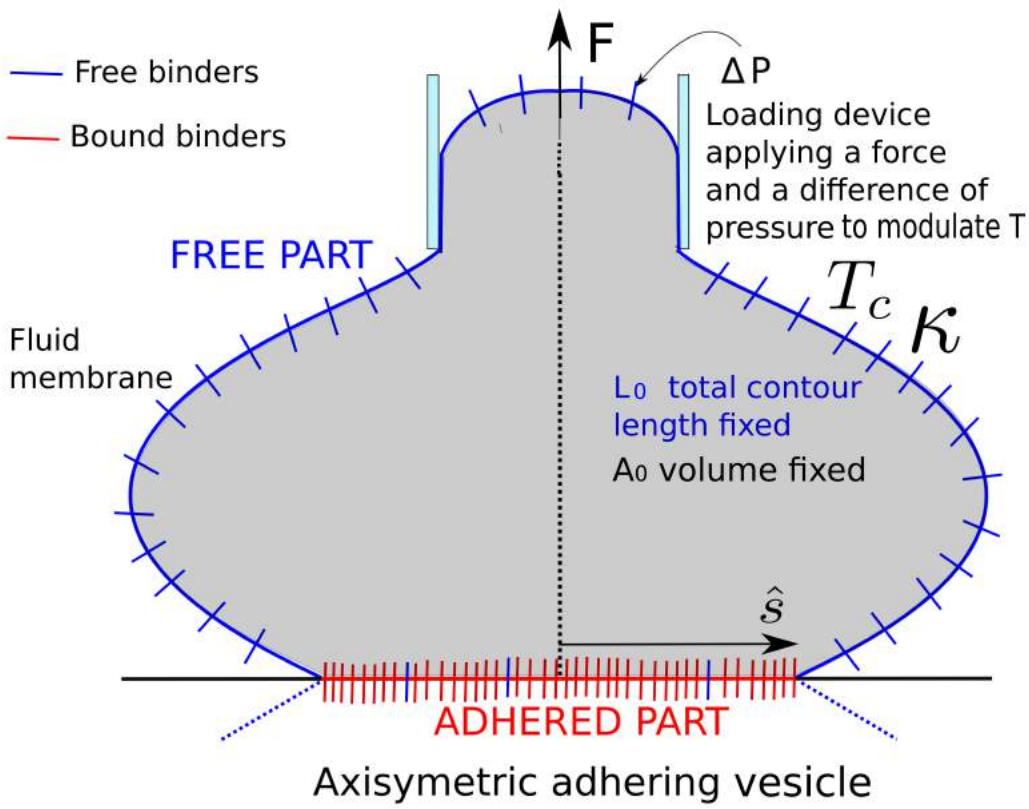

Figure 9.1: Sketch of the problem.

not have self-interaction, attractive or repulsive. Naturally, this leads to a phase-separation into a region where adjacent membranes are in close proximity and the concentration of bound binders is high, and another region with a very low or vanishing concentration of bound binders and potentially a large distance to the neighboring vesicle. To treat these two phases, a sharp interface bounding the adhesion patch has been often considered, with bound molecules only on one side of this interface, the adhesion patch [Brochard-Wyart and de Gennes, 2002a, 2003].

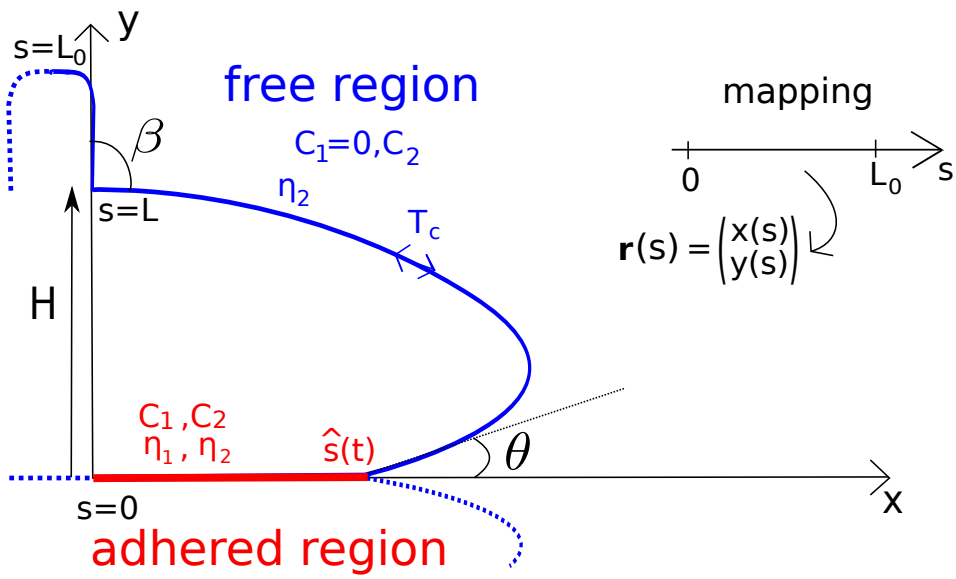

Figure 9.2: Simplified sketch of the problem. The position on the vesicle is mapped by the arc-length s with $s \in [0, L_0]$. Binders and bonds are treated as concentrations as respectively $c_1(s)$ and $c_2(s)$. The system is divided in two domains: the adhered domain $[0, \hat{s}]$ where $c_1 \neq 0$ and $c_2 \neq 0$ and a free domain where $c_1 = 0$ and $c_2 \neq 0$.

Here, we adopt a classical description of the adhesion patch, according to which its boundary is sharply defined. No bonds can exist outside of the adhered region. We do assume capillarity for the vesicle, whose shape is given by the prescribed tension T_c and an enclosed volume constraint. To focus on the chemo-mechanical coupling and simplify all other aspects of the model, we consider a 2D model, see Fig. 9.2, where a curve represents a vesicle partially adhering to another symmetric curve. This model is easily extended to axisymmetry by appropriately introducing geometrical factors. The conceptual extension to 3D is straightforward, although the numerical implementation becomes more complex. The 2D curve representing the vesicle is parameterized by arc-length, s. The interface between the bound and the

unbound parts of the curve is labeled by $s = \hat{s}(t)$.
Along this inextensible curve of total length L_0, two fields, $c_1(s)$ and $c_2(s)$, describe the *number concentration* of bound and free binders. Obviously, $c_1(s) = 0$ for $s > \hat{s}$. For the moment, we neglect the force sensitivity of the bonds and in a first step, the concentrations of bonds and binders are also considered small enough to be in the dilute limit. Thus, if c_{max} is the maximum concentrations of adhesion molecules allowed on the membrane because of steric constraints, we have $(c_1 + c_2)/c_{max} \ll 1$ in $[0, \hat{s}]$ and $c_2/c_{max} \ll 1$ in $[\hat{s}, L_0]$. We revisit these hypotheses in Chapter 11 and Chapter 12.
We consider an idealized loading device that can remove or release membrane length to control tension so that the actual length of the adhered and free parts of the vesicle is $L \leq L_0$. As a first approximation, we assume that unbound binders can freely enter this device, thus the whole domain accessible to the free binders is $[0, L_0]$. The loading device can also apply a vertical force to drive binding or unbinding of the vesicles. We assume that this device does not affect the volume (area) enclosed by the vesicle (curve), which is constrained. This constraint imposes a pressure difference between the inside and the outside of the vesicle.

If the vesicle is large enough, or tension is large enough, bending elasticity can be neglected to determine the vesicle configuration and the mechanical force acting at the boundary of the adhesion patch (the triple point $s = \hat{s}$ in Fig. 9.2). Indeed, the competition between tension T_c and bending stiffness κ gives a length-scale $\ell_1 = \sqrt{\kappa/T_c}$, which defines the typical radius of curvature near the rim of adhesion patch and near the loading device. If ℓ_1 is much smaller than the system size, then one can model the vesicle as a purely capillary system, thus allowing kinks in the vesicle shape and a well-defined macroscopic contact angle θ at $s = \hat{s}$ and at the contact point between the micropipette and the vesicle t $s = L_0$, see Fig. 9.2.
The same statement can be made considering the competition between the elasticity of bonds and the tension, which is characterized by the length-scale $\ell_2 = \sqrt{\frac{T_c}{k_0 c_0}}$, where c_0 is a typical bond concentration. Thus, if $\ell_2 \ll L_0$, we can neglect the effect of the stretching of the bonds on the mechanics in the patch.

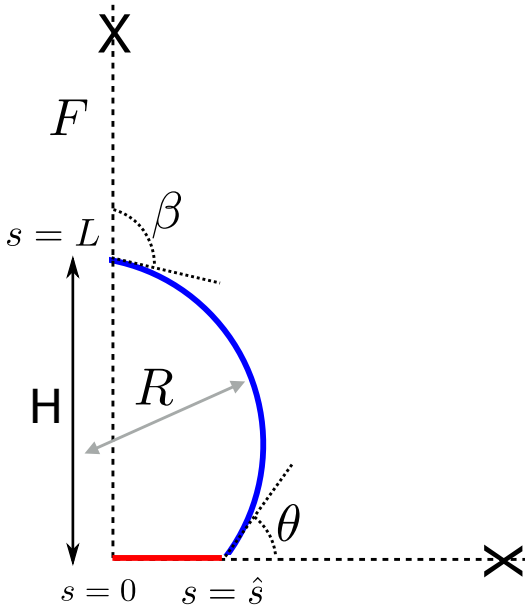

Figure 9.3: Sketch for the parameterization of the mechanics of the vesicle. As a pure capillary system, three parameters are sufficient to characterize the mechanics of the vesicle: the position of the interface $\hat{s}$ and the two contact angles θ and β.

For reasonable values of the parameters $c_0 = 2.5 \cdot 10^3$ molecules/μm^2, $\kappa = 10^{-19}$ N·m, $T_c = 10^{-4}$ N·m^{-1}, $k_0 = 2.5 \cdot 10^{-4}$ N·m^{-1} and $L_0 = 30$ μm we have $\ell_1 = 32$ nm $\ll L_0$ and $\ell_2 = 13$ nm $\ll L_0$. The two length scales are comparable and the previous approximations are then justified and will be considered and discussed in the following chapter. Since tension in the free part is constant, the resulting shape of the free part of the curve is an arc of a circle. In fact, because the concentration field $c_2(s)$ is not necessarily uniform in the free part of the membrane, there will be a non-uniform osmotic component of tension, that will lead to a non-circular shape in general. However, we expect this osmotic tension to be much smaller than T_c and therefore decouple vesicle shape from the concentration of unbound binders.

Considering the parameterization depicted in Fig. 9.3, elementary geometric considerations allow us to express, in terms of these variables, the radius of the arc of circle R, the area enclosed by the curve A, the length of the curve L and the distance between the adhesion patch and the loading device H in terms of $\hat{s}$ and the two contact angles θ and β.

$$R(\theta,\beta,\hat{s}) = \hat{s}/\left(\sin\theta + \cos\beta\right), \tag{9.1}$$

$$A(\theta,\beta,\hat{s}) = R^2\left(3\pi/2 - \theta - \beta + \sin\theta\cos\theta + \sin\beta\cos\beta + 2\cos\theta\cos\beta\right), \tag{9.2}$$

$$L(\theta,\beta,\hat{s}) = 2R\left(3\pi/2 - \theta - \beta + \sin\theta + \cos\beta\right), \tag{9.3}$$

$$H(\theta,\beta,\hat{s}) = R\left(\cos\theta + \sin\beta\right). \tag{9.4}$$

9.2 Goal and plan

In Part II of the thesis, we develop a chemo-mechanical model based on Onsager's principle, describing the dynamics of the shape of the vesicle (given here by the two contact angles, θ and β and the position of the adhesion interface $\hat{s}$) and of the concentration of bound and unbound binders that evolve due to diffusion and reaction in the bound region. The focus is made on the coupling between the mechanics, the reaction kinetics and the diffusion by discussing the different hypotheses detailed above and the consequences on the dynamics when these hypothesis are lifted. Chapter 9 discusses the case of rigid ideal bonds while Chapter 10 and Chapter 11 discuss the effect of compliant bonds and of slip bonds. In Chapter 12, we lift the assumption of a dilute limit, by introducing molecular crowding to consider cases in which $c_1 + c_2 \sim c_{max}$.

9.3 Model ingredients

States variables

Let us start by identifying the state variables of the system. At any given instant, the mechanical state of the system can be parameterized by the three

scalars θ, β and $\hat{s}$, see Fig. 9.3. The chemical state is parameterized by the number concentration of bound and free binders c_1 and c_2. Thus the system can be described by the set of state variables Z:

$$Z = \left(\theta, \beta, \hat{s}, c_1, c_2\right). \tag{9.5}$$

Free energy

In order to apply the variational principle, it is necessary to detail the free energy of the system and compute the variation of the free energy. Considering a capillary free energy contribution, the potential energy for the force applied by the loading device and an ideal gas entropy, in the dilute limit, for the bound and unbound non-interacting binders, the chemo-mechanical free energy is

$$\begin{aligned}\mathcal{F}(Z) = T_c \cdot L(\theta, \beta, \hat{s}) - F \cdot H(\theta, \beta, \hat{s}) \\ + \frac{k_B T}{2} \int_0^{\hat{s}} c_1 \left(\log \frac{c_1}{c_0} - 1\right) ds + \frac{1}{2} \int_0^{\hat{s}} \mu_1^0 c_1 \, ds \\ + k_B T \int_0^{\hat{s}} c_2 \left(\log \frac{c_2}{c_0} - 1\right) ds + \int_0^{\hat{s}} \mu_2^0 c_2 \, ds \\ + k_B T \int_{\hat{s}}^{L_0} c_2 \left(\log \frac{c_2}{c_0} - 1\right) ds + \int_{\hat{s}}^{L_0} \mu_2^0 c_2 \, ds,\end{aligned} \tag{9.6}$$

where μ_i^0 is the so-called standard chemical potential of either bound ($i = 1$) or unbound ($i = 2$) binders and c_0 is an arbitrary reference concentration.
We note that μ_2^0 could, in principle, be different at the adhesion patch or out of it, given the different chemical environment. We will consider that μ_2^0 is equal in both regions. As we are modeling only half of a symmetric system, and the bound binders are shared by the two vesicles, the terms in the second line of this equation are multiplied by a 1/2 factor. The tension T_c and force applied by the loading device F are parameters in the model. Note that the integrals in the last line extend to L_0, the constant total length relevant to diffusion, and not to the smaller and variable length L of the membrane, exterior to the loading device, since we assume that unbound binders can freely enter this device.

To enforce our assumption that the enclosed area (volume) remains constant so that $A = A_0$, we introduce the Lagrangian

$$\mathcal{L}(Z, P) = \mathcal{F}(Z) - P\left[A(\theta, \beta, \hat{s}) - A_0\right], \tag{9.7}$$

where P is the pressure difference enforcing the constraint. Thus, this Lagrangian is a function of the extended set of state variables $\bar{Z}$ as:

$$\bar{Z} = \left(\theta, \beta, \hat{s}, c_1, c_2, P\right). \tag{9.8}$$

Process variables and jump conditions

To investigate, both equilibrium and dynamics, we examine how the state can change in time. We denote by ω, γ, $\hat{v}$, and Q the rates of change of θ, β, $\hat{s}$, and P. To parameterize the changes in concentration, we recall the local form of the balance of mass for each of the chemical species, noting that s is a Lagrangian coordinate:

$$\dot{c}_i + (c_i w_i)' \mp r = 0, \tag{9.9}$$

where $w_i(s, t)$ denotes the diffusive flux of species i, $r(s, t)$ is the net rate of binding within the adhesion patch, the dot denotes partial differentiation with respect to time, and the prime partial differentiation with respect to s. Therefore, we can define the process variables describing the rate of change of the system as

$$\bar{W} = \left(\omega, \gamma, \hat{v}, w_1, w_2, r, Q\right), \tag{9.10}$$

and the process operator relating changes in $\bar{Z}$ to $\bar{W}$ as

$$\dot{\bar{Z}} = \mathcal{P}(\bar{W}) = \left(\omega, \gamma, \hat{v}, -(c_1 w_1)' + r, -(c_2 w_2)' - r, Q\right). \tag{9.11}$$

We note that, because c_1 is only different from zero in the adhesion patch, then r vanishes for $s > \hat{s}$. Furthermore, because of symmetry, $w_i(0) = w_i(L_0) = 0$ for both species.

There are additional process equations which relate w_i at the interface and $\hat{v}$, as a result of mass conservation. The global statement of conservation of bound binder molecules is

$$\frac{d}{dt}\int_0^{\hat{s}} c_1 \, ds = \int_0^{\hat{s}} r \, ds, \tag{9.12}$$

which, using Leibniz rule and the local statement of mass conservation, becomes

$$c_1(\hat{s})\,\hat{v} + \int_0^{\hat{s}} \dot{c}_1 \, ds = c_1(\hat{s})\,\hat{v} + \int_0^{\hat{s}} [-(c_1 w_1)' + r] \, ds = \int_0^{\hat{s}} r \, ds, \tag{9.13}$$

and applying the fundamental theorem of calculus, we obtain

$$\hat{v} = w_1(\hat{s}), \tag{9.14}$$

which states that the flux of bound binders at the interface occurs due to the motion of the interface. Invoking global conservation of number of unbound binders,

$$\frac{d}{dt}\left(\int_0^{\hat{s}} c_2 \, ds + \int_{\hat{s}}^{L_0} c_2 \, ds\right) = -\int_0^{\hat{s}} r \, ds, \tag{9.15}$$

and following an analogous procedure to above, we find

$$[\![c_2]\!]\,\hat{v} = [\![c_2 w_2]\!]\,, \tag{9.16}$$

where the symbol $[\![f]\!] = f(\hat{s}^+) - f(\hat{s}^-)$ denotes the jump operator across the interface.

Equilibrium

To get a first insight into the problem, it is worth to look at the equilibrium. Minimization of the free energy $\mathcal{F}$ with respect to Z subject to the area constraint yields the equilibrium equations for Z and P. Alternatively, these equations can be written abstractly by making the Lagrangian stationary with respect to $\bar{Z}$ as

$$0 = \frac{d\mathcal{L}}{dt} = D_{\bar{Z}}\mathcal{L}(\bar{Z}) \cdot \mathcal{P}(\bar{W}) \quad \forall \bar{W} \tag{9.17}$$

To obtain these equations, we calculate the variation of the Lagrangian

$$\begin{aligned}
D_{\bar{Z}}\mathcal{L}(\bar{Z})\cdot\mathcal{P}(\bar{W}) = &\left[T_c\,\partial_\theta L(\theta,\beta,\hat{s}) - F\,\partial_\theta H(\theta,\beta,\hat{s}) - P\,\partial_\theta A(\theta,\beta,\hat{s})\right]\omega \\
&+\left[T_c\,\partial_\beta L(\theta,\beta,\hat{s}) - F\,\partial_\beta H(\theta,\beta,\hat{s}) - P\,\partial_\beta A(\theta,\beta,\hat{s})\right]\gamma \\
&+\left[A(\theta,\beta,\hat{s}) - A_0\right]Q \\
&+\frac{1}{2}\int_0^{\hat{s}}\left(k_BT\log\frac{c_1}{c_0}+\mu_1^0\right)\left[-(c_1w_1)'+r\right]ds \\
&+\int_0^{\hat{s}}\left(k_BT\log\frac{c_2}{c_0}+\mu_2^0\right)\left[-(c_2w_2)'-r\right]ds \\
&+\int_{\hat{s}}^{L_0}\left(k_BT\log\frac{c_2}{c_0}+\mu_2^0\right)\left[-(c_2w_2)'\right]ds \\
&+\left[T_c\,\partial_{\hat{s}} L(\theta,\beta,\hat{s}) - F\,\partial_{\hat{s}} H(\theta,\beta,\hat{s}) - P\,\partial_{\hat{s}} A(\theta,\beta,\hat{s})\right]\hat{v} \\
&+\frac{1}{2}\left[c_1\left(k_BT\log\frac{c_1}{c_0}+\mu_1^0\right)-k_BTc_1\right]_{s=\hat{s}}\hat{v} \\
&-\left[\!\left[c_2\left(k_BT\log\frac{c_2}{c_0}+\mu_2^0\right)-k_BTc_2\right]\!\right]\hat{v}.
\end{aligned} \tag{9.18}$$

Using the arbitrariness of $\bar{W}$, the first three lines provide three purely mechanical nonlinear algebraic equilibrium equations uncoupled to c_1 and c_2, which allow us to obtain θ^{equil}, β^{equil} and P^{equil} as a function of $\hat{s}$. These quantities are consistent with Laplace's law, which in this 2D setting is simply:

$$T_c = P^{\text{equil}}(\hat{s})R\left(\theta^{\text{equil}}(\hat{s}),\beta^{\text{equil}}(\hat{s}),\hat{s}\right). \tag{9.19}$$

Therefore, these three mechanical variables can be solved for a give $\hat{s}$ and eliminated from the problem.
We identify the chemical potentials of the bound and unbound binders as:

$$\mu_1 = \mu_1^0 + k_BT\log\frac{c_1}{c_0}. \tag{9.20}$$

$$\mu_2 = \mu_2^0 + k_BT\log\frac{c_2}{c_0}. \tag{9.21}$$

It is a classical result in capillarity that the third-to-last line can be written as

$$\left[T_c\,\partial_{\hat{s}} L(\theta,\beta,\hat{s}) - F\,\partial_{\hat{s}} H(\theta,\beta,\hat{s}) - P\,\partial_{\hat{s}} A(\theta,\beta,\hat{s})\right]\hat{v} = T_c\left(1-\cos\theta^{\text{equil}}(\hat{s})\right)\hat{v}. \tag{9.22}$$

Thus, assuming equilibrium for θ, β and P, integrating by parts the fourth to sixth lines in the previous expression and using the no-flux conditions at the symmetry endpoints of the domain, the variation of the Lagrangian takes the form

$$\begin{aligned} D_{\bar{Z}}\mathcal{L}(\bar{Z})\cdot\mathcal{P}(\bar{W}) = &\int_0^{\hat{s}} \left[\left(\frac{1}{2}\mu_1 - \mu_2\right) r + \frac{1}{2}c_1 w_1\, \mu_1' + c_2 w_2\, \mu_2'\right] ds \\ &+ \int_{\hat{s}}^{L_0} c_2 w_2\, \mu_2'\, ds \\ &- \frac{1}{2}\left[c_1 w_1 \mu_1\right]_{s=\hat{s}} + \left[\!\left[c_2 w_2 \mu_2\right]\!\right] \\ &+ T_c\left(1 - \cos\theta^{\text{equil}}(\hat{s})\right)\hat{v} \\ &+ \frac{1}{2}\left[c_1\mu_1 - k_B T c_1\right]_{s=\hat{s}}\hat{v} - \left[\!\left[c_2\mu_2 - k_B T c_2\right]\!\right]\hat{v}, \end{aligned} \tag{9.23}$$

where the third line collects the terms at the interface remaining from integration by parts. Using the relation $\left[\!\left[fg\right]\!\right] = \left[\!\left[f\right]\!\right]\langle g\rangle + \langle f\rangle\left[\!\left[g\right]\!\right]$, where $\langle\cdot\rangle$ is the average operator across the interface, and rearranging terms, we can rewrite this equation as

$$\begin{aligned} D_{\bar{Z}}\mathcal{L}(\bar{Z})\cdot\mathcal{P}(\bar{W}) = &\int_0^{\hat{s}} \left[\left(\frac{1}{2}\mu_1 - \mu_2\right) r + \frac{1}{2}c_1 w_1\, \mu_1' + c_2 w_2\, \mu_2'\right] ds \\ &+ \int_{\hat{s}}^{L_0} c_2 w_2\, \mu_2'\, ds \\ &+ T_c\left(1 - \cos\theta^{\text{equil}}(\hat{s})\right)\hat{v} - \frac{1}{2}k_B T c_1(\hat{s})\hat{v} + k_B T\, [\![c_2]\!]\,\hat{v} \\ &+ \frac{1}{2}\left[c_1\mu_1\right]_{s=\hat{s}}\hat{v} - \frac{1}{2}\left[c_1 w_1 \mu_1\right]_{s=\hat{s}} \\ &+ [\![c_2 w_2]\!]\,\langle\mu_2\rangle + \langle c_2 w_2\rangle\left[\!\left[\mu_2\right]\!\right] - [\![c_2]\!]\,\langle\mu_2\rangle\hat{v} - \langle c_2\rangle\left[\!\left[\mu_2\right]\!\right]\hat{v}, \end{aligned} \tag{9.24}$$

Now, recalling the conditions at the interface in Eqs. (9.14,9.16), several terms cancel out in the fourth and fifth lines, and we obtain

$$
\begin{aligned}
D_{\bar{Z}}\mathcal{L}(\bar{Z})\cdot\mathcal{P}(\bar{W}) = &\int_0^{\hat{s}} \left[\left(\frac{1}{2}\mu_1 - \mu_2\right) r + \frac{1}{2}c_1 w_1\, \mu_1' + c_2 w_2\, \mu_2'\right] ds \\
&+ \int_{\hat{s}}^{L_0} c_2 w_2\, \mu_2'\, ds \\
&+ T_c\left(1 - \cos\theta^{\text{equil}}(\hat{s})\right)\hat{v} - \frac{1}{2}k_B T c_1(\hat{s})\hat{v} + k_B T\, [\![c_2]\!]\, \hat{v} \\
&+ \left[\!\left[\mu_2\right]\!\right] \left(\langle c_2 w_2\rangle - \langle c_2\rangle \hat{v}\right). \qquad (9.25)
\end{aligned}
$$

Developing the average operator and using Eqs. (9.16), the last line can be rewritten to obtain the final expression

$$
\begin{aligned}
D_{\bar{Z}}\mathcal{L}(\bar{Z})\cdot\mathcal{P}(\bar{W}) = &\int_0^{\hat{s}} \left[\left(\frac{1}{2}\mu_1 - \mu_2\right) r + \frac{1}{2}c_1 w_1\, \mu_1' + c_2 w_2\, \mu_2'\right] ds \\
&+ \int_{\hat{s}}^{L_0} c_2 w_2\, \mu_2'\, ds \\
&+ T_c\left(1 - \cos\theta^{\text{equil}}(\hat{s})\right)\hat{v} - \frac{1}{2}k_B T c_1(\hat{s})\hat{v} + k_B T\, [\![c_2]\!]\, \hat{v} \\
&+ \left[\!\left[\mu_2\right]\!\right] c_2(\hat{s}^+)\left[w_2(\hat{s}^+) - \hat{v}\right]. \qquad (9.26)
\end{aligned}
$$

Note that the mechanical part of the problem only enters here through $\theta^{\text{equil}}(\hat{s})$. We can now invoke the arbitrariness of w_1, w_2, r and $\hat{v}$ to obtain the remaining equilibrium equations.
Starting with the variation of w_2 at $\hat{s}$, we obtain

$$
\left[\!\left[\mu_2\right]\!\right] c_2(\hat{s}^+) = 0. \qquad (9.27)
$$

Since c_2 will be different from zero, we conclude that the chemical potential of the unbound binders is continuous across the interface.

From the other variations we obtain:

$$
\mu_1' = 0 \text{ in } (0, \hat{s}) \qquad (9.28)
$$

$$
\mu_2' = 0 \text{ in } (0, L_0). \qquad (9.29)
$$

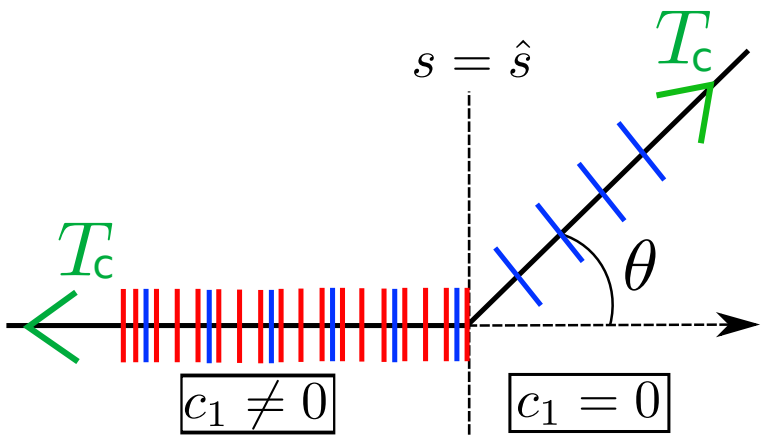

Figure 9.4: Schematic view of the configurational equilibrium at the interface $s = \hat{s}$.

We conclude that μ_1 is uniform in $(0, \hat{s})$ and that μ_2 is uniform in $(0, L_0)$. We also obtain the following equality

$$\mu_1 = 2\mu_2 \text{ in } (0, \hat{s}). \tag{9.30}$$

Furthermore, the equilibrium condition at the interface is

$$0 = T_c \left(1 - \cos\theta^{\text{equil}}(\hat{s})\right) - \frac{1}{2} k_B T c_1(\hat{s}) + k_B T \left[\!\left[c_2\right]\!\right],$$

showing that the mechanical force is balanced by the osmotic tension difference of the bound and unbound binders across the interface.
Recalling Eq. (9.20), if we assume that the bonds are ideal, μ_1^0 is uniform and that μ_2^0 is uniform and takes the same value at the adhesion patch and out of it, then we conclude $[\![c_2]\!] = 0$, the concentrations c_i are uniform, and the configurational equilibrium at the interface simplifies to

$$0 = T_c \left(1 - \cos\theta^{\text{equil}}(\hat{s})\right) - \frac{1}{2} k_B T c_1. \tag{9.31}$$

This configurational equilibrium corresponds to the equilibrium between osmotic forces and tension at the interface as shown in Fig. 9.4.

Furthermore, recalling Eq. (9.30), the uniform bound and unbound concentrations satisfy the relation

$$\frac{c_0 c_1}{c_2^2} = \exp\left(\frac{2\mu_2^0 - \mu_1^0}{k_B T}\right) = K \quad \text{in} \quad (0, \hat{s}), \tag{9.32}$$

where K is the dimensionless equilibrium constant of the reaction. Seeing the problem from a chemical kinetics point of view, at the adhesion patch we have the following reaction

$$U^a + U^b \underset{k_{\text{off}}}{\overset{k_{\text{on}}}{\rightleftharpoons}} B, \tag{9.33}$$

where U^a and U^b are unbound binder molecules in vesicles a and b, B is a bound pair of binders, and k_{on} and k_{off} are the reaction rates. Because of our assumption of symmetry between the two adhering vesicles, in equilibrium, we have the following law of mass action

$$\frac{c_1}{c_2^2} = \frac{k_{\text{on}}}{k_{\text{off}}}. \tag{9.34}$$

Comparison with Eq. (9.32) shows that the ratio between reaction rates is a purely thermodynamic quantity. Eqs. (9.31,9.32), together with the equation expressing that the total number of binders, free or bound, is fixed

$$c_1 \hat{s} + c_2 L_0 = N_{\text{tot}}, \tag{9.35}$$

allow us to solve for c_1, c_2, and $\hat{s}$. These results for equilibrium are consistent with previous theoretical results citepBell1984a,Maitre2012a.
Then, the equilibrium state can be obtained from the equations

$$\frac{c_0 c_1}{c_2^2} = \exp\left(\frac{2\mu_2^0 - \mu_1^0}{k_B T}\right) \quad \text{in} \quad (0, \hat{s}), \tag{9.36}$$

$$N_{\text{tot}} = \int_0^{\hat{s}} c_1 \, ds + c_2 L_0, \tag{9.37}$$

$$0 = T_c \left(1 - \cos \theta^{\text{equil}}(\hat{s})\right) - \frac{1}{2} k_B T c_1, \tag{9.38}$$

which allow us to solve for c_1, c_2, $\hat{s}$ invoking the mechanical equilibrium, for P, θ and β.

Dissipation

To model the dynamics, we introduce a dissipation potential expressed in terms of the process variables W:

$$\Psi(W;Z) = \int_0^{\hat{s}} \frac{1}{2\bar{k}} r^2 ds + \int_0^{\hat{s}} \left(\frac{\eta_1 c_1}{4} w_1^2 + \frac{\eta_2 c_2}{2} w_2^2 \right) ds + \int_{\hat{s}}^{L_0} \frac{\eta_2 c_2}{2} w_2^2 ds + \frac{k\mu}{\theta} \hat{v}. \tag{9.39}$$

The first term accounts for the dissipation induced by the chemical reactions of forming or breaking bonds, where $\bar{k}$ is a kinetic parameter, which may depend on the concentration of species and must be positive for consistency with the second law of thermodynamics [Mielke, 2012]. We will provide a precise definition later. The parameter η_1 may be viewed as a molecular drag coefficient of bound binders, which could be obtained from an extension of Saffman-Delbruck theory [Saffman and Delbrück, 1975]. Consequently, $\eta_1 c_1 w_1/2$ will be a drag force density on one of the adjacent membranes for a dilute collection of bound binders moving at a diffusive velocity w_1, and the integrand a dissipation power density for this force. The parameter η_2 is analogous for the free binders, and may depend on whether we are on the adhesion patch or out of it. The last term accounts for the dissipation in the bulk fluid resulting from moving the contact point at speed $\hat{v}$, where k is a numerical factor, μ the solution viscosity and θ the contact angle [de Gennes et al., 2004]. Given the time-scales of vesicle unbinding mediated by bond breaking or motion, this contribution will be ignored in the rest of the thesis. We note that $\Psi(W;Z)$ depends also on the state Z through $\hat{s}$, θ and $c_i(s)$.

9.4 Onsager's variational principle

Onsager's variational principle allows us to derive the dynamics of the system by, at any given state Z, minimizing the Rayleighian

$$\mathcal{R}(W) = \Psi(W;Z) + D_Z\mathcal{F}(Z) \cdot \mathcal{P}(W), \tag{9.40}$$

with respect to W subject to the constraints (here the fixed area constraint). Given the minimizer W, we can integrate in time the state $Z(t)$ using the process operator. To deal with the constraint, we need to extremize the Lagrangian

$$\mathcal{M}(\bar{W}) = \Psi(W;Z) + D_{\bar{Z}}\mathcal{L}(\bar{Z}) \cdot \mathcal{P}(\bar{W}), \tag{9.41}$$

with respect to $\bar{W}$.

Since the dissipation potential does not depend on ω, γ and Q, the mechanical equilibrium equations are still algebraic equations that allow us to solve for $\theta^{\text{equil}}(\hat{s})$, $\beta^{\text{equil}}(\hat{s})$ and $P^{\text{equil}}(\hat{s})$. Now, combining Eqs. (9.26,9.39), we can take variations with respect to the remaining process variables w_1, w_2, r and $\hat{v}$ to obtain the dynamical equations. Making variations with respect to w_1 stationary, we obtain the appropriate version of Fick's law

$$\boxed{w_1 = -\frac{1}{\eta_1}\mu_1' = -\frac{1}{\eta_1}\left(k_B T \frac{c_1'}{c_1}\right) \quad \text{in} \quad (0,\hat{s}).} \tag{9.42}$$

Assuming that μ_2^0 is uniform in $(0, L_0)$, we obtain from taking variations with respect to w_2 that

$$\boxed{w_2 = -\frac{k_B T}{\eta_2}\frac{c_2'}{c_2} \quad \text{in} \quad (0,\hat{s}) \cup (\hat{s}, L_0) \quad \text{and} \quad [\![c_2]\!] = 0,} \tag{9.43}$$

where in principle η_2 could depend on whether we are at the adhesion patch or not.

Taking variations with respect to the reaction rate r, we obtain

$$r = \bar{k}\left(\mu_2 - \frac{1}{2}\mu_1\right). \tag{9.44}$$

Arrived at this point, a modeling choice is needed for $\bar{k}$. Following [Mielke, 2012], we will make a choice consistent with the law of mass action. Considering the following choice for $\bar{k}$:

$$\bar{k} = k\frac{c_2^2/c_0 - \exp\left(\frac{\mu_1^0 - 2\mu_2^0}{k_B T}\right)c_1}{\mu_2 - \frac{1}{2}\mu_1}, \tag{9.45}$$

where $k > 0$ is a rate constant. A direct calculation shows that

$$\bar{k} = \frac{2kc_0}{k_B T} \exp\left(-\frac{2\mu_2^0}{k_B T}\right) \frac{\exp\left(\frac{2\mu_2}{k_B T}\right) - \exp\left(\frac{\mu_1}{k_B T}\right)}{\frac{2\mu_2}{k_B T} - \frac{\mu_1}{k_B T}}, \tag{9.46}$$

which is clearly positive as required by the second law of thermodynamics. Plugging Eq. (9.45) into Eq. (9.44), we obtain

$$\boxed{r = k_{\text{on}}^0 c_2^2 - k_{\text{off}}^0 c_1 \quad \text{in} \quad (0, \hat{s}),} \tag{9.47}$$

where

$$\boxed{k_{\text{on}} = \frac{k}{c_0} \ , \ k_{\text{off}} = k \exp\left(\frac{\mu_1^0 - 2\mu_2^0}{k_B T}\right).} \tag{9.48}$$

Thus, the model is consistent with the law of mass action but, unlike what was discussed in Chapter 3, the binding and unbinding rates are constant and independent of the dynamics. We will revisit this in Chapter 10 and 11. Taking variations with respect to $\hat{v}$, we obtain the configurational force-balance at the interface

$$\boxed{0 = T_c \left(1 - \cos\theta^{\text{equil}}(\hat{s})\right) - \frac{1}{2} k_B T c_1(\hat{s}),} \tag{9.49}$$

9.5 Final set of equations

Now, we can plug Eqs. (9.42,9.43,9.47) into the local conservation equations for the bound and unbound binders to obtain the final system of equations.

Set of coupled equations and boundary/jump conditions

At any given instant, we assume the current state Z is known. Given the location of the interface $\hat{s}$, the large-scale mechanical model requires extremizing the function

$$\mathcal{L}_{\text{mech}}(\theta, \beta, P) = T \cdot L(\theta, \beta, \hat{s}) - F \cdot H(\theta, \beta, \hat{s}) - P\left[A(\theta, \beta, \hat{s}) - A_0\right], \tag{9.50}$$

which provides three nonlinear equations to solve for $\theta^{\text{equil}}(\hat{s})$, $\beta^{\text{equil}}(\hat{s})$ and $P^{\text{equil}}(\hat{s})$. The final set of coupled equations for the chemistry and its set of chemical and mechanical boundary conditions at $s = 0$, $s = \hat{s}$ and $s = L_0$ are:

$$\dot{c}_1 = D_1 c_1'' + k_{\text{on}} c_2^2 - k_{\text{off}}^0 \, c_1 \qquad \text{in } (0, \hat{s}), \tag{9.51}$$

$$\dot{c}_2 = D_2 c_2'' - k_{\text{on}} c_2^2 + k_{\text{off}}^0 \, c_1 \qquad \text{in } (0, \hat{s}), \tag{9.52}$$

$$\dot{c}_2 = D_2 c_2'' \qquad \text{in } (\hat{s}, L_0), \tag{9.53}$$

where the diffusion coefficients are $D_i = k_B T / \eta_i$.
The chemical and mechanical boundary/jump conditions are:

$$\boxed{\text{at } s = 0} \qquad c_1'(0) = 0, \qquad c_2'(0) = 0, \tag{9.54}$$

$$\boxed{\text{at } s = \hat{s}} \qquad [\![c_2]\!] = 0, \qquad \left[\!\left[D_2 c_2'\right]\!\right] = 0, \qquad -D_1 c_1'(\hat{s}) = c_1(\hat{s})\, \hat{v}, \tag{9.55}$$

$$k_B T \; c_1(\hat{s}) = 2T_c \left(1 - \cos \theta^{\text{equil}}(\hat{s})\right) \tag{9.56}$$

$$\boxed{\text{at } s = L_0} \qquad c_2'(L_0) = 0. \tag{9.57}$$

Mathematically, we are allowed to impose two boundary conditions on c_1 at $s = \hat{s}$ (of Robin and Dirichlet type) because the location of this interface is also an unknown. It is easy to check that these partial differential equations, boundary and jump conditions are consistent with global conservation of binders.

Discussion

Two different time-scales appear naturally from the previous system of equations. The first time-scale τ_{diff} is related to diffusion and expresses the average time for a bond to diffuse from one end to the other of the patch a size $\hat{s}_0$. The second time-scale τ_{reac} is related to the chemical reaction and expresses the average time to break bonds one after the other in a patch with a uniform concentration of bonds c_0. The initial number of bonds in the patch is N^0_{bonds}.

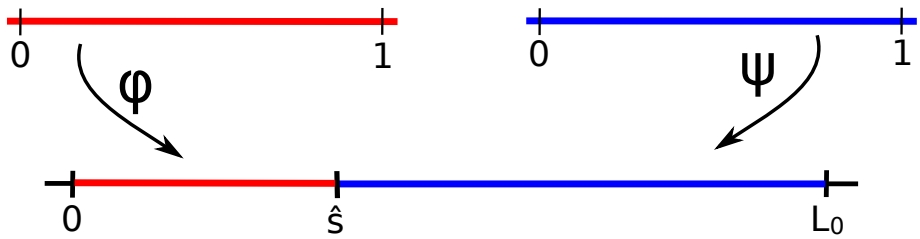

Figure 9.5: Sketch of the rescaling of the time-dependent domains into fixed domains using the transformations φ and ψ .

We have:

$$\tau_{diff} = \frac{\hat{s}_0^2}{2D_1} \quad \text{and} \quad \tau_{reac} = \frac{N^0_{bonds}}{k^0_{off}} = \frac{c_0 \hat{s}_0}{k^0_{off}}. \tag{9.58}$$

Depending on the chosen parameters, we expect different behaviors depending on which time-scale is relevant in the considered problem. For $\tau_{diff} << \tau_{reac}$, the dynamics will be driven by diffusion while for $\tau_{diff} >> \tau_{reac}$, the system will be dominated by reaction dynamics. This provides a first criterion to study the extreme cases of the process of vesicle unbinding.

9.6 Solving the equations

Rescaling of the problem

We have obtained a set of coupled equations defined on time-dependent domains $(0, \hat{s})$ and $(\hat{s}, L_0)$. Rather than addressing computationally the moving interface problem directly, we will transform it in a problem on a fixed domain using time-dependent mappings. We consider the following time-dependent changes of variables, see Fig. 9.5,

$$\begin{aligned} \varphi(\cdot, t) : [0,1] &\longmapsto [0, \hat{s}] \\ \eta &\longrightarrow \eta \hat{s}(t), \end{aligned} \tag{9.59}$$

$$\begin{aligned}\psi(\cdot,t) : [0,1] &\longmapsto [\hat{s}, L_0] \\ \eta &\longrightarrow \eta L_0 + (1-\eta)\hat{s}(t).\end{aligned} \tag{9.60}$$

We define the concentrations on the re-scaled domain $[0,1]$ as

$$u(\eta,t) = c_1\left(\varphi(\eta,t),t\right), \quad v(\eta,t) = c_2\left(\varphi(\eta,t),t\right), \quad w(\eta,t) = c_2\left(\psi(\eta,t),t\right). \tag{9.61}$$

Applying the chain rule, we have

$$\frac{\partial u}{\partial \eta} = \hat{s}(t)\frac{\partial c_1}{\partial s}, \qquad \frac{\partial^2 u}{\partial \eta^2} = \hat{s}^2(t)\frac{\partial^2 c_1}{\partial s^2}, \tag{9.62}$$

$$\frac{\partial u}{\partial t} = \frac{\partial c_1}{\partial t} + \eta\hat{v}(t)\frac{\partial c_1}{\partial s} = \frac{\partial c_1}{\partial t} + \eta\frac{\hat{v}(t)}{\hat{s}(t)}\frac{\partial u}{\partial \eta}, \tag{9.63}$$

and similarly

$$\frac{\partial w}{\partial \eta} = (L_0 - \hat{s}(t))\frac{\partial c_2}{\partial s}, \qquad \frac{\partial^2 w}{\partial \eta^2} = (L_0 - \hat{s}(t))^2\frac{\partial^2 c_2}{\partial s^2}, \tag{9.64}$$

$$\frac{\partial w}{\partial t} = \frac{\partial c_2}{\partial t} + (1-\eta)\frac{\hat{v}(t)}{L_0 - \hat{s}(t)}\frac{\partial w}{\partial \eta}. \tag{9.65}$$

Substituting these expressions into the system of reaction-diffusion equations, we find

$$\dot{u} = \frac{D_1}{\hat{s}^2}u'' + \eta\frac{\hat{v}}{\hat{s}}u' + k_{\text{on}}v^2 - k^0_{\text{off}}\,u \qquad \text{in } (0,1), \tag{9.66}$$

$$\dot{v} = \frac{D_2}{\hat{s}^2}v'' + \eta\frac{\hat{v}}{\hat{s}}v' - k_{\text{on}}v^2 + k^0_{\text{off}}\,u \qquad \text{in } (0,1), \tag{9.67}$$

$$\dot{w} = \frac{D_2}{(L_0 - \hat{s})^2}w'' + (1-\eta)\frac{\hat{v}}{L_0 - \hat{s}}w' \qquad \text{in } (0,1), \tag{9.68}$$

which is an advection-reaction-diffusion system with time-dependent coefficients but on a fixed domain. The boundary conditions, omitting dependence on time for notational simplicity, read

$$u'(0) = 0, \quad v'(0) = 0, \quad v(1) = w(0), \quad \frac{D_2}{\hat{s}}v'(1) = \frac{D_2}{L_0 - \hat{s}}w'(0) \tag{9.69}$$

$$\hat{s}\ \hat{v}\ u(1) = -D_1 u'(1), \quad k_B T u(1) = 2T_c \left(1 - \cos\theta^{\text{equil}}(\hat{s})\right), \quad w'(1) = 0. \tag{9.70}$$

It is easy to show that these equations are consistent with the global balance of adhesion molecules in the re-scaled domain, that is

$$0 = \frac{d}{dt}\left[\hat{s}\int_0^1 (u+v)d\eta + (L_0 - \hat{s})\int_0^1 w\ d\eta\right]. \tag{9.71}$$

Time and spatial discretization

We describe below a straightforward approach to time-discretization. The method is implicit in the concentrations but explicit in the interface location. The chemo-mechanical coupling is staggered. Super-indices below denote quantities evaluated at discrete time instants.

1. Initialize the problem with $\hat{s}^0$, $\hat{v}^0$, u^0, v^0 and w^0.
2. Given $\hat{s}^n$, compute the contact angles θ^n, β^n and the pressure P^n extremizing Eq. (9.50).
3. Solve for u^{n+1}, v^{n+1} and w^{n+1} using

$$\begin{aligned}
\frac{u^{n+1} - u^n}{\Delta t} &= \frac{D_1}{(\hat{s}^n)^2} u^{n+1\prime\prime} + \eta\frac{\hat{v}^n}{\hat{s}^n} u^{n+1\prime} + k_{\text{on}}(v^{n+1})^2 - k^0_{\text{off}}\, u^{n+1} && \text{in } (0,1),\\
\frac{v^{n+1} - v^n}{\Delta t} &= \frac{D_2}{(\hat{s}^n)^2} v^{n+1\prime\prime} + \eta\frac{\hat{v}^n}{\hat{s}^n} v^{n+1\prime} - k_{\text{on}}(v^{n+1})^2 + k^0_{\text{off}}\, u^{n+1} && \text{in } (0,1),\\
\frac{w^{n+1} - w^n}{\Delta t} &= \frac{D_2}{(L_0 - \hat{s}^n)^2} w^{n+1\prime\prime} + (1-\eta)\frac{\hat{v}^n}{L_0 - \hat{s}^n} w^{n+1\prime} && \text{in } (0,1),
\end{aligned}$$

subject to

$$\begin{aligned}
&u^{n+1\prime}(0) = 0, \quad u^{n+1}(1) = \frac{2T_c}{k_B T}(1 - \cos\theta^n)\, v^{n+1\prime}(0) \quad = 0, \quad v^{n+1}(1) = w^{n+1}(0),\\
&w^{n+1\prime}(1) = 0, \quad \frac{D_2}{\hat{s}^n} v^{n+1\prime}(1) = \frac{D_2}{L_0 - \hat{s}^n} w^{n+1\prime}(0).
\end{aligned}$$

The above system of partial differential equations can be made linear by replacing $(v^{n+1})^2$ by $v^n v^{n+1}$.

4. Update the interface velocity and position

$$\hat{v}^{n+1} = -\frac{D_1}{\hat{s}^n u^{n+1}(1)} u^{n+1\prime}(1), \qquad \hat{s}^{n+1} = \hat{s}^n + \Delta t \hat{v}^{n+1}. \tag{9.72}$$

5. Set $n+1 \longrightarrow n$ and go to step 2.

We discretize this problem in space using a Galerkin finite element method combined with B-splines basis functions, see Appendix B. Despite the advective term in the partial differential equation we did not find the need to stabilize the formulation.

9.7 Results and discussion

Preparation of an equilibrium state

Before running out-of-equilibrium calculations, we prepare the system in a equilibrium state, chemical and mechanical, with $F = 0$, as follows. We consider two vesicles with a radius $R = 10$ μm coated with binders with a concentration $c_0^* = 2.5 \cdot 10^3$ molecules $/\mu\text{m}^2$. To map areal concentration to line concentration in our 2D problem, we consider a ribbon of the membrane of width $l_{lat} = 1/\sqrt{2500}$ μm. Thus the reference concentration c_0 on the ribbon is $c_0 = c_0^* l_{lat} = 50$ molecules$/\mu$m. Making the following choice for the difference of the standard chemical potentials: $2\mu_2^0 - \mu_1^0 = \log(2) k_B T$, Eq. (9.32) gives $K = 2$. The binders will cluster and form bonds in a patch of radius $\hat{s}_0 = 2.5$ μm. The concentration of free binders is constant in the patch and out of the patch and obeys the law of mass action: $v_0 = \sqrt{\frac{u_0}{K}}$. We obtain the number concentrations u_0, v_0 and w_0 by fixing the total number of molecules as $N_{tot} = c_0 L_0$ and solving the corresponding system of equations:

$$N_{tot} = u_0 \hat{s}_0 + v_0 \hat{s}_0 + w_0 (L_0 - \hat{s}_0) \tag{9.73}$$

$$v_0 = \sqrt{\frac{u_0}{K}} \tag{9.74}$$

$$w_0 = v_0 \tag{9.75}$$

The contact angles are chosen such as $\beta = \pi/2$ (so that $F = 0$) and θ =asin($\frac{1}{4}$) so that $\hat{s}_0 = 2.5\ \mu\text{m} = R/4$. We fix the tension T_c such that there is mechanical equilibrium between the osmotic forces and the mechanical forces at $s = \hat{s}_0$ given by Eq. (9.49). The tension is then $T_c = 2.48 \cdot 10^{-4}$ N·m^{-1}. For such a preparation, the chemical and the mechanical equilibrium are achieved and the system is at equilibrium. The evolution of this system is governed by the set of equations, obtained in the previous section. A sketch of the prepared system is given in Fig. 9.6.

To study the dynamics, the system can be brought out of equilibrium in various ways, here we displace the system from equilibrium by applying a force F to the top of the vesicle. This induces a change in the shape of the vesicle that modifies contact angles, and thus, because of the chemo-mechanical coupling at $s = \hat{s}$, this affects the chemistry inside of the patch.
We focus our numerical studies on two cases: we first examine the pure diffusive case, where $\tau_{reac} \gg \tau_{diff}$. We then look at the dynamics in the case of a reaction-diffusion problem where $\tau_{reac} \sim \tau_{diff}$. To do so we keep $\tau_{diff} = 31$ s by setting $D_1 = 0.1\ \mu\text{m}^2\cdot\text{s}^{-1}$. This choice is justified by different studies [Cai et al., 2016], and corresponds to the lower bound of diffusion constant of cadherins for low Ca^{2+} concentration. We modify k^0_{off} to switch from one case to the other.

Verification of the numerical implementation

We checked that, starting from a variety of equilibrium states satisfying the conditions derived above, the dynamics of the system were stationary. Furthermore, we performed mesh refinement and considered a variety of time-steps to verify numerical convergence. This study allowed us to design adapted meshes, refined close to the interface $s = \hat{s}$, showing a balance between accuracy and efficiency. We do checked balance of mass, obtaining typical relative errors of 10^{-4}. We note that here balance of mass requires proper treatment of jump conditions at the moving interface.

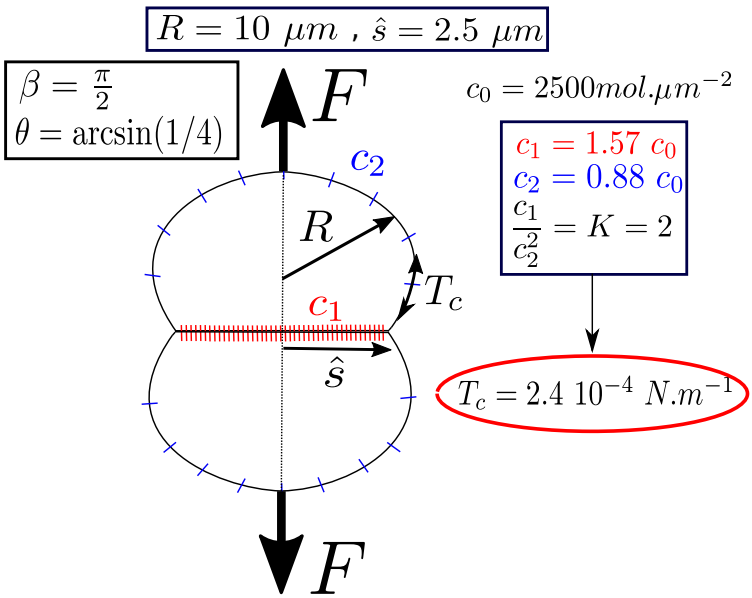

Figure 9.6: Sketch of the equilibrium definition. By setting the radius of curvature R of the vesicle, the size of the patch $\hat{s}$, the equilibrium constant K and the reference concentration c_0 we determine the concentration of bonds c_1, of binders c_2 and the tension T_c.

Finally, to check the consistency of our formulation and numerical implementation with Onsager's variational principle, we track the dissipation in the system and the energy change along time and verify the following relation , see Eq. (8.44):

$$\dot{\mathcal{F}}(t) = -2\mathcal{D}(t) \tag{9.76}$$

We consider here the reaction-diffusion case with an applied ramp of force F such as $F(t) = F_{max}\frac{t}{\tau_{diff}}$ for $0 < t < \tau_{diff}$ and $F(t) = F_{max}$ for $t > \tau_{diff}$ with $F_{max} = 0.2\ T_c$. The result is given in the following 9.7. The figure shows that the relation expected between energy change and dissipation is verified during time. Thus our model complies with the second law of thermodynamics.

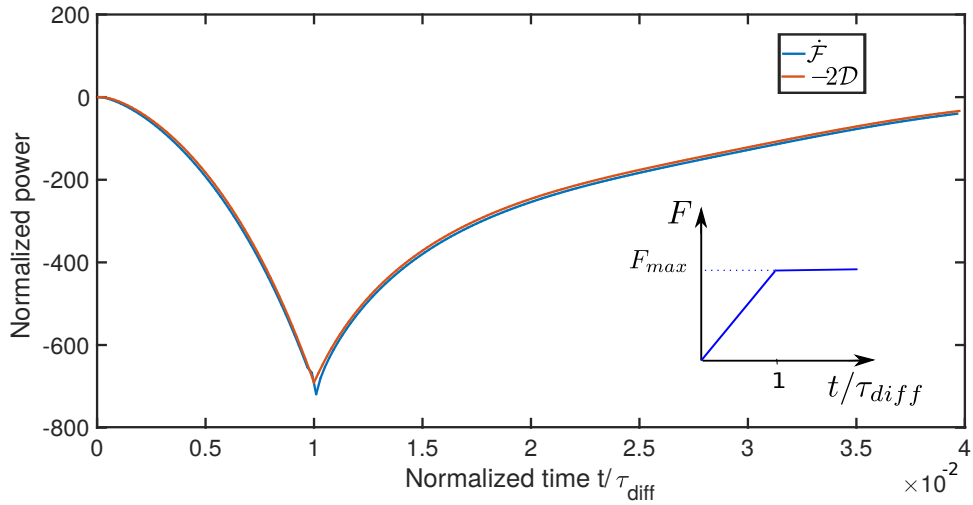

Figure 9.7: $\dot{\mathcal{F}}$ and $-2\mathcal{D}$ as a function of time.The time is here normalized by τ_{diff}. In the right corner: profile of force applied. $F_{max} = 0.2\ T_c$

Diffusion-dominated regime

Considering the case of pure diffusion, i.e. the case of $\tau_{reac} \gg \tau_{diff}$, we look at the effect of a pulling force on the system. To do so we set $k_{off} = 0$ and $k_{on} = 0$ and we displace the equilibrium by applying a force F to the top of the vesicle.

A series of snapshots capturing the evolution of the size of the patch and the concentration of bonds is given in Fig. 9.8. It shows a reduction of the size of the patch associated with an increase of the concentration of chemical bonds. By increasing the applied force, the contact angle is increased. This leads to an increase of the concentration of bonds at the interface (Eq. (9.57)), which creates a gradient in bond concentration, inducing a diffusive flux towards uniformization of bonds concentration. In turn, diffusive flux at the interface requires motion of the interface, see Eq. (9.55). This result in a "packed" patch, smaller and more concentrated. This is clearly illustrated in Fig 9.8(a,c) and summarized in Fig. 9.8(b). The system reaches a new equilibrium when the

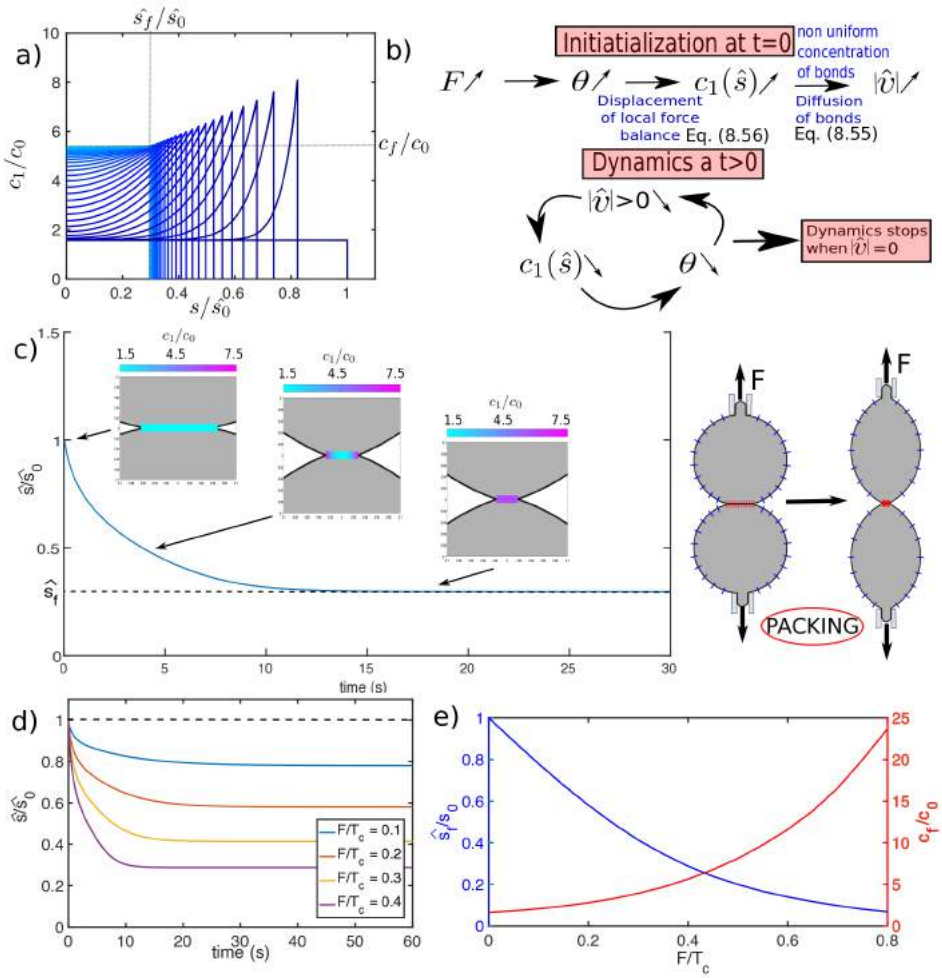

Figure 9.8: Diffusion dominated regime. a) Series of plots of the profile of normalized concentration of bonds in the patch at different instants. Lighter blue represents later times. b) Scenario after sudden F increase. c) Time evolution of the normalized position of the interface $\hat{s}/\hat{s}_0$ for an applied force $F = 0.4T_c$. A series of snapshots of the adhesion patch at different instant of the dynamics illustrate the change in concentration of bonds as the change in the size of the patch. d)Time evolution of the normalized position of the interface $\hat{s}/\hat{s}_0$ for different applied force. e) Final normalized concentration c_f/c_0 and final normalized position of the interface $\hat{s_f}/\hat{s}_0$ as a function of the applied force.

concentration of the bonds reaches a certain value for which the mechanical equilibrium at $s_f = \hat{s}$ is achieved. A larger applied force leads to a more highly packed patch (smaller and more concentrated), see Fig. 9.8(d,e), but the patch cannot dissociate since reactions are not possible with $k_{on} = k_{off} = 0$. We note that this kind of behavior has been observed in cells [Maître et al., 2012a] although our 2D model does not capture the typical tethering observed in these experiments and more generally in fluid membranes under localized force [Rahimi and Arroyo, 2012].

Reaction-Diffusion regime

By setting $k^0_{off} = 10$ s^{-1} we have $\tau_{reac} = 12.5$ s $\sim \tau_{diff}$. For such a set of parameters, the time to break one by one the bonds of the patch is nominally equivalent to the time to move a bond from the interface to the center of the patch. Here the interplay between the reaction and diffusion is expected to modify the dynamics of the problem.

For low applied forces, the system is driven out of the equilibrium by the force but finally reaches a new quasi-equilibrium, when the osmotic pressure equilibrates with tensile forces, see Eq. (9.57), for which the time-scale of evolution involves slow reactions and is way longer than the time of the experiment and the system can be considered as nearly stable. The time evolution of the position of the interface is given in Fig. 9.9(a). This regime is similar to the "packing" of bonds discussed in the previous section with some degree of bond breaking along the process.
For larger forces, see Fig. 9.9(b), the system never reaches the regime of quasi-equilibrium and is instead driven out of equilibrium until full separation in a relatively short time scale. An interesting observation is illustrated in Fig. 9.9(c), where the lifetime τ_f of the patch is plotted as a function of the applied force. The transition between stability and instability seems like a threshold: there is a very narrow domain of applied force that separates a stable patch, with a very large lifetime from a unstable one, for which the

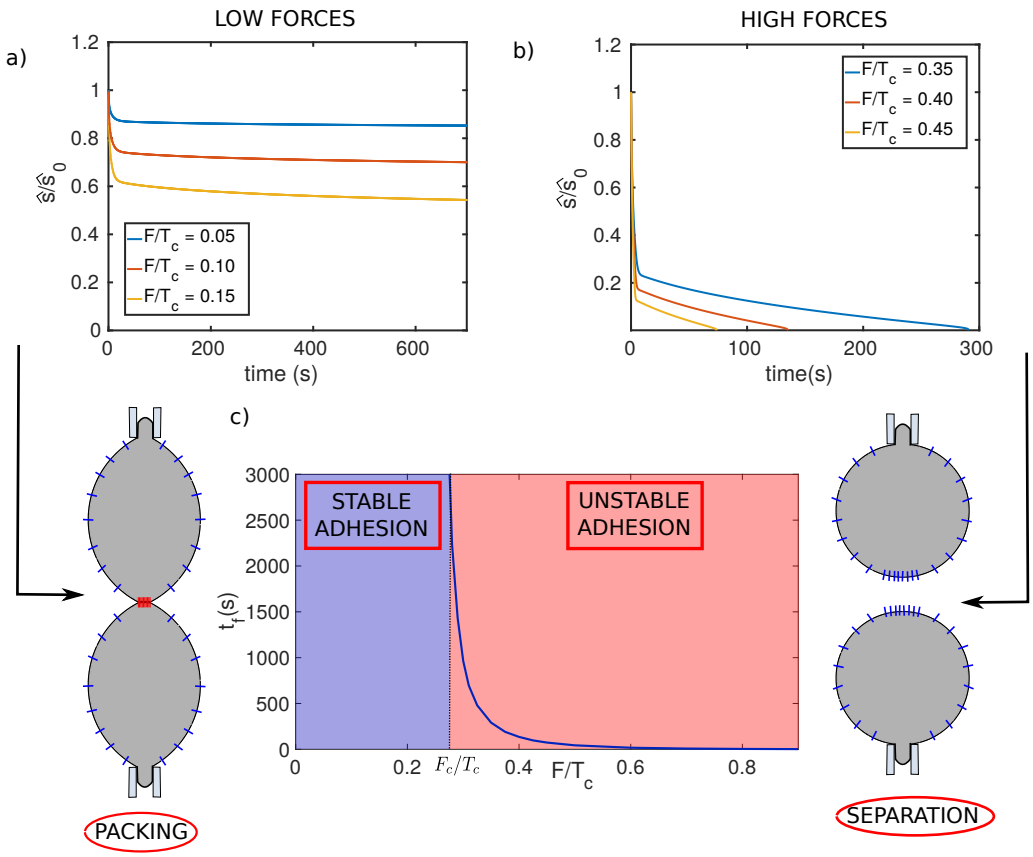

Figure 9.9: Reaction-diffusion regime. a) Time evolution of the normalized position of the interface $\hat{s}/\hat{s}_0$ at low applied forces. For this regime of forces. the system evolves towards a quasi-equilibrium state. b)Time evolution with of the normalized position of the interface $\hat{s}/\hat{s}_0$ at high applied forces. For this regime of forces, the system evolves until the two vesicles are completely detached. c) Lifetime of adhesion patch as a function of the applied force F/T_c. F_c is the critical force for which lower applied forces $F < F_c$ lead to an infinite lifetime of the adhesion patch.

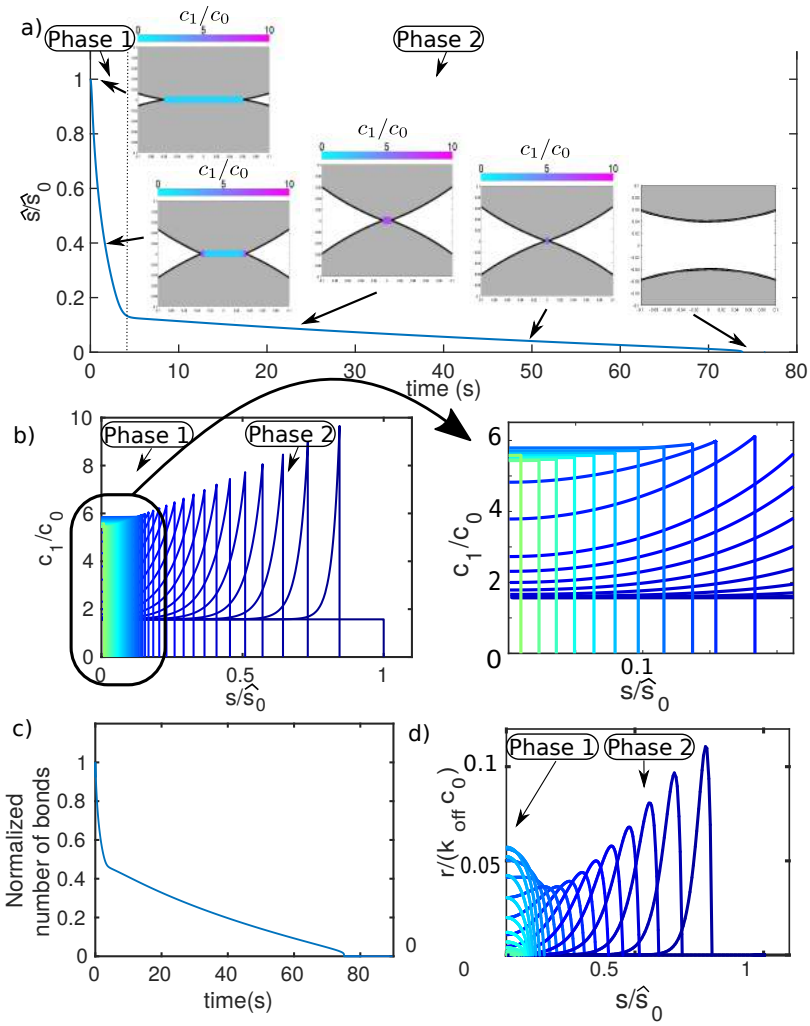

Figure 9.10: Reaction-diffusion regime at large forces. a) Time evolution of the normalized position of the interface $\hat{s}/\hat{s}_0$ for an applied force $F = 0.4T_c$. A series of snapshots of the adhesion patch at different instant of the dynamics illustrate the change in concentration of bonds as the change in the size of the patch. b) (right) Series of plots of the profile of normalized concentration of bonds in the patch at different instants. Lighter color represents later times. (left) Zoom on the evolution of the concentration during the second phase of the process. Bonds are packed, and the patch shrinks slowly while the bond concentration decreases slowly. c) Time evolution of the normalized number of bonds. d) Series of plots of the net unbinding rate $r(s/\hat{s}_0)$ on the patch at different instants. Color coding coincides with that in (b)

lifetime is very small. In analogy with remarks made multiple times in Part I of the thesis, see section 4.2 and section 5.3, we can identify a critical force F_c such that for $F < F_c$ the system is stable and for $F > F_c$ the system is unstable. To better illustrate the dynamics of the system for large forces, a series of snapshots capturing the dynamics is given in Fig. 9.10(a). We can identify two phases: a first phase, where the patch gets "packed" (it shrinks and becomes more concentrated) in the presence of high concentration gradients, and hence bonds diffuse towards teh center of the patch, see Fig. 9.10(a,b). In contrast with the diffusion-dominated case, during this phase bonds also break at a high speed, as a result of a high breaking rate r localized near the edge of the patch, see Fig. 9.10(d). This phase stops when the osmotic pressure equilibrates the mechanical forces. This phase is also present at low forces. The second phase corresponds to another process: now, the gradient of bond concentration in the patch is very small, and thus so is diffusion. The "packing" of the patch, by increasing the concentration of bonds in the patch, brought the chemical reaction in the patch far from the equilibrium: the reaction quotient $Q = c_1 c_0 / c_2^2$ is such as $Q > K = 2$. Thus, reactions continue to happen towards bond breaking (the breaking rate is positive in the patch during this phase, see 9.10(d)), reducing the number of bonds in such a way that the osmotic tension cannot balance the increased mechanical force. This out-of-equilibrium regime happen on a longer time-scale than the first regime and is clearly visible on Fig. 9.10(c(left)): the concentration in the patch is uniform and the patch shrinks slowly towards full separation with a low and more uniform breaking rate in the patch, see Fig. 9.10(d), decreasing along time as the reaction in the patch is evolving towards chemical equilibrium without ever reaching it.

Growth and maturation

In previous examples, we have applied a separation force starting from an equilibrium state. However, this is not necessarily the case, as in the experiments reported by Chu et al. [2004a], where they measure the critical

separation force F_c as a function of the maturation time of the patch, i.e. the time spent after the establishment of a nascent adhesion between two cells. They found a strong dependence of F_c on maturation time: for the first part of growth, the critical force increases rapidly by several fold while, after an hour, the critical force reaches a plateau. To explain this dependence they discuss the influence of Ca^{2+} concentration and immobilization of bonds through actin binding, as discussed in the introduction. We examine this kind of behavior with our model next. We place two vesicles in contact, forming a small adhesion patch with low concentration of adhesion molecules. Tension is kept constant. The time evolution of the process is given in Fig. 9.11(a,b).

We observe two phases during the process: a first phase of growth, between 30 s and 4 min, for which the the size of the patch increases while the patch is poorly concentrated and the concentration is constant, it is the "growth phase", and a second phase for which the patch grows slowly and the concentration of bonds inside the patch increases by "pumping" binders from the free part of the vesicles due to diffusion: its the "maturation phase". Thus the first phase evolves towards mechanical equilibrium between tension and osmotic pressure and stops when the mechanical equilibrium at the interface is reached while the second phase is due to an equilibration of the chemical potential of the binders by recruitment of binders from out of the patch and its coupling with bond formation in the patch, where binders react to form bonds. After an hour, the system stops to evolve and an equilibrium is achieved. By applying a separation force during the maturation process, we compute the dependence of the critical force F_c necessary to unbind the vesicles on maturation time, see Fig. 9.11(c). We recover a similar dependence than the one observed by Chu et al. [2004a], even though in these experiments the situation is likely more complex as cadherins are known to progressively couple to the cytoskeleton and become increasingly immobilized, see Introduction. Here the plateau is simply a result of the equilibration of the chemo-mechanical coupling and no other process is necessary to explain this observation.

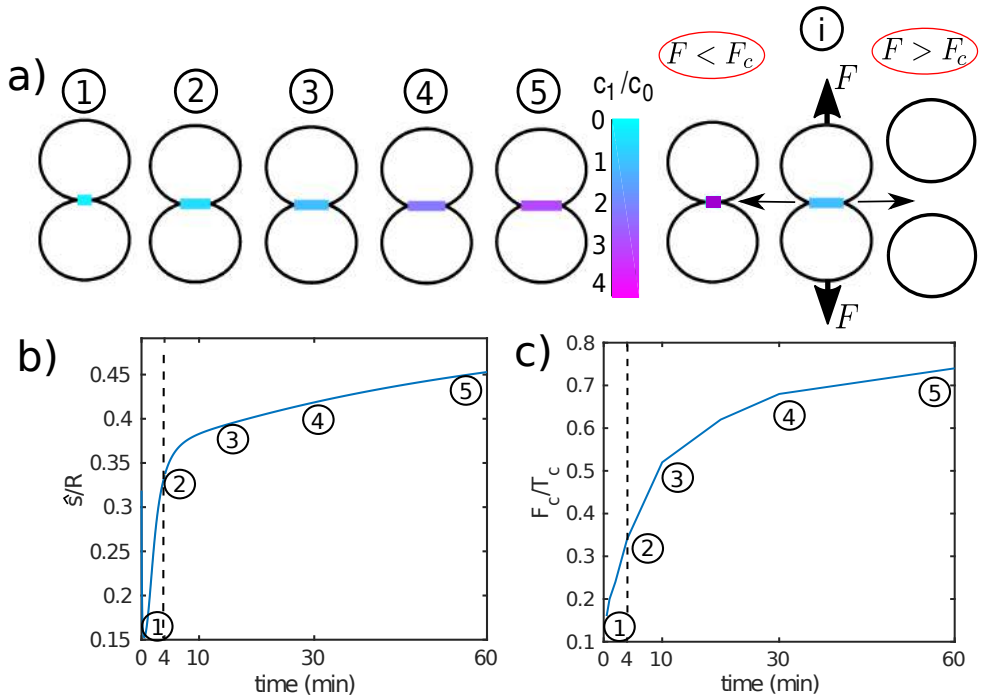

Figure 9.11: a) (left) Series of snapshots of the vesicle doublet at different instants during growth and maturation of the adhesion patch. The number corresponds to the times given by the same number on Fig.(b,c). The normalized concentration of bonds in the patch is shown with a color gradient. (right) Definition of the critical force F_c as the minimum force necessary to unbind the vesicles. b) Time evolution of the normalized position of the interface $\hat{s}/\hat{s}_0$. c) Dependence of the critical force F_c on the maturation time of the adhesion. To generate this plot, the separation force is applied at different instants during maturation. $R = 5\ \mu$m, $T_c = 2.5 \cdot 10^{-4}$ N·m^{-1}, $D_1 = 2.5 \cdot 10^{-2}$ μm^2 ·s^{-1}, $k_{off} = 10$ s^{-1}, $K = 1$, $c_0 = 2500$ molecules/μm^2.

Chapter 10

Binding/unbinding dynamics with compliant ideal bonds

In the previous chapter, we have assumed that bonds are rigid. This hypothesis has several consequences. From the point of view of the microscopic mechanics, it allows us to ignore the effect of bond compliance on vesicle shape, which is reasonable. However, bond rigidity prevents us from resolving the force distribution on the bonds in a microscopic region near $s = \hat{s}$. This force distribution will have chemical consequences, even for ideal bonds, since its stored elastic energy in the bonds will contribute to their chemical potential. A molecular bond would rather be in an unstressed configuration, which has lower elastic energy and will create a driving force moving bonds away from the crack tip. In this chapter, we study the influence of the bond compliance on the dynamics of adhesion patches in the case of ideal bonds. We exploit the scale separation between the overall vesicle mechanics, governed by capillarity, and the microscopic mechanics near $s = \hat{s}$, depending on the bond compliance and bending rigidity of the membrane, which we resolve with a microscopic model using the large-scale capillary model to set the boundary conditions.

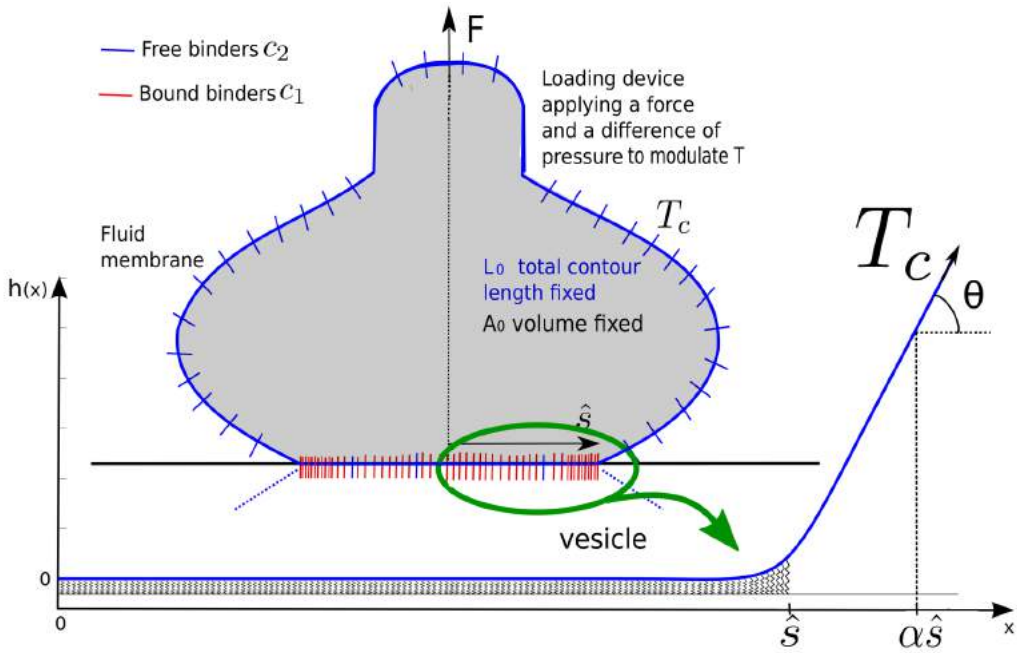

Figure 10.1: Sketch of the two-scale approach to examine the mechanics of the problem which includes a micro-scale model to determine the elongation h of the bonds in the patch. We treat the adhesion patch as an elastic beam lying on a continuous concentration of bonds. Minimization of the free energy of this problem gives h as a function of s. The boundary conditions for this problem (θ and T_c) are given by a large-scale capillary problem.

10.1 Micro-scale modeling around the contact point

Sketch of the micro-scale model

To determine the separation $h(s)$, and hence the force distribution on the bonds, we resort to a more detailed model, since the simple capillary mechanical model predicts that all the vertical force transmitted by the membrane on the adhered part is resisted by a concentrated reaction at the triple point. To overcome this issue, we consider a model for an elastic beam on an elastic

foundation as depicted in Fig. 10.1, which takes as data from the larger-scale model $c_1(s)$, $\hat{s}$ and θ. We parameterize the deformed shape (a planar curve) as $x \longmapsto (x, h(x))$ for $x \in (0, \alpha\hat{s})$, where $\alpha > 1$ is a factor determining the domain size, large enough so that at the right-end of the domain bending is negligible. The adhesion patch is given by $x \in (0, \hat{s})$. Note that this is an approximation because the parameter x is not exactly arc-length s, however, since $s(x) = \int_0^x \sqrt{1 + h'^2(y)}dy$, x and s are expected to be very close within the adhesion patch because the slope of the curve will be small there. Therefore, in this region, the concentration of bound binders can be well approximated by $c_1(x)$ instead of $c_1(s(x))$.

How to solve the problem

The free energy consists of five terms. The first one is due to the tension of the vesicle, simply the product of the tension T_c times the length of the curve. The second models the bending elastic energy, which is non-negligible near the interface $s = \hat{s}$ and takes the form $(\kappa/2)\int C^2\, ds$, where κ is the bending rigidity, $c = h''/(1 + h')^{3/2}$ is the curvature of the curve and $ds = \sqrt{1 + h'^2}dx$. The third term is the energy stored in the elastic foundation whose stiffness is given by the number concentration of bound binders c_1 times the stiffness to stretching of one bound binder molecule, k_0, with c_1 computed thanks to the bigger scale capillary model. The fourth term accounts for the pressure inside the vesicle, which presses against the molecular bonds. The last term is the potential energy of the tension force at the boundary of the domain. Thus, the free energy takes the form

$$\tilde{\mathcal{F}}[h] = T_c \int_0^{\alpha\hat{s}} \sqrt{1 + h'^2}dx + \frac{\kappa}{2}\int_0^{\alpha\hat{s}} \frac{h''^2}{\left(1 + h'^2\right)^{5/2}}dx \tag{10.1}$$

$$+ \int_0^{\hat{s}} \frac{k_0 c_1}{2} h^2 dx + \int_0^{\hat{s}} Ph\, dx - T_c \sin\theta\, h(\alpha\hat{s}). \tag{10.2}$$

Because of symmetry considerations, we should impose the condition $h'(0) = 0$. Minimization of this functional provides a method to obtain $h(x)$, and thus the force distribution $f(x) = k_0 c_1(x) h(x)$ (which is approximately $h(s)$ and $f(s)$ in the adhesion patch) as a function of $c_1(s)$, $\hat{s}$ and θ given by the large-scale capillary model. We note that treating the large-scale and the small-scale aspects of the mechanics in a unified model poses practical difficulties as a result of ill-conditioning. Thus, our two-scale approach is appealing conceptually and useful computationally.

Separation distance profile in the adhesion patch

A closer look to the mechanics in the patch is given in Fig. 10.2, where the separation distance over the adhesion patch $h(s)$ is given for different values of k_0. We can form two different characteristics lengths x_γ and ℓ_2. $x_\gamma = \sqrt{\frac{k_B T}{k_0}}$ is a characteristic length that scales the vertical elongation of the bonds at the interface as can be seen on Fig. 10.2. The second characteristic length $\ell_2 = \sqrt{\frac{T_c}{k_0 c_0}}$ is shown for each curve and scales the horizontal extension of the region where bond elongation is perturbed, and thus where bonds bear force. The figure shows how $h(s) \neq 0$ is localized in a small region of extension ℓ_2 near $s = \hat{s}$, justifying the two-scale modeling approach.

10.2 Governing equations

Free energy

To apply Onsager's variational principle, it is necessary to detail the new free energy of the system and compute its variation. Considering a capillary free energy contribution, the elastic energy of the stretched bonds, the potential for the force applied by the loading device and an ideal gas entropy for the bound and unbound binders, the new chemo-mechanical free energy is

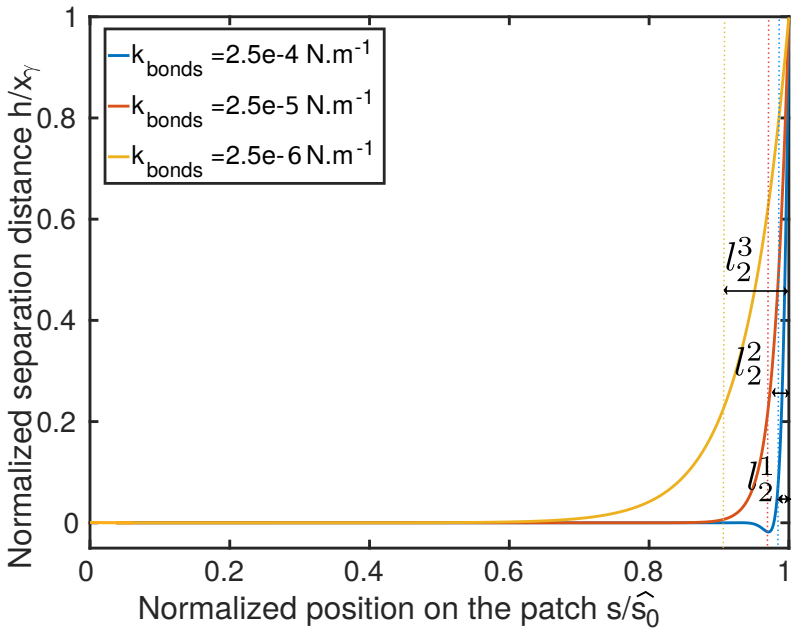

Figure 10.2: Profile of the normalized separation distance h/x_γ in the patch for different values of k_0. The characteristic length ℓ_2 is shown for each value of k_0.

$$
\begin{aligned}
\mathcal{F}(Z) = {} & T_c \cdot L(\theta, \beta, \hat{s}) - F \cdot H(\theta, \beta, \hat{s}) \\
& + \frac{k_B T}{2} \int_0^{\hat{s}} c_1 \left(\log \frac{c_1}{c_0} - 1 \right) ds + \frac{1}{2} \int_0^{\hat{s}} \mu_1^0 c_1 \, ds + \frac{k_B T}{2} \int_0^{\hat{s}} \left(\frac{h}{x_\gamma} \right)^2 c_1 \, ds \\
& + k_B T \int_0^{\hat{s}} c_2 \left(\log \frac{c_2}{c_0} - 1 \right) ds + \int_0^{\hat{s}} \mu_2^0 c_2 \, ds \\
& + k_B T \int_{\hat{s}}^{L_0} c_2 \left(\log \frac{c_2}{c_0} - 1 \right) ds + \int_{\hat{s}}^{L_0} \mu_2^0 c_2 \, ds,
\end{aligned} \tag{10.3}
$$

where h is determined from the small-scale model described before. As stated in the previous chapter, to enforce our assumption that the enclosed area (volume) remains constant so that $A = A_0$, we introduce the Lagrangian

$$
\mathcal{L}(Z, P) = \mathcal{F}(Z) - P \left[A(\theta, \beta, \hat{s}) - A_0 \right], \tag{10.4}
$$

where P is the pressure difference enforcing the constraint. Thus, this Lagrangian is a function of the extended set of state variables $\bar{Z}$ as:

$$\bar{Z} = \left(\theta, \beta, \hat{s}, c_1, c_2, P\right). \tag{10.5}$$

Following the same framework used in the previous chapter, we can now identify the two following chemical potentials.

$$\mu_1(h) = \mu_1^{chem} + \mu_1^{mech}(h) = \mu_1^0 + k_B T \log \frac{c_1}{c_0} + k_B T \left(\frac{h}{x_\gamma}\right)^2, \tag{10.6}$$

$$\mu_2 = \mu_2^0 + k_B T \log \frac{c_2}{c_0}, \tag{10.7}$$

with $\mu_1(h)$ now exhibiting a chemical and a mechanical part, the latter one expressing a dependence on the distance h and thus establishing an additional coupling between the vesicle mechanics and the chemistry.

Process variables and jump conditions

The set of process variables W is unchanged and the continuity equations of mass conservation 9.9 are not affected by the compliance of the bonds and thus gives us the same jump conditions than the one obtained for the rigid bonds

$$\hat{v} = w_1(\hat{s}), \tag{10.8}$$

$$[\![c_2]\!]\, \hat{v} = [\![c_2 w_2]\!]. \tag{10.9}$$

Using the new expression for the chemical potentials and these jump conditions, we are able to express the rate of change of the free energy as:

$$\begin{aligned} D_{\bar{Z}}\mathcal{L}(\bar{Z}) \cdot \mathcal{P}(\bar{W}) = &\int_0^{\hat{s}} \left[\left(\frac{1}{2}\mu_1(h) - \mu_2\right) r + \frac{1}{2} c_1 w_1\, \mu_1'(h) + c_2 w_2\, \mu_2'\right] ds \\ &+ \int_{\hat{s}}^{L_0} c_2 w_2\, \mu_2'\, ds + T_c \left(1 - \cos\theta^{\text{equil}}(\hat{s})\right) \hat{v} - \frac{1}{2} k_B T c_1(\hat{s}) \hat{v}. \end{aligned} \tag{10.10}$$

Dissipation

Similarly, by definition, the dissipation in the system is not affected by the elastic contribution of stretched bonds. Thus we can express the dissipation potential as:

$$\Psi(W;Z) = \int_0^{\hat{s}} \frac{1}{2\bar{k}} r^2 ds + \int_0^{\hat{s}} \left(\frac{\eta_1 c_1}{4} w_1^2 + \frac{\eta_2 c_2}{2} w_2^2 \right) ds + \int_{\hat{s}}^{L_0} \frac{\eta_2 c_2}{2} w_2^2 ds. \tag{10.11}$$

Biased diffusion

Invoking Onsager's variational principle and forming the Rayleighian by combining Eqs. (10.10,10.11), we can take variations with respect to the remaining process variables w_1, w_2, r and $\hat{v}$ to obtain the dynamical equations. Making variations with respect to w_1 stationary we obtain the appropriate version of Fick's law

$$\boxed{w_1 = -\frac{1}{\eta_1}\mu_1'(h) = -\frac{k_B T}{\eta_1}\left(\frac{c_1'}{c_1} + 2\frac{hh'}{x_\gamma^2}\right) \quad \text{in } (0,\hat{s}).} \tag{10.12}$$

The second term in this equation is a bias with respect to Fickian diffusion due to the non-uniform stretching energy stored in the bonds. Assuming that μ_2^0 is uniform in $(0, L_0)$, we obtain from taking variations with respect to w_2 that

$$\boxed{w_2 = -\frac{k_B T}{\eta_2}\frac{c_2'}{c_2} \quad \text{in } (0,\hat{s}) \cup (\hat{s}, L_0) \quad \text{and} \quad [\![c_2]\!] = 0,} \tag{10.13}$$

Taking variations with respect to the reaction rate r, we obtain

$$r = \bar{k}\left(\mu_2 - \frac{1}{2}\mu_1(h)\right). \tag{10.14}$$

Reaction rates

Arrived at this point, a modeling choice is needed for $\bar{k}$. Following [Mielke, 2012], we will make a choice consistent with the law of mass action. Consider

the following choice:

$$\bar{k} = k \frac{c_2^2/c_0 \exp\left(\frac{-h^2}{x_\gamma^2}\right) - \exp\left(\frac{\mu_1^0 - 2\mu_2^0}{k_B T}\right) c_1}{\mu_2 - \frac{1}{2}\mu_1(h)}, \tag{10.15}$$

where $k > 0$ is a rate constant. A direct calculation shows that

$$\bar{k} = \frac{2kc_0}{k_B T} \exp\left(-\frac{2\mu_2^0}{k_B T}\right) \frac{2\pi k_B T}{k_0} \exp\left(\frac{-h^2}{x_\gamma^2}\right) \frac{\exp\left(\frac{2\mu_2}{k_B T}\right) - \exp\left(\frac{\mu_1(h)}{k_B T}\right)}{\frac{2\mu_2}{k_B T} - \frac{\mu_1(h)}{k_B T}}, \tag{10.16}$$

which is clearly positive as required by the second law of thermodynamics. Plugging Eq. (10.15) into Eq. (10.14), we obtain

$$\boxed{r = k_{\text{on}}^0 \exp\left(\frac{-h^2}{x_\gamma^2}\right) c_2^2 - k_{\text{off}}^0 c_1 \quad \text{in} \quad (0, \hat{s}),} \tag{10.17}$$

where

$$\boxed{k_{\text{on}}^0 = \frac{k}{c_0} \quad \text{and} \quad k_{\text{off}}^0 = k \exp\left(\frac{\mu_1^0 - 2\mu_2^0}{k_B T}\right).} \tag{10.18}$$

Interpretations of $k_{on}(h)$

In order to interpret this dependence of the binding rate on the separation distance h between the two vesicle, we recall the discussion in Chapter 3 about the process of formation of a bond, see section 3.1. The reaction consisting of binding of two binders is actually a combination of two events [Erdmann and Schwarz, 2006, 2007, Qian et al., 2008]. First, the binder has to come close enough to the opposite binder and then react when they are in a close-enough range.

We keep the classical view of the binder as attached to a spring of rest length l_b and stiffness k_0. As it is stuck between the two surfaces, the binder is allowed to move only in a zone delimited between $z = -l_b$ and $z = 2h + l_b$ in the potential $U(z)$, with $U(z)$ such as:

$$U(z) = \frac{k_0 z^2}{2} \text{for z} \in [-l_b, 2h + l_b]. \tag{10.19}$$

As a classical result of statistical mechanics, the Boltzmann statistics gives the probability density function $P(z)$ for the binder to be in a position z such as:

$$P(z) = \frac{1}{Z}\exp\left(\frac{U(z)}{K_B T}\right) = \frac{1}{Z}\exp\left(\frac{k_0 z^2}{2K_B T}\right), z \in [-l_b, h + l_b], \tag{10.20}$$

where Z is the partition function satisfying the normalization condition:

$$\int_{-l_b}^{2h-l_b} P(z)dz = 1. \tag{10.21}$$

Letting the limits of integration to infinity we can approximate Z such as:

$$Z = \sqrt{\frac{\pi k_B T}{2k_0}}, \tag{10.22}$$

We thus can compute the probability $p(h)$ of having the spring elongated to $z = h$ as

$$p(h) = \frac{l_{bind}}{Z}\exp\left(\frac{-k_0 h^2}{2k_B T}\right). \tag{10.23}$$

With k_{on}^0 the reaction rate for binders separated by a distance $z < l_{bind}$, and considering $l_{bind} \ll l_b$ such that p is considered constant on $[h - l_{bind}, h + l_{bind}]$, the rebinding rate can be approximated as:

$$\boxed{k_{on}(h) = k_{on}^0 p(h) = k_{on}^0 \frac{2l_{bind}}{l_b Z}\exp\left(\frac{-k_0 h^2}{2k_B T}\right).} \tag{10.24}$$

Thus, our model is consistent with the law of mass action and the following chemical reaction:

$$\boxed{Binder(h) + Binder(h) \underset{k_{\text{off}}}{\overset{k_{\text{on}}(h)}{\rightleftharpoons}} Bond(h)} \tag{10.25}$$

which states that at a given s, only the binder with an elongation $h(s)$ can react to form a bond that bridges the separation $h(s)$ between the two vesicles. At the equilibrium the concentrations of bonds and binders in the patch obey

$$\frac{c_0 c_1}{c_2^2} = \exp\left(\frac{2\mu_2^0 - \mu_1^0}{k_B T}\right)\exp\left(\frac{-h^2}{x_\gamma^2}\right) \quad \text{in } (0, \hat{s}), \tag{10.26}$$

This equation has potential experimental implications. Indeed, suppose that the equilibrium concentrations $c_1(s)$ and c_2 are measured, e.g. using fluorescence microscopy. Suppose also that the tension and contact angle are measured. Then, it is possible to infer the distribution $h(s)$ in the adhesion patch and obtain an expression for the stiffness of the bonds k_0. Interestingly, this function can also be mapped out from single molecule stiffness measurement experiments. Thus, this theory can help us confront single molecule and large-scale collective measurements of adhesion molecules.

Final set of equations

Following the same procedure detailed in the previous chapter, see section 9.5, we obtain the following system of coupled advection-diffusion-reaction equations

$$\dot{c}_1 = D_1 c_1'' + k_{\text{on}} \exp\left(\frac{-h^2}{x_\gamma^2}\right) c_2^2 - k_{\text{off}}\, c_1 + D_1 \left(2c_1 \frac{hh'}{x_\gamma^2}\right)' \qquad \text{in } (0, \hat{s}), \tag{10.27}$$

$$\dot{c}_2 = D_2 c_2'' - k_{\text{on}} \exp\left(\frac{-h^2}{x_\gamma^2}\right) c_2^2 + k_{\text{off}}\, c_1 \qquad \text{in } (0, \hat{s}), \tag{10.28}$$

$$\dot{c}_2 = D_2 c_2'' \qquad \text{in } (\hat{s}, L_0), \tag{10.29}$$

where the diffusion constants are $D_i = k_B T/\eta_i$ and $x_\gamma = \sqrt{\frac{k_B T}{k_0}}$,

completed by the chemo-mechanical boundary/jump conditions

Boundary/jump conditions:

$\boxed{\text{at } s = 0}$

$$\left[2c_1 \frac{hh'}{x_\gamma^2} + c_1'\right]_{s=0} = 0, \qquad c_2'(0) = 0, \tag{10.30}$$

$\boxed{\text{at } s = \hat{s}}$

$$[\![c_2]\!] = 0, \qquad \left[\!\!\left[\frac{c_2'}{\eta_2}\right]\!\!\right] = 0, \qquad -D_1 \left[2c_1 \frac{hh'}{x_\gamma^2} + c_1'\right]_{s=\hat{s}} = c_1(\hat{s})\, \hat{v}, \tag{10.31}$$

$$k_B T\, c_1(\hat{s}) = 2T_c \left(1 - \cos\theta^{\text{equil}}(\hat{s})\right) \tag{10.32}$$

$\boxed{\text{at } s = L_0}$

$$c_2'(L_0) = 0. \tag{10.33}$$

Careful inspection shows that this chemical problem, the large-scale capillary mechanical problem, and the smaller-scale mechanical problem, are tightly coupled. The chemical problem is informed about the large-scale mechanical problem through $\theta^{\text{equil}}(\hat{s})$ and about the smaller-scale mechanical problem through $h(s)$. In turn, the smaller-scale mechanical problem needs $c_1(s)$ from the chemical problem and $\theta^{\text{equil}}(\hat{s})$ from the large-scale mechanical problem. All problems depend on the location of the interface, whose velocity is determined by the conditions at the interface.

Solving the problem

To solve the system of equations, we rescale the problem using the same time-dependent change of variables described in section 9.6. The small-scale mechanical problem is an equilibrium problem, and therefore the fact that the interface is moving does not play any role. Once $h(x)$ is obtained, as before we make the approximation $h(x) \approx h(s)$, and then apply the change of variables

to feed the result into the re-scaled chemical problem. The separation distance h can be rescaled on $[0, 1]$ as:

$$\delta(\eta, t) = h\left(\varphi(\eta, t), t\right), \tag{10.34}$$

and applying the chain rule, we have

$$\frac{\partial \delta}{\partial \eta} = \hat{s}(t)\frac{\partial h}{\partial s}, \qquad \frac{\partial^2 \delta}{\partial \eta^2} = \hat{s}^2(t)\frac{\partial^2 h}{\partial s^2}. \tag{10.35}$$

Using this rescaling we are able to solve the set of equations on a fixed interval $[0, 1]$.

10.3 Results and discussion

In this section, we examine how the stretching of the bonds affects the dynamics of the problem.

New equilibrium

Looking again at Fig. 10.2, we see that the profile of separation distance in the patch is such that the equation 10.31 dos not hold with the initial set of conditions defined as a starting point in section 9.7. In other words, the chemical potential of the bonds $\mu_1(h)$ is not uniform in the patch with uniform bond concentration. Thus at $F = 0$, the system evolves towards uniformization of $\mu_1(h)$. In Fig. 10.3, we see that the new quasi-equilibrium position of the interface and bond concentration are largely independent of the stiffness of the bond k_0. By quasi equilibrium we mean a state rapidly reached before eventual much slower dynamics. Nevertheless the bonds stiffness controls the extent of the zone in which the concentration of the bonds is not uniform i.e. the zone in which the separation distance is significantly large. As discussed in 10.1, this extension is related to the characteristic length $\ell_2 = \sqrt{\frac{T_c}{k_0 c_0}}$.

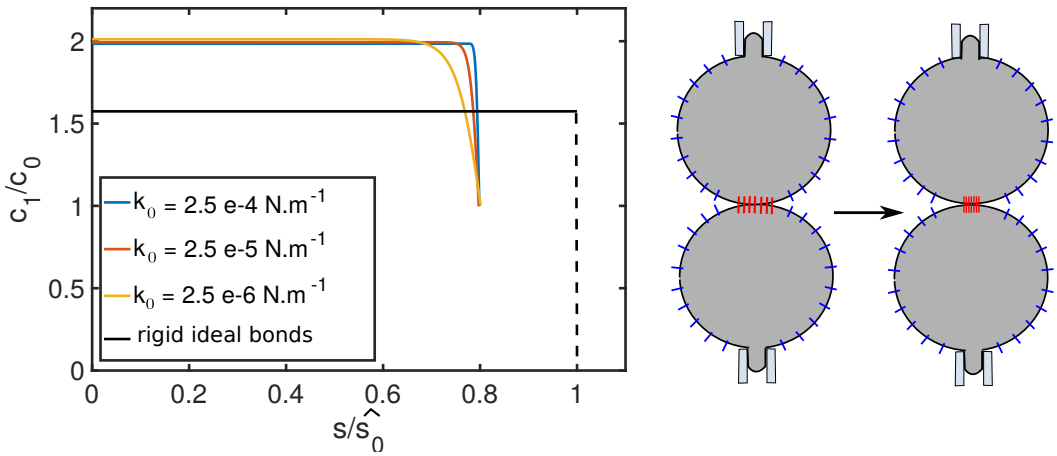

Figure 10.3: Profile of the concentrations of bonds in the adhesion patch after re-equilibration for different values of k_0. The initial profile of concentrations is given in black. The system evolved towards uniformization of the chemical potentials.

Diffusion-dominated regime

Considering the case of pure diffusion, for which $\tau_{reac} \gg \tau_{diff}$, we look at the effect of a pulling force on the system. To do so, we set $k_{off} = 0$ and $k_{on} = 0$ and we displace the equilibrium by applying a force F to the top of the vesicle. We update the Fig. 9.8(c) to compare the dynamics of rigid ideal bonds and that of compliant ideal bonds due to application of force. The results are given in Fig. 10.4. We see that, making bonds compliant increases the effect of "packing", due to the biased diffusion of the bonds: the stretched bonds diffused faster than the resting ones. For a given force F, the patch retracts to a smaller final size $\hat{s}_f$ for compliant bonds and the corresponding concentration in the center of the patch is also larger.

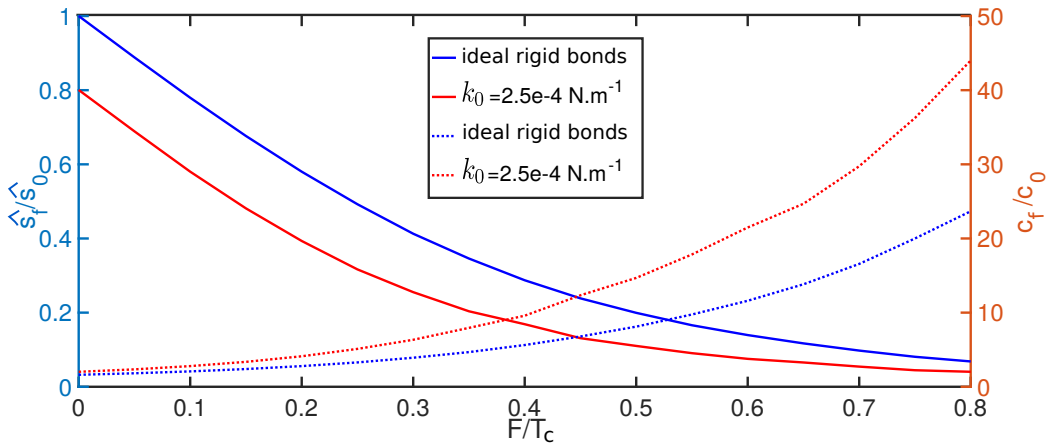

Figure 10.4: Final normalized concentration c_f/c_0 (dotted line) and final normalized position of the interface $\hat{s}_f/\hat{s}_0$ (solid line) as a function of the applied force. The curve corresponding to rigid bonds is also given in blue.

Diffusion-reaction regime

We now have a look at the influence of the rigidity of the bonds on the more general mixed diffusion-reaction case. To illustrate it, Fig. 10.5 describes the time evolution of the position of the interface for three different values of k_0. We see that the general behavior does not depend on the stiffness of the bonds. The difference appears when the size of the patch comes close to $\ell_2 = \sqrt{\frac{T_c}{k_0 c_0}}$. Then, the whole patch is affected by the applied force, the separation between the bonds is non-zero and $k_{on} < 1$ everywhere, making rebinding more difficult in the whole patch, and thus the adhesion patch dramatically fails. Thus the characteristic length ℓ_2 selects the instant when the adhesion finally fails. This effect is clearly visible in the figure inset.
This effect drifts the threshold in the lifetime of the patch as a function of the force. The softer the bonds are, the more unstable the patch is, see Fig. 10.6. We note that, because of the steepness of the relation between the lifetime and force, a relatively small change in the threshold can lead to a very large

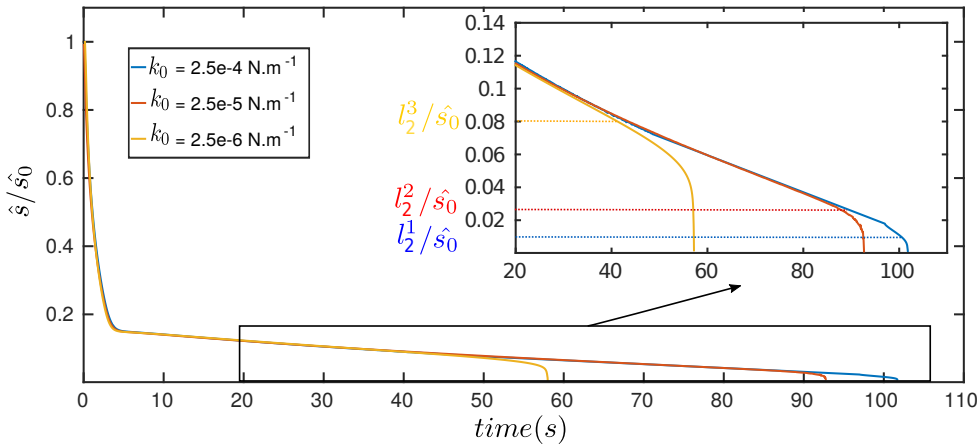

Figure 10.5: Time evolution of the normalized position of the interface $\hat{s}/\hat{s}_0$ for different values of k_0. (inset) Zoom on the last instants of the separation is given to illustrate how the system finally fail and how ℓ_2 selects when it fails.

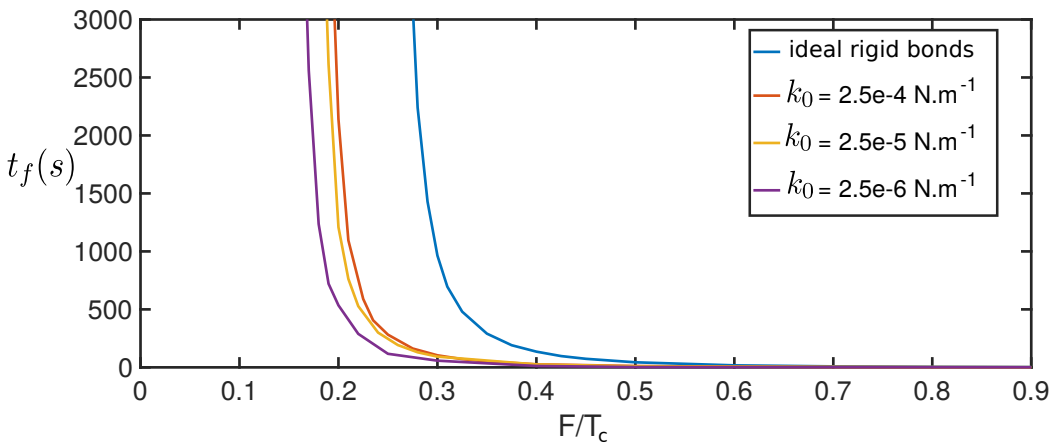

Figure 10.6: Lifetime of adhesion patch as a function of the applied force F/T_c for different values of k_0. The ideal rigid bonds is also given (blue plot).

change in the lifetime near the critical force. The dependence on bonds

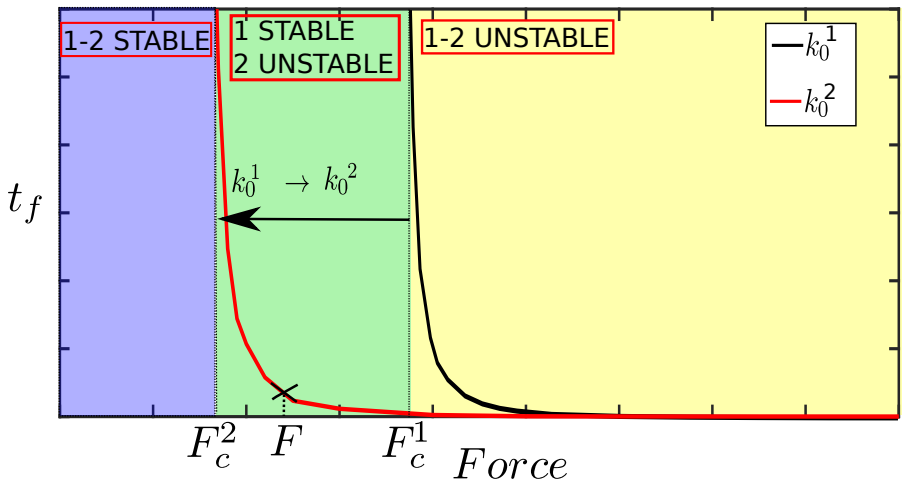

Figure 10.7: Simplified sketch of the proposed switching process for the system to pass from a stable mode to an unstable one: by changing the stiffness of the chemical bonds to change its stability.

stiffness of the strength of the patch could be another physical mechanism allowing cells to control adhesion. Both experimental and numerical studies, show a strong dependence of the stiffness of cadherins on the concentration of Ca^{2+} ions [Nagar et al., 1996, Sotomayor and Schulten, 2008]. The binding process also shows such a dependence [Pokutta et al., 1994]. The conformation of these molecules is affected by the presence of Ca^{2+} ions and thus their physical properties are affected. Moreover, studies also show the prominent role of calcium intracellular signaling in cell adhesion mediated by cadherins or integrins [Sheng et al., 2013]. Thus, calcium signaling could modify locally the rigidity of the bonds and their affinity to bind, and thus, switch from a stable patch to an unstable one. This could provide a mechanism for cells to easily switch from strong adhesion to weak adhesion in processes such as remodeling or cell migration. An illustration of this switching process is given in Fig. 10.7, where a patch with bonds of stiffness k_0^1 is stable under an applied force $F < F_c^1$. A change in the concentration of Ca^{2+} would change the stiffness of the bonds such as a softening $k_0^1 \rightarrow k_0^2$, reducing the critical

force such that $F > F_c^2$, driving the patch towards instability.

Chapter 11

Binding/unbinding dynamics with compliant slip bonds

Most biological bonds exhibit force-dependent unbinding kinetics. The experimental characterization and theoretical modeling of such force-sensitivity has been a major theme of research over the last decades [Bell, 1978a, Evans and Ritchie, 1997]. in this chapter we discuss the most general form of force-sensitivity, that of slip bonds following Bell's law, for references see section 3.1. In particular we explore how to introduce the Bell's law in the thermodynamically consistent framework based on Onsager's variational principle. We present results about the effect of force-sensitivity in the unbinding rate. In Fig.11.1, we recall the slip bond effect. In this picture the applied force tilts the energy landscape and accelerates the dissociation of the non-covalent receptor-ligand bond by modifying the height of the barrier at $x = x_b$, leading to the force-dependence of the unbinding rate $k_{off} = k^0_{off} e^{\frac{F}{F_\beta}}$, with $F_\beta = \frac{k_B T}{x_b}$ [Bell, 1978a]. Based on this definition of a slip bond, the next section 11.2 examines and discusses different approaches to include this effect in the Onsager's variational framework we detailed in the previous chapters.

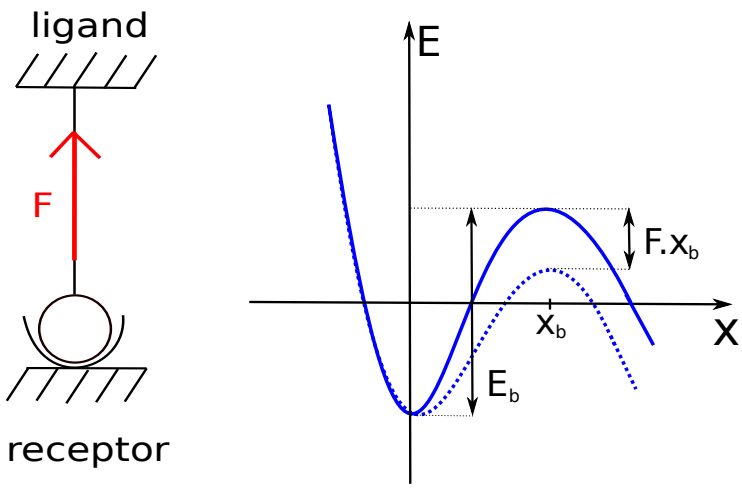

Figure 11.1: Schematic representation of the energy landscape for receptor-ligand interaction. The solid blue curve represents the energy landscape for an unstressed bond and the dotted blue line corresponds to the modified energy landscape in the case of an applied force F, which lowers the energy barrier at a rate controlled by x_b.

11.1 Modeling the slip bond complex as a spring and a slip bond

A slip bond can be seen as a combination in series of two springs: the "tail" of the binder of stiffness k_0 and a molecular complex acting like the slip bond itself with a stiffness k_{slip}, which is the reacting part of the molecule. A schematic view is given in Fig. 11.2. If we consider the stiffness of the slip bond $k_{slip} \gg k_0$, we can approximate the stiffness of the complex k as: $k \sim k_0$. Thus, the force F exerted by the vesicle to a bond is transmitted through the spring to the slip bond and affects its energy landscape of unbinding by reducing its transition barrier by $\frac{F}{F_\beta} k_B T$.
According to our model, at any position s in $[0, \hat{s}]$, is assigned a separation $h(s)$, such as the bond at s is stretched by $h(s)$ from its rest position. As the force is transmitted to the slip bond, we can state that the force exerted on

the bond is $F(s) = k_0 h(s)$. Thus we can re-write the change in the energy of the barrier as $\frac{h(s)}{x_\beta} k_B T$ with $x_\beta = F_\beta / k_0$. Eventually, according to Bell's law, the unbinding rate k_{off} can be written as a function of $h(s)$ as :

$$k_{off}(h(s)) = k^0_{off} \exp \frac{h(s)}{x_\beta} \tag{11.1}$$

In the next section 11.2, we review the different options available from the Onsager's variational principle to obtain this unbinding rate, which in principle can only be based on:

1. Modifying the free energy $\mathcal{F}(Z)$ of the system,
2. Modifying the kinetics only with a different structure for $\bar{k}$,
3. Adding a power input $P_{tilt}(W)$ to the system,
4. Modifying the dissipation potential $\mathcal{D}_{reac}(Z; W)$ associated to the reaction.

11.2 Modeling slip bonds with Onsager's principle

Through the free energy

A first way to introduce the change in the barrier height would be to see the decrease of the transition barrier as a force-dependent increase of the energy of the bonds, which would bias the system towards dissociation. The first approach considered would thus be to suppose that μ^0_1 is an affine function of h as:

$$\mu^0_1(h) = \bar{\mu}_1(h) + k_0 h x_b = \bar{\mu}_1(h) + k_B T \frac{h}{x_\beta}, \tag{11.2}$$

with $\bar{\mu}_1(h)$ the chemical potential of a compliant ideal bond given by Eq.(10.6). At first sight, this modeling choice seems to lead to the right form of k_{off}.

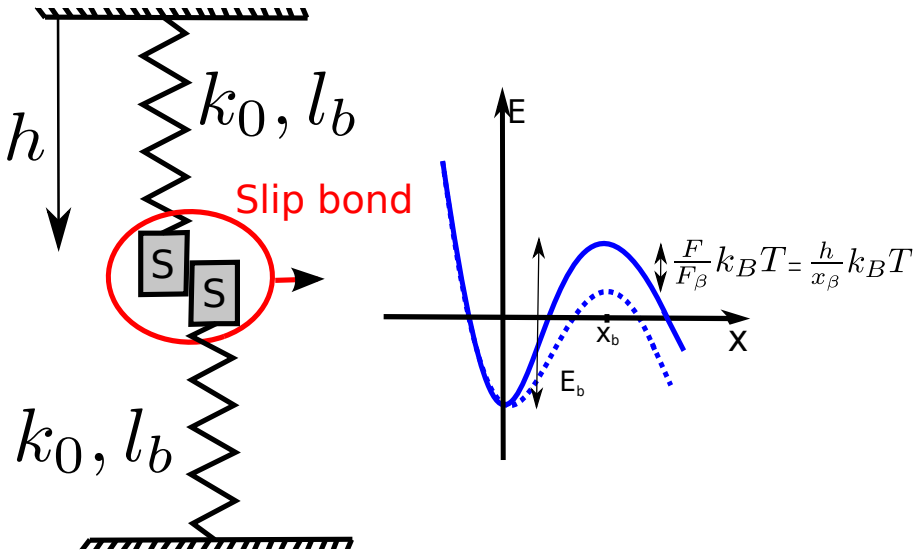

Figure 11.2: Schematic representation of the slip bond complex as a combination of two springs and a slip bond in series.

Indeed, recalling Eq. (10.15) we find that

$$k_{\text{off}} = k^0_{\text{off}} \exp\left(\frac{h}{x_\beta}\right), \qquad \text{with} \quad k^0_{\text{off}} = k \exp\left(\frac{\bar{\mu}_1 - 2\mu^0_2}{k_B T}\right), \tag{11.3}$$

with $x_\beta = \frac{k_B T}{k_0 x_b}$. Recalling the definition of F_β given previously, we conclude that this result is in agreement with Bell's law.

However this modeling choice also biases the diffusion of bonds. Recalling Eq. (10.12), we now have:

$$\boxed{w_1 = -\frac{1}{\eta_1}\mu_1'(h) = -\frac{1}{\eta_1}\bar{\mu}_1'(h) - \frac{k_B T}{\eta_1}\frac{h'}{x_\beta} \quad \text{in} \quad (0, \hat{s}).} \tag{11.4}$$

Thus this modeling choice adds a new force dependence on diffusion. This additional force-sensitivity on the diffusion of the bonds, different from that resulting from the bond compliance, captured by the term $-\frac{1}{\eta_1}\bar{\mu}_1'(h)$,

and studied in the previous chapter, does not seem physically meaningful. Indeed, the applied force lowers the barrier for thermally activated unbinding transitions but does not change the free energy of bonds, other than by the storage of elastic energy already studied in the previous chapter. Including this linear tilt in the chemical potential (last term in Eq. (11.2)) seems to "work" to capture the right reaction kinetics, but since the chemical potential also drives diffusion, we get a spurious bias to diffusion. Modifying the energy of the unbound state would also give the desired rate but would lead to another bias in the diffusion. Thus, modifying the energy of the bonds or the free binders appears to be a dead end because the chemical potential drives both reaction and diffusion.

Through $\bar{k}$

The previous remarks suggest to introducing force-sensitivity in a way that affects only reaction kinetics and not diffusion. A straightforward way to do so would be to modify directly the general structure $\bar{k}$ as:

$$\bar{k} = k \frac{\exp\left(\frac{2\mu_2}{k_B T}\right) - \exp\left(\frac{\mu_1(h)}{k_B T}\right) c_1}{2\mu_2 - \mu_1(h)}, \tag{11.5}$$

Consider the following choice:

$$\bar{k} = k \frac{c_2^2/c_0 \exp\left(\frac{-h^2}{x_\gamma^2}\right) - \exp\left(\frac{h}{x_\beta}\right) \exp\left(\frac{\mu_1^0 - 2\mu_2^0}{k_B T}\right) c_1}{\mu_2 - \frac{1}{2}\mu_1(h)}, \tag{11.6}$$

where $k > 0$ is a rate constant. This modeling choice would also give us the desired unbinding rate. But a direct calculation shows that

$$\bar{k} = \frac{2kc_0}{k_B T} \exp\left(-\frac{2\mu_2^0}{k_B T}\right) \exp\left(-\frac{h^2}{x_\gamma^2}\right) \frac{\exp\left(\frac{2\mu_2}{k_B T}\right) - \exp\left(\frac{h}{x_\beta}\right) \exp\left(\frac{\mu_1(h)}{k_B T}\right)}{\frac{2\mu_2}{k_B T} - \frac{\mu_1(h)}{k_B T}}, \tag{11.7}$$

which cannot be guaranteed to always be positive. Thus, this choice for $\bar{k}$ does not ensure the modeling to be thermodynamically consistent since the rate of

reaction could either dissipate or pump energy into the system depending on the state.

Through a power input

One last idea would be to consider the tilting of the energy landscape with a power input $P_{tilt}(W)$ in the problem acting directly on the net rate of unbinding r as:

$$P_{tilt} = \frac{1}{2}\int_0^{\hat{s}} r k_0 h x_b \, ds = \frac{1}{2}\int_0^{\hat{s}} k_B T \frac{h}{x_\beta} r \, ds \tag{11.8}$$

This way, applying the Onsager's variational principle we obtain, minimizing the Rayleighian with respect to r:

$$r = \bar{k}\left(\mu_2 - \frac{1}{2}\mu_1(h) - \frac{1}{2}k_B T \frac{h}{x_\beta}\right). \tag{11.9}$$

Considering the following choice for $\bar{k}$:

$$\bar{k} = k\frac{c_2^2/c_0 \exp\left(-\frac{h^2}{x_\gamma^2}\right) - \exp\left(\frac{\mu_1^0 + k_B T h/x_\beta - 2\mu_2^0}{k_B T}\right) c_1}{\mu_2 - \frac{1}{2}\mu_1(h) - \frac{1}{2}k_B T h/x_\beta}, \tag{11.10}$$

where $k > 0$ is a rate constant, a direct calculation shows that

$$\bar{k} = \frac{2kc_0}{k_B T}\exp\left(-\frac{2\mu_2^0}{k_B T}\right)\exp\left(-\frac{h^2}{x_\gamma^2}\right)\frac{\exp\left(\frac{2\mu_2}{k_B T}\right) - \exp\left(\frac{\mu_1(h) + k_B T h/x_\beta}{k_B T}\right)}{\frac{2\mu_2}{k_B T} - \frac{\mu_1(h) + k_B T h/x_\beta}{k_B T}}, \tag{11.11}$$

which is clearly positive as required by the second law of thermodynamics. Plugging Eq. (11.10) into Eq. (11.9), we obtain

$$\boxed{r = k_{\text{on}}^0 \exp\left(-\frac{h^2}{x_\gamma^2}\right) c_2^2 - k_{\text{off}}^0 \exp\left(\frac{h}{x_\beta}\right) c_1 \quad \text{in} \quad (0, \hat{s}),} \tag{11.12}$$

where

$$\boxed{k_{\text{on}} = \frac{k}{c_0}\exp\left(-\frac{h^2}{x_\gamma^2}\right) \quad \text{and} \quad k_{\text{off}} = k\exp\left(\frac{\mu_1^0 - 2\mu_2^0}{k_B T}\right)\exp\left(\frac{h}{x_\beta}\right)}. \tag{11.13}$$

Thus, biasing the energy landscape towards the unbinding reaction through a power input allows us to obtain the desired structure for the rates. However, this approach is not fully satisfactory. Indeed, a generic calculation shows that

$$\dot{\mathcal{F}}(Z, W) + \mathcal{P}(W) = -\mathcal{D}(W) \tag{11.14}$$

Although in most cases $\mathcal{P}(W)$ will be positive, this cannot be guaranteed and thus this approach does not ensure the decrease of the free energy along the dynamics. It is clear that we bias the system towards unbinding reaction in a force-dependent manner, but this bias is internal to the system and thus, the interpretation of this power input in the global energy balance is unclear. The previous results suggest that:

- The effect of the force should not be included in the free energy because it would drive diffusion of one of the species.
- It is not possible to introduce the slip bond effect through a state dependent coefficient $\bar{k}$ and guarantee a positive dissipation rate.
- Introducing the slip bond effect through a power input leads to the correct equations, but the physical interpretation is unclear since the free energy can no longer be guaranteed to be decreasing during the dynamics.

Up to now, we have not attempted to modify the dissipation potential to obtain the slip bond effect. This effect could appear from an interaction with the spring in a natural way by considering a more general set of state variables including the separation h and through an appropriately constructed dissipation potential of the form:

$$\mathcal{D}(r, \dot{h}) = \frac{1}{2}\begin{pmatrix} r & \dot{h} \end{pmatrix}\begin{pmatrix} \bar{k}^{-1} & \eta \\ \eta & \nu \end{pmatrix}\begin{pmatrix} r \\ \dot{h} \end{pmatrix}, \tag{11.15}$$

with ν characterizing the viscous friction opposing to change in separation h, due to the surrounding fluid for example, and η characterizing the coupling between elongation of the bond and reaction. To relate to our previous models, ν should be chosen very small, and to ensure that the problem is thermodynamically consistent, we need the following relation to be verified:

$$\frac{\nu}{\bar{k}} - \eta^2 > 0 \tag{11.16}$$

A more detailed discussion about this last approach is given in the Appendix C, using a more simple set-up, considering fixed adhesion molecules attached between two rigid plates.

11.3 Final system of equations

Considering the previous observations, we use the definition of slip bonds through a power input, which has its drawbacks but has the advantage to provide the expected dependence on h of the chemical rates. Using this definition, we obtain the following system of equations:

$$\dot{c}_1 = D_1 c_1'' + k_{\text{on}}^0 \exp\left(\frac{-h^2}{x_\gamma^2}\right) c_2^2 - k_{\text{off}}^0 \exp\left(\frac{h}{x_\beta}\right) c_1 + D_1 \left(\frac{2c_1 h h'}{x_\gamma^2}\right)' \quad \text{in } (0, \hat{s}), \tag{11.17}$$

$$\dot{c}_2 = D_2 c_2'' - k_{\text{on}}^0 \exp\left(\frac{-h^2}{x_\gamma^2}\right) c_2^2 + k_{\text{off}}^0 \exp\left(\frac{h}{x_\beta}\right) c_1 \quad \text{in } (0, \hat{s}), \tag{11.18}$$

$$\dot{c}_2 = D_2 c_2'' \quad \text{in } (\hat{s}, L_0), \tag{11.19}$$

with respect to the following boundary conditions

$\boxed{\text{at } s = 0}$

$$\left[\frac{2c_1 hh'}{x_\gamma^2} + c_1'\right]_{s=0} = 0, \qquad c_2'(0) = 0, \tag{11.20}$$

$\boxed{\text{at } s = \hat{s}}$

$$[\![c_2]\!] = 0, \qquad \left[\!\!\left[\frac{c_2'}{\eta_2}\right]\!\!\right] = 0, \qquad -D_1\left[\frac{2c_1 hh'}{x_\gamma^2} + c_1'\right]_{s=\hat{s}} = c_1(\hat{s})\,\hat{v}, \tag{11.21}$$

$$k_B T\, c_1(\hat{s}) = 2T_c\left(1 - \cos\theta^{\text{equil}}(\hat{s})\right) \tag{11.22}$$

$\boxed{\text{at } s = L_0}$

$$c_2'(L_0) = 0. \tag{11.23}$$

These equations need to be solved in conjunction with mechanical equations resulting from the large-scale capillary problem and for the small-scale problem in the vicinity $s \sim \hat{s}$.

11.4 Results and discussion

Reaction-diffusion

The previous section illustrated the fact that the slip bond effect only affects the reaction and not the diffusion. Thus, the purely diffusive case will not be affected by a change in the nature of the bond (ideal or slip). Thus, let us have a look at how the reaction-diffusion case is affected by the change in the reaction. To illustrate this effect, we update Fig. 10.6 for slip bonds. The updated version is given in Fig. 11.3

As observed for the case of ideal compliant bonds, the change in the nature of the bonds modifies the strength of the patch and, for slip bonds and at

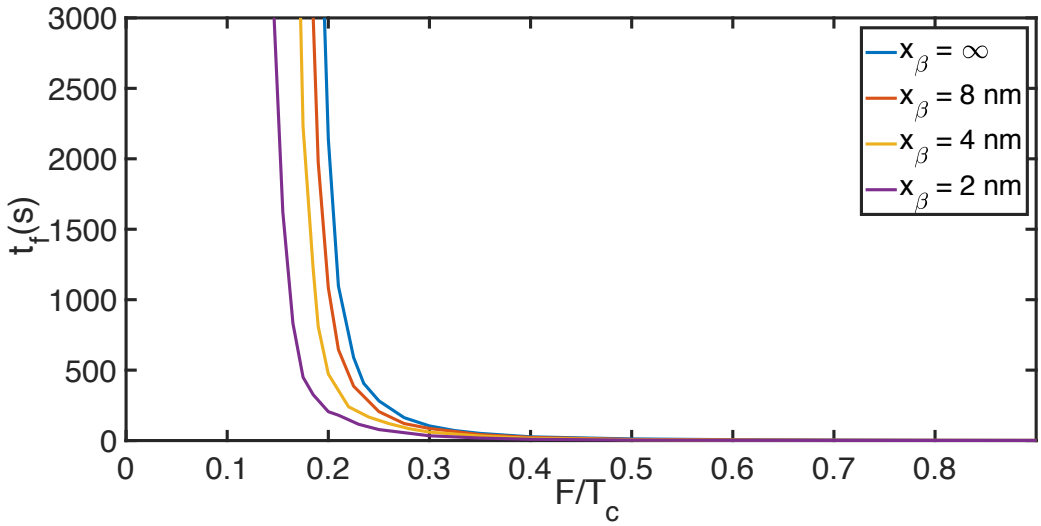

Figure 11.3: Lifetime of adhesion patch as a function of the applied force F/T_c for different values of x_β and $k_0 = 2.5 \cdot 10^{-4}$ N·m^{-1}. The blue curve corresponds to the previous case considering ideal compliant bonds.

a given force F, shifts the critical force towards more instability. As Ca^{2+} concentration is thought to tune the affinity and the stiffness of the bonds, it also tunes the nature of the bond itself: by modifying its conformation, the bond can switch between different behaviors: ideal, slip and catch. This is supported by different studies [Rakshit et al., 2012, Sivasankar, 2013]. Thus, similarly to the switching process illustrated in Fig. 10.7, a change in the concentration of ions could make the adhesion patch switch between stability and instability. Despite these quantitative changes in the critical force, which can lead to very strong changes in lifetime near the critical force, we did not find qualitatively different behaviors between slip compliant bonds and ideal compliant bonds for the problem considered here. In a different context, like clutch model for mechanosensitivity [Elosegui-Artola et al., 2016] or the tear-out behavior detailed next, the slip bond nature of the bonds could lead to much more significant changes on the dynamics.

Tear-out

We end this chapter by examining the tear-out scenario [de Gennes et al., 2003], in which, if reaction are sufficiently fast as compared to diffusion, the shrinking of the adhesion patch under force should be the result of the progressive breaking of bonds very much like unbinding from a solid substrate with immobile receptors. However, faster kinetics can also mean faster rebinding in the case of ideal bonds. The tear-out scenario is eased by the slip bond behavior, which can increase the unbinding rate very significantly near the rim of the adhesion patch due to the uneven force distribution in the patch. To study the case where reaction dominates the dynamics, for which $\tau_{reac} \ll \tau_{diff}$, we set $k^0_{off} = 1000\ \mathrm{s}^{-1}$ and keeping the same diffusion constants. To look at this extreme case, we also choose $x_\gamma = 2$ nm for the slip bonds, such that bonds are very sensitive to the transmitted force and $h(\hat{s}) > x_\beta$. To probe this case, we apply a ramp of force on the top of the vesicle and we look at the resulting dynamics. A series of snapshots capturing the evolution of the size of the patch and the concentration of bonds is given in Fig. 11.4(a). It shows a fast transition at small time-scales and then, a linear dependence with time of the position of the interface.

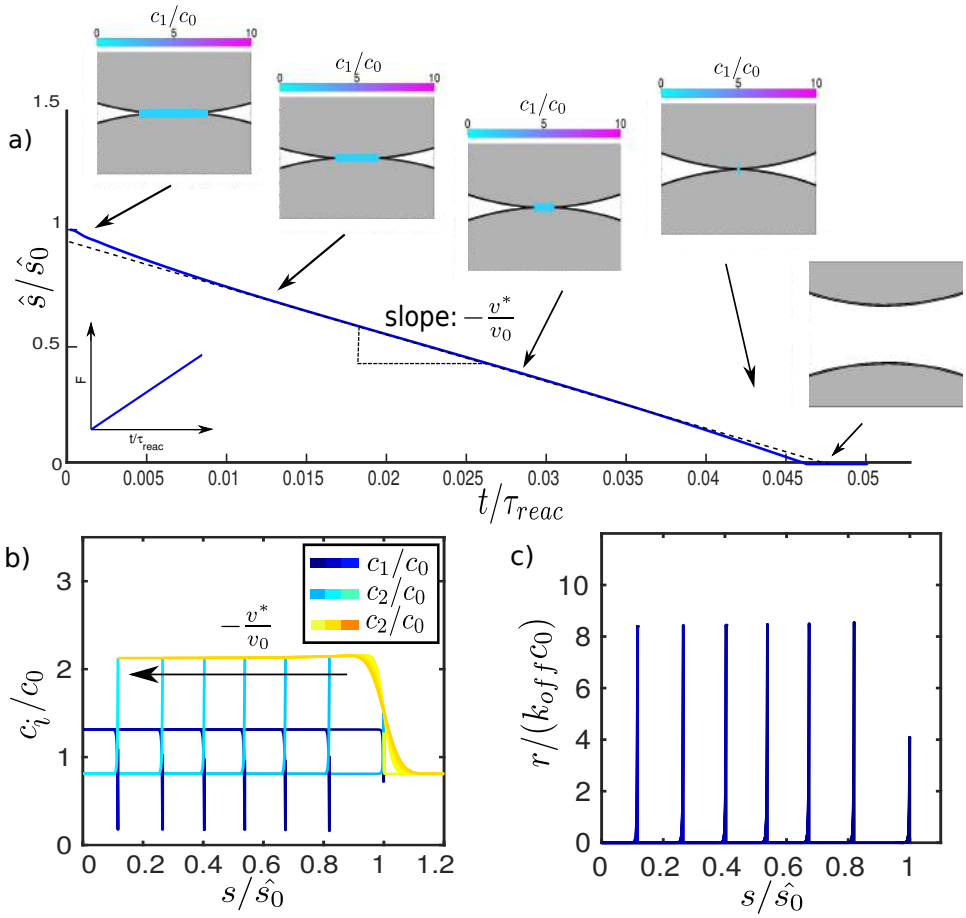

Figure 11.4: a) Time evolution of the normalized position of the interface $\hat{s}/\hat{s}_0$ while imposing a ramp of force such as $F(t)/T_c = 6.5 \cdot 10^{-2}\, t/\tau_{reac}$. The time evolution of F is given as an inset. A series of snapshots of the adhesion patch at different instants during the dynamics illustrate the change in concentration of bonds as the change in size of the patch. The dashed line is give as an illustration of the linear dependence of $\hat{s}$ with time . The slope of the dashed line is $-v^*/v_0$ with $v_0 = \hat{s}_0/\tau_{reac}$. b) Profiles of normalized concentration of bonds c_1 and binders c_2 in the patch and outside of the patch at different instants. Clearer colors indicate later times. c) Profiles of the unbinding rate $r(s/\hat{s}_0)$ on the patch at different instants. Clearer colors indicate later times.

This is also illustrated in Fig. 11.4(b) and Fig. 11.4(c), where we see that the concentration of bonds at the interface and the bond breaking rate appear to exhibit a well defined travelling profile. The linear dependence can be approximated by a linear function with a slope v^*/v_0, where v_0 is a characteristic speed such as $v_0 = \hat{s}^0/\tau_{reac}$. Along the dynamics, the figure shows that the concentration in the patch is not affected by the tearing process: the bonds break before they have time to diffuse in a region of the patch where their transmitted force is lower. There is propagation of local breaking at $s = \hat{s}$, with no large-scale diffusion of bonds and only a noticeable diffusion of free binders c_2 at $s = \hat{s}$. Thus, we obtain a behavior that looks like a classic tear-out, as we would observe in the case of immobile bonds [Prechtel et al., 2002, Pierrat et al., 2004b]. However, in contrast with the classical tear-out, here diffusion should play a role. Indeed, the time-scale of diffusion $\tau_{diff} = \frac{\ell}{2D_1}$ is strongly size-dependent. Thus, even if at the length-scale of the whole patch ($\ell = \hat{s}^0$) $\tau_{reac} \ll \tau_{diff}$, there should be a small length scale for which $\tau_{reac} \sim \tau_{diff}$. Following this reasoning, even if reaction should normally dominate the dynamics of the system, there should be a small region near the edge of the adhesion patch where it competes with diffusion of bonds. The interesting question is if this small-scale diffusion has macroscopic consequences, e.g. in the velocity of propagation as suggested by Eq. (11.21). To interrogate these ideas with our model, we examined the influence of bond diffusivity on the tear-out dynamics, see Fig 11.5. According to the theory, the length-scale L_p where the bond concentration is locally perturbed because of diffusion close to $s = \hat{s}$ should increase with D_1. Our results, reported on the figure, are consistent with this prediction.

To study this effect more systematically, we consider a simplified set-up where we uncouple the vesicle mechanics with the micromechanics and the chemistry by fixing the angle $\theta = \theta_0$ and the tension T_c at $s = \hat{s}$, as illustrated in Fig. 11.6(a). Thus, in this problem, the mechanical driving force is constant, see Eq. (11.22). In Fig. 11.6(b), we represent the time evolution of the position of the interface for different values of the diffusion constant D_1 (with

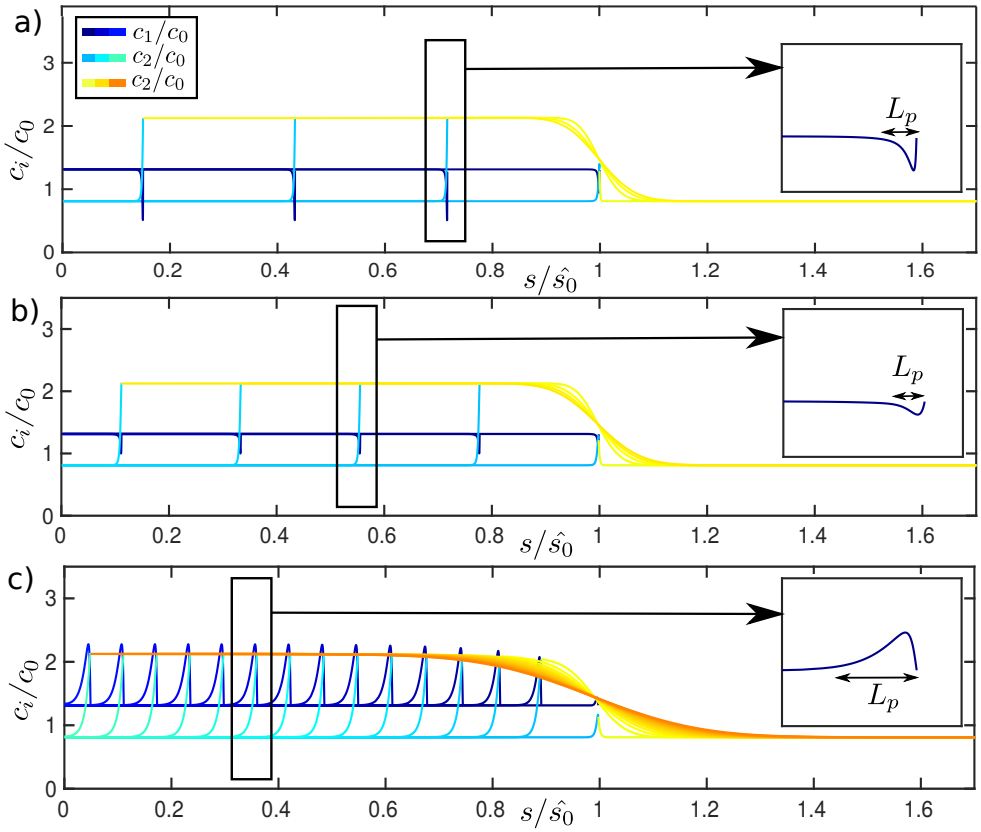

Figure 11.5: Series of plots of the profile of normalized concentration of bonds c_1 and binders c_2 in the patch and outside of the patch at different instants during propagation. Clearer colors indicate later times. The local shape of the propagating profile of concentration near $s = \hat{s}$ is given in the right corner and its size is denoted L_p. $D_1^0 = 0.5\ \mu\text{m}^2\cdot\text{s}^{-1}$. a) $D_1 = 5D_1^0$. b) $D_1 = 15D_1^0$. c) $D_1 = 45D_1^0$.

$D_2 = 2D_1$), providing an effective kinetic law for the tear-out process. From these results, we compute the slope v^*/v_0 for each value of D_1. Fig. 11.6(c) shows the systematic dependence of velocity v^* and extent of the diffusion zone L_p on the diffusion constant of bonds D_1. The figure shows that the propagation velocity decreases with increasing D_1, whereas increasing D_1

leads to a larger diffusion zone. During the propagation of the stationary profile, local transport by diffusion must keep up with the propagation velocity. It is therefore natural that larger L_p requires more time for diffusive transport, and hence can only be compatible with a slower propagation velocity. This study shows a strong observable effect of small-scale (hence fast) diffusion in this nominally reaction-dominated tear-out regime. This behavior is a new kind of tear-out decohesion distinct from classical tear-out for immobile bonds on a solid substrate, which is independent of membrane fluidity, whereas the behavior reported here is not since fluidity determines bond mobility. These results suggest that a pure tear-out process independent of bond diffusion in adhesion mediated by mobile binders is impossible unless L_p becomes very small, in the nanometer range, where our theory breaks down. These results also highlights the subtility of adhesion mediated by mobile binders. We finally note that one could seek for the traveling wave solutions to the chemo-mechanical equations that result from fixing θ_0 and T_c^0. By performing the change of variables $c_i(s,t) = \bar{c}_i(s + v^* t)$, where $\bar{c}_i$ are time-independent stationary solutions, one realizes that the resulting system is a set of stationary advection-diffusion equations coupled to the small-scale mechanical model, whose analytical solution or even qualitative analysis is far from obvious.

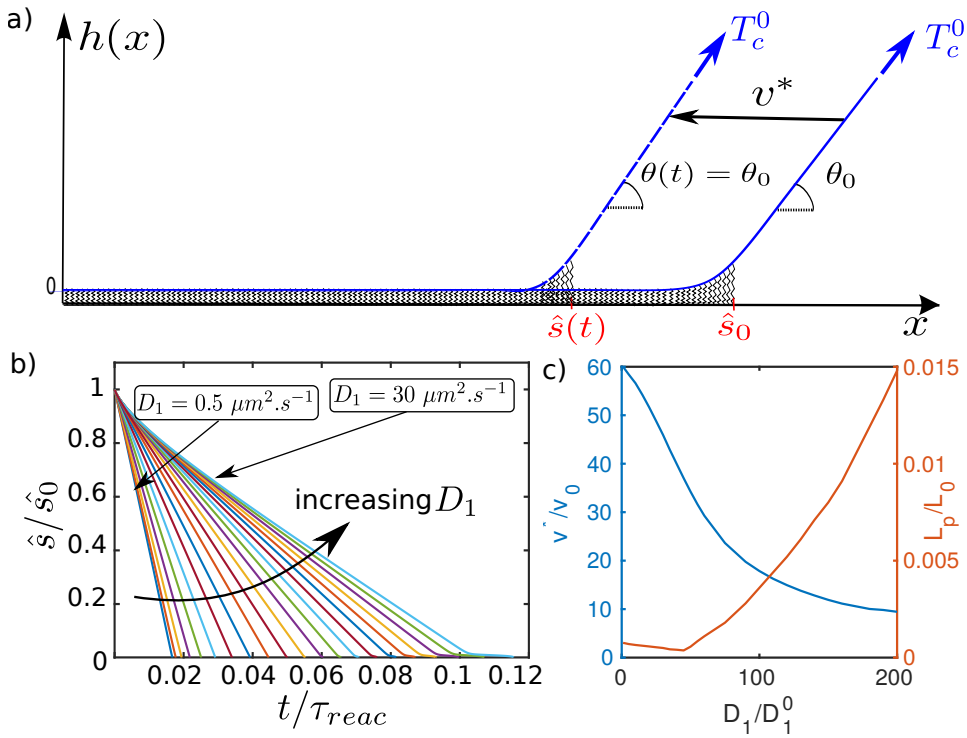

Figure 11.6: a) Simplified problem with a constant driving force set by a fixed angle $\theta = \theta_0$ and tension $T_c = T_c^0$. b) Time evolution of the normalized position of the interface $\hat{s}/\hat{s}_0$ for an applied ramp of forces. the different curves show the dependence on the diffusion constant D_1. c) Normalized speed of the interface v^*/v_0 (blue curve) and normalized size of the propagating structure L_p/L_0 (red curve) as a function of the diffusion constant D_1/D_1^0. $D_1^0 = 0.5\ \mu\text{m}^2\cdot\text{s}^{-1}$.

Chapter 12

Discussion about the crowded limit

In the previous section we assumed that the dilute limit was valid, that is to say, $c_1 \ll c_{max}$ and $c_2 \ll c_{max}$. This assumption may break down. Actually, for usual vesicle membranes and adhesion molecules of the size of E-cadherins, the maximum possible concentration is of about $c_{max} = 50000\,\text{mol}\cdot\mu\text{m}^2$=20 c_0 [Pontani et al., 2016]. It is possible to modify the available space for the molecules on the membrane by adding some non-interacting molecules on the vesicles. Thus, by modifying the concentration of such molecules, the maximum concentration c_{max} can be reduced. The overcrowding of the vesicle limits the diffusion as it limits the available space for a molecule to move on the membrane, but at a given s, the binding/unbinding kinetics is not affected by the level of crowding of its surrounding. However, if crowding severely limits the ability of the system to evolve by bond motion, then it may lead to a change in behavior dominated by reaction.
In order to verify these statements and to study the influence of an overcrowding of molecules on the membrane, we relax the dilute-limit assumption in the present section.

12.1 Considering a maximum concentration c_{max}

Considering a capillary free energy contribution, the potential for the force applied by the loading device and a more general expression for entropy of bonds, based on Flory-Huggins theory, that includes the entropy of the adhesion molecules and the entropy of the free space on the membrane, the chemo-mechanical free energy is

$$\begin{aligned}\mathcal{F}(Z) = {} & T_c \cdot L(\theta,\beta,\hat{s}) - F \cdot H(\theta,\beta,\hat{s}) \\ & + \frac{k_B T}{2}\int_0^{\hat{s}} c_1 \left(\log\frac{c_1}{c_0}+1\right) ds + \frac{1}{2}\int_0^{\hat{s}} \mu_1^0 c_1\, ds + \frac{1}{2}\int_0^{\hat{s}} k_0 h^2 c_1\, ds \\ & + k_B T \int_0^{\hat{s}} c_2 \log\frac{c_2}{c_0}\, ds + \int_0^{\hat{s}} \mu_2^0 c_2\, ds \\ & + k_B T \int_0^{\hat{s}} (c_{max}-c_1-c_2)\log\left(\frac{c_{max}-c_1-c_2}{c_{max}}\right) ds \\ & + k_B T \int_{\hat{s}}^{L_0} c_2 \log\frac{c_2}{c_0}\, ds + \int_{\hat{s}}^{L_0} \mu_2^0 c_2\, ds \\ & + k_B T \int_{\hat{s}}^{L_0} c_2\,(c_{max}-c_2)\log\left(\frac{c_{max}-c_2}{c_{max}}\right) ds \end{aligned} \tag{12.1}$$

We can check that, in the dilute limit (i.e. $\frac{c_1+c_2}{c_{max}} \ll 1, \frac{c_2}{c_{max}} \ll 1$), to first order in $\frac{c_1+c_2}{c_{max}}$ and $\frac{c_1}{c_{max}}$, the free energy simplifies to :

$$\begin{aligned}\mathcal{F}(Z) = {} & T_c \cdot L(\theta,\beta,\hat{s}) - F \cdot H(\theta,\beta,\hat{s}) \\ & + \frac{k_B T}{2}\int_0^{\hat{s}} c_1 \left(\log\frac{c_1}{c_0}-1\right) ds + \frac{1}{2}\int_0^{\hat{s}} \mu_1^0 c_1\, ds + \frac{1}{2}\int_0^{\hat{s}} k_0 h^2 c_1\, ds \\ & + k_B T \int_0^{\hat{s}} c_2 \left(\log\frac{c_2}{c_0}-1\right) ds + \int_0^{\hat{s}} \mu_2^0 c_2\, ds \\ & + k_B T \int_{\hat{s}}^{L_0} c_2 \left(\log\frac{c_2}{c_0}-1\right) ds + \int_{\hat{s}}^{L_0} \mu_2^0 c_2\, ds, \end{aligned} \tag{12.2}$$

which are precisely the expression for the free energy of the model previously used, see Eq. (10.3).

12.2 Deriving the dynamics from Onsager's variational principle

Minimization of the free energy $\mathcal{F}$ with respect to Z subject to the area constraint yields the equilibrium equations for Z and P. Alternatively, these equations can be written abstractly by making the Lagrangian stationary with respect to $\bar{Z}$ as

$$0 = \frac{d\mathcal{L}}{dt} = D_{\bar{Z}}\mathcal{L}(\bar{Z}) \cdot \mathcal{P}(\bar{W}) \quad \forall \bar{W}. \tag{12.3}$$

To obtain these equations, we calculate the variation of the Lagrangian

$$\begin{aligned}
D_{\bar{Z}}\mathcal{L}(\bar{Z}) \cdot \mathcal{P}(\bar{W}) = {} & \left[T_c\, \partial_\theta L(\theta,\beta,\hat{s}) - F\, \partial_\theta H(\theta,\beta,\hat{s}) - P\, \partial_\theta A(\theta,\beta,\hat{s})\right] \omega \\
& + \left[T_c\, \partial_\beta L(\theta,\beta,\hat{s}) - F\, \partial_\beta H(\theta,\beta,\hat{s}) - P\, \partial_\beta A(\theta,\beta,\hat{s})\right] \gamma \\
& + \left[A(\theta,\beta,\hat{s}) - A_0\right] Q \\
& + \frac{1}{2}\int_0^{\hat{s}} \left(k_B T \log\left(\frac{c_{max}^2 c_1}{c_0(c_{max}-c_1-c_2)^2}\right) + \mu_1^0 + k_0 h^2\right) \dot{c}_1 ds \\
& + \int_0^{\hat{s}} \left(k_B T \log\left(\frac{c_{max} c_2}{c_0(c_{max}-c_1-c_2)}\right) + \mu_2^0\right) \dot{c}_2 ds \\
& + \int_{\hat{s}}^{L_0} \left(k_B T \log\left(\frac{c_2 c_{max}}{c_0(c_{max}-c_2)}\right) + \mu_2^0\right) \dot{c}_2 ds \\
& + \left[T_c\, \partial_{\hat{s}} L(\theta,\beta,\hat{s}) - F\, \partial_{\hat{s}} H(\theta,\beta,\hat{s}) - P\, \partial_{\hat{s}} A(\theta,\beta,\hat{s})\right] \hat{v} \\
& + \frac{1}{2}\left[c_1\left(k_B T \log\left(\frac{c_{max}^2 c_1}{c_0(c_{max}-c_1-c_2)^2}\right) + \mu_1^0 + k_0 h^2\right)\right]_{s=\hat{s}^-} \hat{v} \\
& + \frac{k_B T}{2}\left[c_1\right]_{s=\hat{s}^-} \hat{v} \\
& + \left[c_2\left(k_B T \log\left(\frac{c_{max} c_2}{c_0(c_{max}-c_1-c_2)}\right) + \mu_2^0\right)\right]_{s=\hat{s}^-} \hat{v} \\
& + \left[c_{max} k_B T \log\left(\frac{c_{max}-c_1-c_2}{c_{max}}\right)\right]_{s=\hat{s}^-} \hat{v} \\
& - \left[c_2\left(k_B T \log\left(\frac{c_{max} c_2}{c_0(c_{max}-c_2)}\right) + \mu_2^0\right)\right]_{s=\hat{s}^+} \hat{v} \\
& - \left[c_{max} k_B T \log\left(\frac{c_{max}-c_2}{c_{max}}\right)\right]_{s=\hat{s}^+} \hat{v}
\end{aligned}$$

As before, the first three lines provide three purely mechanical nonlinear algebraic equilibrium equations, which allow us to obtain θ^{equil}, β^{equil} and P^{equil} as a function of $\hat{s}$. We identify the chemical potentials of the bound and unbound binders as

$$\mu_1 = \mu_1^{chem} + \mu_1^{mech}(h) = \mu_1^0 + k_B T \frac{c_1}{c_0} - 2\log\left(\frac{c_{max} - c_1 - c_2}{c_{max}}\right) + k_0 h^2 \quad (12.4)$$

$$\mu_2^{in} = \mu_2^0 + k_B T \frac{c_2}{c_0} - \log\left(\frac{c_{max} - c_1 - c_2}{c_{max}}\right) \quad (12.5)$$

$$\mu_2^{out} = \mu_2^0 + k_B T \frac{c_2}{c_0} - \log\left(\frac{c_{max} - c_2}{c_{max}}\right). \quad (12.6)$$

Because the chemical potential of one specie depends on the concentration of other species, this model will result in what is called cross-diffusion. Then, we can write equation 12.4 as:

$$\begin{aligned} D_{\bar{Z}}\mathcal{L}(\bar{Z}) \cdot \mathcal{P}(\bar{W}) = & \int_0^{\hat{s}} \frac{1}{2}\mu_1 \dot{c}_1 \, ds + \int_0^{\hat{s}} \mu_2^{in} \dot{c}_2 \, ds + \int_{\hat{s}}^{L_0} \mu_2^{out} \dot{c}_2 \, ds \\ & + \frac{1}{2}\left[c_1 \mu_1\right]_{s=\hat{s}} \hat{v} \\ & + k_B T c_{max} \left(\left[\log\left(\frac{c_{max} - c_1 - c_2}{c_{max}}\right)\right]_{s=\hat{s}^-} - \left[\log\left(\frac{c_{max} - c_2}{c_{max}}\right)\right]_{s=\hat{s}^+} \right) \hat{v} \\ & + \frac{k_B T}{2}\left[c_1\right]_{s=\hat{s}^-} \hat{v} \\ & + T\left(1 - \cos\theta^{\text{equil}}(\hat{s})\right) \hat{v} \\ & + \left(\left[\mu_2^{in} c_2\right]_{s=\hat{s}^-} - \left[\mu_2^{out} c_2\right]_{s=\hat{s}^+} \right) \hat{v}, \end{aligned} \quad (12.7)$$

Finally using the local form of balance of mass:

$$\dot{c}_i + (c_i w_i)' \mp r = 0, \quad (12.8)$$

We can rewrite the Eq. (12.7) as:

$$\begin{aligned} D_{\bar{Z}}\mathcal{L}(\bar{Z}) \cdot \mathcal{P}(\bar{W}) = & \int_0^{\hat{s}} \left[\left(\frac{1}{2}\mu_1 - \mu_2^{in}\right) r + \frac{1}{2} c_1 w_1 \, \mu_1' + c_2 w_2 \, \mu_2^{in\prime} \right] ds + \int_{\hat{s}}^{L_0} c_2 w_2 \, \mu_2^{out\prime} \, ds \\ & - \frac{1}{2}\left[c_1 w_1 \mu_1\right]_{s=\hat{s}^-} - \left[c_2 w_2 \mu_2^{in}\right]_{s=\hat{s}^-} + \left[c_2 w_2 \mu_1^{out}\right]_{s=\hat{s}^+} \end{aligned}$$

$$
\begin{aligned}
&+\frac{1}{2}\left[c_1\mu_1\right]_{s=\hat{s}}\hat{v}\\
&+k_BTc_{max}\left(\left[\log\left(\frac{c_{max}-c_1-c_2}{c_{max}}\right)\right]_{s=\hat{s}^-}-\left[\log\left(\frac{c_{max}-c_2}{c_{max}}\right)\right]_{s=\hat{s}^+}\right)\hat{v}\\
&+\frac{k_BT}{2}\left[c_1\right]_{s=\hat{s}^-}\hat{v}\\
&+T\left(1-\cos\theta^{\text{equil}}(\hat{s})\right)\hat{v}\\
&+\left(\left[\mu_2^{in}c_2\right]_{s=\hat{s}^-}-\left[\mu_2^{out}c_2\right]_{s=\hat{s}^+}\right)\hat{v}.
\end{aligned}
\tag{12.9}
$$

Recalling the conditions at the interface

$$\hat{v}=w_1(\hat{s}) \tag{12.10}$$

$$(c_2(\hat{s}^+)-c_2(\hat{s}^-))\hat{v}=\left[c_2w_2\right]_{s=\hat{s}^+}-\left[c_2w_2\right]_{s=\hat{s}^-}, \tag{12.11}$$

we can simplify Eq. (12.9):

$$
\begin{aligned}
D_{\bar{Z}}\mathcal{L}(\bar{Z})\cdot\mathcal{P}(\bar{W})=&\int_0^{\hat{s}}\left[\left(\frac{1}{2}\mu_1-\mu_2^{in}\right)r+\frac{1}{2}c_1w_1\,\mu_1'+c_2w_2\,\mu_2^{in\prime}\right]ds+\int_{\hat{s}}^{L_0}c_2w_2\,\mu_2^{out\prime}\,ds\\
&+k_BTc_{max}\left(\left[\log\left(\frac{c_{max}-c_1-c_2}{c_{max}}\right)\right]_{s=\hat{s}^-}-\left[\log\left(\frac{c_{max}-c_2}{c_{max}}\right)\right]_{s=\hat{s}^+}\right)\hat{v}\\
&+\frac{k_BT}{2}\left[c_1\right]_{s=\hat{s}^-}\hat{v}\\
&+T\left(1-\cos\theta^{\text{equil}}(\hat{s})\right)\hat{v}\\
&+\left(\left[\mu_2^{out}\right]_{s=\hat{s}^+}-\left[\mu_2^{in}\right]_{s=\hat{s}^-}\right)(w_2(\hat{s}^+)-\hat{v})c_2(\hat{s}^+).
\end{aligned}
\tag{12.12}
$$

To model the dynamics, we introduce a dissipation potential expressed in terms of the process variables W:

$$\Psi(W;Z)=\int_0^{\hat{s}}\frac{1}{2\bar{k}}r^2ds+\int_0^{\hat{s}}\left(\frac{\eta_1c_1}{4}w_1^2+\frac{\eta_2c_2}{2}w_2^2\right)ds+\int_{\hat{s}}^{L_0}\frac{\eta_2c_2}{2}w_2^2ds. \tag{12.13}$$

To take into account the slip bond behavior, we introduce the power input

$$\mathcal{P}=\frac{1}{2}\int_0^{\hat{s}}rk_0hx_b=\frac{1}{2}\int_0^{\hat{s}}k_BT\frac{h}{x_\beta}r. \tag{12.14}$$

Applying the Onsager's variational principle and taking variations with respect to w_1, we find:

$$w_1 = -\frac{1}{\eta_1}\mu_1' = -\frac{k_B T}{\eta_1}\left(\frac{c_1'}{c_1} + 2\frac{c_1' + c_2'}{c_{max} - c_1 - c_2} + \frac{2}{k_B T}k_0 h h'\right) \quad \text{in } (0, \hat{s}). \tag{12.15}$$

Assuming for simplicity that μ_2^0 is uniform in $(0, L_0)$, we obtain from taking variations with respect to w_2 that:

$$w_2 = -\frac{k_B T}{\eta_2}\left(\frac{c_2'}{c_2} + \frac{c_1' + c_2'}{c_{max} - c_1 - c_2}\right) \quad \text{in } (0, \hat{s}), \tag{12.16}$$

$$w_2 = -\frac{k_B T}{\eta_2}\left(\frac{c_2'}{c_2} + \frac{c_2'}{c_{max} - c_2}\right) \quad \text{in } (\hat{s}, L_0). \tag{12.17}$$

As expected, these expressions show that the diffusion is affected by the crowding of the membrane. Paradoxically, they show that for very crowded membranes ($c_1 + c_2 \sim c_{max}$), diffusive fluxes are higher than in the dilute limit. When the the membrane is crowded, a single molecule moves slower, due to the limitation of the available free space around it, but the collective diffusive fluxes (here w_1 and w_2) are faster. This paradox is discussed in another context by Bruna and Chapman [2012].

Invoking the arbitrariness of w_2 at $s = \hat{s}$ we found:

$$\left[\mu_2^{out}\right]_{s=\hat{s}^+} - \left[\mu_2^{in}\right]_{s=\hat{s}^-} = 0 \text{ since } c_2 \neq 0 \text{ so: } \mu_2 \text{ continuous across the interface,} \tag{12.18}$$

which means :

$$\frac{c_2(\hat{s}^-)}{c_{max} - c_1(\hat{s}^-) - c_2(\hat{s}^-)} = \frac{c_2(\hat{s}^+)}{c_{max} - c_2(\hat{s}^+)}. \tag{12.19}$$

This equation can also be expressed:

$$\frac{c_2(\hat{s}^+)}{c_2(\hat{s}^-)} = \frac{c_{max}}{c_{max} - c_1(\hat{s}^-)}. \tag{12.20}$$

Taking variations with respect to the reaction rate r, we obtain

$$r = \bar{k}\left(\mu_2^{in} - \frac{1}{2}\mu_1 - \frac{1}{2}\frac{h}{x_\beta}\right). \tag{12.21}$$

Considering the following choice for $\bar{k}$

$$\bar{k} = k \frac{c_2^2/c_0 \exp\left(\frac{-h^2 k_0}{k_B T}\right) - \exp\left(\frac{\mu_1^0 - 2\mu_2^0}{k_B T}\right) \exp\left(\frac{h}{x_\beta}\right) c_1}{\mu_2^{in} - \frac{1}{2}\mu_1(h)}, \tag{12.22}$$

where $k > 0$ is a rate constant. A direct calculation shows that

$$\bar{k} = \frac{2kc_0}{k_B T} \exp\left(-\frac{2\mu_2^0}{k_B T}\right) \exp\left(-\frac{h^2 k_0}{k_B T}\right) \frac{\exp\left(\frac{2\mu_2^{in}}{k_B T}\right) - \exp\left(\frac{\mu_1 + k_B T h/x_\beta}{k_B T}\right)}{\frac{2\mu_2^{in}}{k_B T} - \frac{\mu_1 + k_B T h/x_\beta}{k_B T}}, \tag{12.23}$$

which is clearly positive as required by the second law of thermodynamics. Plugging Eq. (12.22) into Eq. (12.21), we obtain

$$\boxed{r = k_{\text{on}}(h) c_2^2 - k_{\text{off}}(h) c_1 = k_{\text{on}}^0 \exp\left(-\frac{h^2 k_0}{k_B T}\right) c_2^2 - k_{\text{off}}^0 \exp\left(\frac{h}{x_\beta}\right) c_1 \quad \text{in} \quad (0, \hat{s}),} \tag{12.24}$$

where

$$\boxed{k_{\text{on}}^0 = \frac{k}{c_0} \quad \text{and} \quad k_{\text{off}}^0 = k \exp\left(\frac{\mu_1^0 - 2\mu_2^0}{k_B T}.\right).} \tag{12.25}$$

As expected, the reaction inside the patch is independent on the level of crowding on the membrane and we recover the reaction rate r for slip bonds given in Eq. (11.12). Finally we derive the equilibrium condition at the interface with the minimization with respect to the speed of the contact point $\hat{v}$:

$$0 = T_c \left(1 - \cos\theta^{\text{equil}}(\hat{s})\right) + k_B T c_{max} \left(\left[\log\left(\frac{c_{max} - c_1 - c_2}{c_{max}}\right)\right]_{s=\hat{s}^-} - \left[\log\left(\frac{c_{max} - c_2}{c_{max}}\right)\right]_{s=\hat{s}^+}\right) + \frac{k_B T}{2} c_1(\hat{s}^-) \tag{12.26}$$

And using Eq. (12.20) we can simplify as:

$$0 = T_c \left(1 - \cos\theta^{\text{equil}}(\hat{s})\right) + k_B T c_{max} \left[\log\left(\frac{c_{max} - c_1}{c_{max}}\right)\right]_{s=\hat{s}^-} + \frac{k_B T}{2} c_1(\hat{s}^-). \tag{12.27}$$

12.3 Final system of equations

Putting together all the previous equations, we obtain the following system of advection-diffusion-reaction equations exhibiting cross diffusion: the diffusion of each specie is influenced by the other specie. One can check that, in the dilute limit we recover the system of equations given in section 11.3 for slip bonds.

Governing equations:

$$\dot{c}_1 = D_1 \left(c_1' + 2c_1 \frac{c_1' + c_2'}{c_{max} - c_1 - c_2} \right)' + k_{\text{on}} \exp\left(\frac{-h^2}{x_\gamma^2} \right) c_2^2 \tag{12.28}$$

$$- k_{\text{off}}^0 \exp\left(\frac{h}{x_\beta} \right) c_1 + D_1 \left(\frac{2hh'c_1}{x_\gamma^2} \right)' \qquad \text{in } (0, \hat{s}),$$

$$\dot{c}_2 = D_2 \left(c_2' + c_2 \frac{c_1' + c_2'}{c_{max} - c_1 - c_2} \right)' - k_{\text{on}} \exp\left(\frac{-h^2}{x_\gamma^2} \right) c_2^2 \tag{12.29}$$

$$+ k_{\text{off}}^0 \exp\left(\frac{h}{x_\beta} \right) c_1 \qquad \text{in } (0, \hat{s}),$$

$$\dot{c}_2 = D_2 \left(c_2' \frac{c_{max}}{c_{max} - c_2} \right)' \qquad \text{in } (\hat{s}, L_0), \tag{12.30}$$

with its following set of boundary/jump conditions,

Boundary conditions:

$\boxed{\text{at } s = 0}$

$$\left[\frac{2c_1hh'}{x_\gamma^2} + c_1' + 2c_1\frac{c_1' + c_2'}{c_{max} - c_1 - c_2}\right]_{s=0} = 0, \quad \left[c_2' + c_2\frac{c_1' + c_2'}{c_{max} - c_1 - c_2}\right]_{s=0} = 0, \tag{12.31}$$

$\boxed{\text{at } s = \hat{s}}$

$$\frac{c_2(\hat{s}^+)}{c_2(\hat{s}^-))} = \frac{c_{max}}{c_{max} - c_1(\hat{s}^-)}, \tag{12.32}$$

$$c_2'(\hat{s}^+)\frac{c_{max}}{c_{max} - c_2(\hat{s}^+)} - c_2'(\hat{s}^-)\frac{c_{max} - c_1(\hat{s}^-)}{c_{max} - c_2(\hat{s}^-) - c_1(\hat{s}^-)} \tag{12.33}$$

$$= -\frac{[\![c_2]\!]\,\hat{v}}{D_2} + \frac{c_2(\hat{s}^-)c_1'(\hat{s}^-)}{c_{max} - c_2(\hat{s}^-) - c_1(\hat{s}^-)} \tag{12.34}$$

$$-D_1\left[\frac{2c_1hh'}{x_\gamma^2} + c_1' + 2c_1\frac{c_1' + c_2'}{c_{max} - c_1 - c_2}\right]_{s=\hat{s}} = c_1(\hat{s})\,\hat{v}, \tag{12.35}$$

$$0 = T_c\left(1 - \cos\theta^{\text{equil}}(\hat{s})\right) + k_BTc_{max}\left[\log\left(\frac{c_{max} - c_1}{c_{max}}\right)\right]_{s=\hat{s}^-} + \frac{k_BT}{2}c_1(\hat{s}^-) \tag{12.36}$$

$\boxed{\text{at } s = L_0}$

$$c_2'(L_0) = 0. \tag{12.37}$$

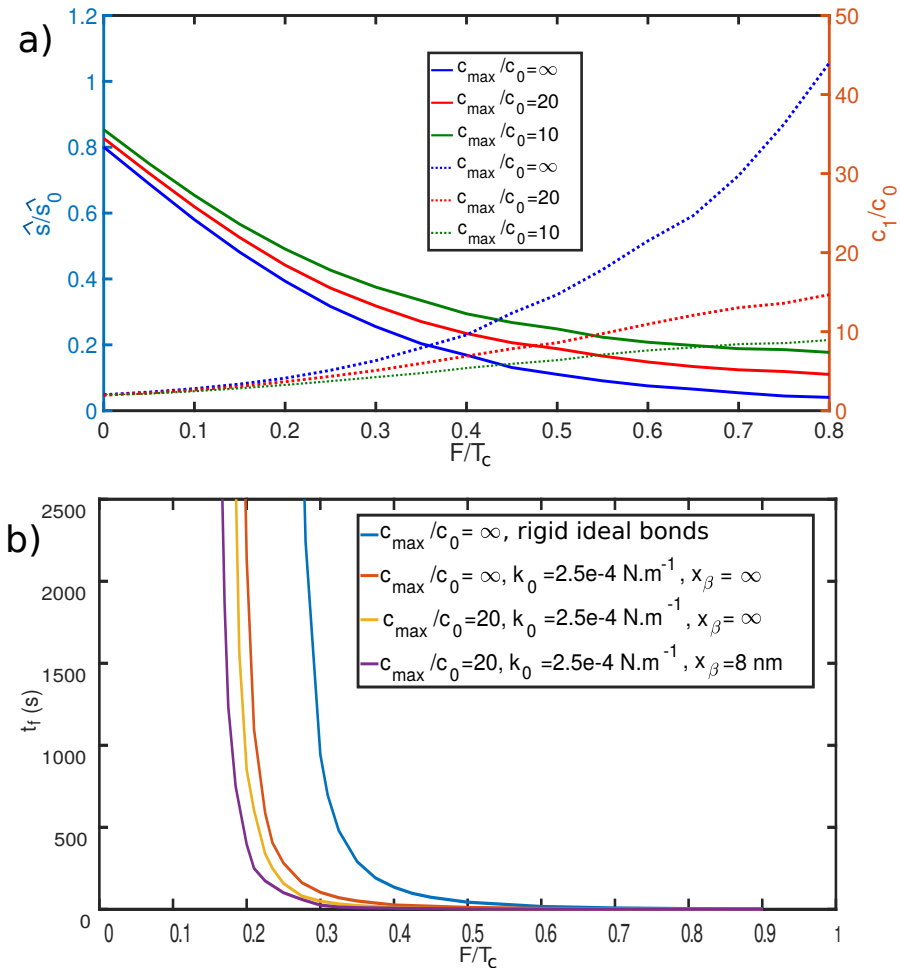

Figure 12.1: a) Purely diffusive problem: Final normalized concentration c_1/c_0 in the patch (dotted line) and final normalized position of the interface $\hat{s}/\hat{s}_0$ (solid line) as a function of the applied force for different values of c_{max}. The bonds are ideal and compliant and such as $k_0 = 2.5 \cdot 10^{-4}$ N·m^{-1}. b) Reaction-Diffusion problem: Influence of the overcrowding of the vesicle on the lifetime of the adhesion patch and its dependence on the applied force F/T_c for ideal compliant ideal bonds and slip bonds.

12.4 Results and discussion

In this last section, we examine the influence of the level of crowding of the vesicle on diffusion-dependent regimes.
First let us look at the diffusion-dominated case, where $\tau_{reac} \gg \tau_{diff}$, for a vesicle under a pulling force in the presence of crowding. To do so we set $k_{off} = 0$ and $k_{on} = 0$ and we consider different values for c_{max}. The results are given in Fig. 12.1(a). The blue curves correspond to the case of compliant ideal bonds when $c_1, c_2 << c_{max}$. The more overcrowded the vesicle is, the less packed the patch is: the shrinking of the patch is reduced as the total concentration of adhesion molecules in the patch is limited. Overcrowding thus limits diffusion of the adhesion molecules and limits the packing in the diffusion-dominated regime.
In the mixed regime of reaction diffusion, when $\tau_{reac} \sim \tau_{diff}$, Fig. 12.1(b) shows how overcrowding on the membrane tends to weaken the adhesion patch of any type of bonds by reducing its lifetime. Thus adding non-interacting molecules on the patch weakens it and could destabilize a adhesion patch stable at a given force while having no effects on the binding/unbinding kinetics.

Chapter 13

Summary and Conclusion to Part II

We have examined the dynamics of unbinding under force of adhesive vesicles mediated by mobile binders. This is an elementary model required to understand the more complex problem of cell-cell adhesion, which however has remained poorly understood beyond scaling and qualitative insights [Brochard-Wyart and de Gennes, 2003, 2002a] .

We have formalized the problem in the framework of Onsager's variational principle, providing a systematic and elegant procedure to generate the governing coupled equations of the problem that captures the tight interplay between diffusion, reaction and mechanics. In particular, we have shown how microscopic properties of adhesion molecules, such as their compliance, force-sensitivity, mobility or crowding, have a strong influence on the macroscopic behavior of an adhesion patch, including its dynamics and lifetime. To focus on this complex chemo-mechanical interplay, we have focused on a simplified 2D setting. However, the extension to axisymmetry or to 3D is straightforward, and our results should be general, albeit with quantitative differences. Our modeling approach exploits scale separation between the overall mechanics of

the vesicle and the detailed mechanics near the edge of the adhesion patch. Indeed, the length-scale over which bending plays a role and the displacements due to the compliance of the bonds in the patch are very small on the scale of the whole vesicle. This allows us to treat the mechanics of the problem with a two-scale model, a large-scale capillary model that determines macroscopic quantities such as the contact angle and or the pressure in the vesicle, and a small-scale model that determines the force distribution in the bonds in the vicinity of the edge of the patch. To examine the resulting family of coupled nonlinear models, we have resorted to numerical calculations.

This framework is able to recover the classical equilibrium picture. It also describes several anticipated regimes [de Gennes et al., 2003] depending on the model parameters. When the time-scale for reactions is much longer than that for diffusion, we have described a diffusion-dominated or packing regime in which where the adhesion patch responds to the force by shrinking and increasing bond concentration. The larger bond concentration in the patch creates an osmotic tension that balances the increasing mechanical force on the patch interface. When the slip-bond behavior is accounted for, the larger forces borne by bonds near the edge of the patch can locally increase the unbinding rate, which in turn can lead to a "tear-out" regime in which the patch shrinks by the progressive breaking of bonds near the interface, very much like in the classical tear-out of a vesicle adhered to a solid substrate through immobile receptors [Prechtel et al., 2002, Pierrat et al., 2004b]. Interestingly, we found that the tear-out regime in our model was distinct from that previously described. Indeed, because bonds are mobile and the time-scale for diffusion is strongly size-dependent, there is a small diffusion zone near the edge of the patch where diffusive transport is significant. As a result, and in sharp contrast with classical tear-out, the mobility of binder molecules on the vesicle (quantified by their diffusion coefficient) has a profound effect on the kinetics of patch shrinking, and determines the size of the diffusion zone and more importantly the speed of propagation of the edge. Thus, even if large-scale diffusion does not play a role and decohesion occurs by progressive bond breaking, the process is critically influenced by diffusion in a microscopic diffusion zone

near the "crack tip".

In fact this unusual tear-out regime with small-scale diffusion is an extreme case of the generic intermediate situation described here in which diffusion and reaction interact. We have shown that in this regime, one can define a critical force, below which adhesion is stable for very long times and above which adhesion is unstable. We have shown that this threshold depends on the physico-chemical properties of adhesion molecules, including its stiffness, force-sensitivity or size determining their packing limit. In fact, crowding can also be tuned by the presence of other inactive molecules on the membrane. Interestingly, these properties can be tuned in a biological context, for instance resorting to Ca^{2+} signalling. Given the strong dependence of patch lifetime on $F_c - F$, small changes in F_c modulated by cells could have a strong effect on the stability of adhesion patches, providing a physical tool to adapt adhesion to different physiological requirements such as maintain tissue cohesion under stress or modify junctions during remodelling. Our results also provide a background to design and control the mechanics and dynamics of soft adhesion in tunable and responsive artificial systems.

From a theoretical point of view, we have shown that Onsager's principle is a valuable tool to model problems with a tight interaction between chemical reactions, molecular diffusion and mechanics. We have shown how, in the context of a moving interface problem, it allows us to determine transparently the differential equation on a moving domain and the jump conditions at the interface. Furthermore, we have seen how physical effects such as bond compliance, force sensitivity or molecular crowding, which leads to highly nonlinear models, can be included naturally in this framework. One point that remains open is the formalization of slip bonds, according to which the unbinding rate increases with force, within Onsager's framework. We have accomplished this by including a power input term, which leads to the expected set of equations but does not admit an obvious interpretation from the point of view of global energy balance. Our treatment is similar in spirit to that in [Kumar et al., 2018], where a phase-field damage model with a stress-dependent damage evolution is formulated.

Finally, in an effort to compare this specific type of adhesion mediated by mobile binders with classical types of adhesion, we note that soft adhesion mediated by mobile binders exhibits similarities and differences with classical mechanisms of non-biological adhesion. A general survey of adhesion and the related computational models is given in [Sauer, 2016]. These adhesion mechanisms can be divided in two families depending on the nature of the interaction between the adherent materials.

1 Apparent adhesion, where adhesion arises from interpenetration of materials. Here, local attraction forces at the contact are absent. Instead, as a result of the porosity and surface roughness of the material surface, contact forces lead to intertwining of the two different materials put in contact. Apparent adhesion includes diffusion adhesion, based on interpenetration of polymers. When two polymers are compatible, their polymer chains are able to mix upon contact, resulting in partial penetration between the two materials and an apparent adhesion on a larger scale.

2 Effective adhesion, arising from attractive forces. This type of adhesion includes dispersive adhesion based on van der Waals interactions, or electrostatic adhesion, due to Coulomb attraction between opposite charges. The interplay of these two types of unspecific adhesion is essential in cell adhesion as it results in a typical attraction well keeping lipid bilayers in a closer range allowing chemical adhesion to take place [Bell, 1978a]. This latter type of specific adhesion rely on covalent or hydrogen chemical bonds.

Thus, the adhesion mechanism considered here does not precisely fit into neither of these categories. In the thesis, soft adhesion relies on chemical bonding mediated by mobile proteins binding through hydrogen bonds, resulting in stronger cohesion than with van der Waals interactions but weaker than with covalent bonds. This mechanism is ideal for biological adhesion since it enables strength but also easy remodeling. Chemical binders can exhibit

force-sensitivity, such as the slip bonds described in the thesis, producing chemo-mechanical coupling between the mechanics and the chemistry of the interface. Another particularity of the model discussed in Part II is the mobility of the binders, which plays a major role in tuning the adhesion mechanism by selecting the spatial extent of the cohesive or process zone. In a diffusion-reaction regime, binders diffuse in the whole adhesion domain affecting adhesion on large scale. In a tear-out regime, no global transport of binders is observed and and the the mechanism is similar to the peeling of an adhering surface, with a small process zone where reactions occur. Even in the tear-out regime, however, the mechanism studied here is distinct from classical peeling in that it critically depends on diffusion, even if it happens on a very small length-scale. The problem of soft adhesion mediated by mobile binders is then a subtle adhesion mechanism critically depending on the nature of adhesion molecules, their concentration, their mobility on the membrane or the loading rate. Because of this, this type of adhesion can offer solutions to a wide range of problems where versatility between strength and ability to remodel is required. This highlights the interest of adhesion mediated by mobile binder for tunable bioengineered soft materials.

Decohesion between adhered deformable objects is essentially a problem of interfacial fracture. As such, one can understand it in terms of an energy flux or driving force towards the process zone coming from the surrounding material (the energy release-rate for a bulk elastic material, the mechanical driving force $T_c(1 - \cos\theta)$ in our capillary problem, the force per adhesion molecule $k_0 h$ in our small-scale mechanical model), and a local resistive mechanism encoding the physics of the interface and how the energy flux is dissipated during de-cohesion. This last point can be often described in terms of a simple surface energy (the energy required to expose a new surface), as in Griffith's fracture or in the JKR model [Johnson et al., 1971]. Here, however, these interfacial processes are much more complex and involve diffusion and reactions, and thus are non-local and time-dependent in nature.

Chapter 14

Conclusions and Future directions

Conclusions

In this thesis, we developed different models, both stochastic and continuous, with the objective of understanding the process of soft adhesion mediated by mobile binders, its coupling with the mechanics of the supported deformable surface and the properties of the adhesion molecules. Towards this goal, we have developed theory and performed simulations. Here, we summarize the main achievements of this study.

- We have developed several mechano-stochastic minimalistic models to investigate the influence of surface tension, interstitial pressure and architecture on the stability of molecular bond clusters. We have found that surface tension plays a role in controlling surface-surface separation and thus the kinetics of rebinding. Surface tension also modulates the force distribution over the cluster. For clusters of slip bonds, this modulates the unbinding kinetics. Stability arises from the interplay of these two phenomena. We have found that the effect on rebinding

dominates, and thus surface tension has a toughening effect: it opposes to expansion of cracks. We have enriched model to examine the influence of the mobility of the bonds. From this last investigation we found that the mobility of the bonds allows the system to close cracks and thus increase the stability.

- Moving to the continuum modeling, we developed a systematic and transparent approach to generate complex models coupling multiple physics. This approach is founded on Onsager's variational principle, by which the dynamics result from the interplay between energetic driving forces and dissipative drag forces, each of them deriving from potentials that are the sum of individual contributions for each physical mechanism. This provides an elegant framework for the modeling of vesicle unbinding but could be used for a large range of other problems exhibiting non trivial coupling between mechanics, chemistry and diffusion.

- We used this modeling framework to study a prototypical problem in biophysics but still poorly understood: the dynamics of the unbinding of soft adhered vesicles adhering through mobile binders. This problem exhibits complex coupling between mechanics, diffusion and chemistry.

- We have extended the formulation to account for bond compliance, slip bond behavior and molecular crowding, although the theoretical understanding of slip bond behavior with Onsager's framework is not fully clear.

- We identified two extreme regimes: one dominated by diffusion where the adhesion patch reacts to the force by shrinking and getting more concentrated, the so-called packing regime, and one dominated by the unbinding kinetics where the bonds break from the edge of the patch with no large-scale diffusion, the so called tear-out regime. This tear-out regime, however, is new in that its dynamics crucially depend on diffusive dynamics that take place in a small diffusive zone close to the edge of the patch.

- We identified an intermediate regime, where reaction and diffusion act together and for which it exists a critical force that separates stability from instability. We show how this critical force depends on the physico-chemical properties of the bonds, including their compliance, force-sensitivity, or their size controlling crowding. Thus, our study portrays soft adhesion mediated by mobile binders as highly tunable and rich soft matter system allowing cells to strongly adhere to each other or disengage to remodel, and which may be the basis for artificial biomimetic systems.

Future directions

The range of behaviors and parameter space of our continuum model for soft specific adhesion are huge, as indicated by many calculations not presented here. Here, we have only examined a narrow part of this landscape, representative of only a few processes in cells. We suggest next further modeling and applications, where our model or extensions of it, can help understand complex dynamical phenomena related to cell adhesion and in particular the mechanosensitivity of the adhesion-cytoskeleton complex. To illustrate these ideas, we propose a simplified scenario for the observed clustering of cadherins at the contact rim and its coupling with actin dynamics in a feedback loop [Engl et al., 2014b, Wu et al., 2015]. This scenario is based on different experimental observations and our variational modeling could provide a framework to study this phenomenon by coupling our model with active gel models. A simplified sketch is given in Fig. 14.1, the different subprocesses are specified by numbers . While subprocess ① is well captured by our model, the other subprocesses can be added to the model and will be discussed in the following.

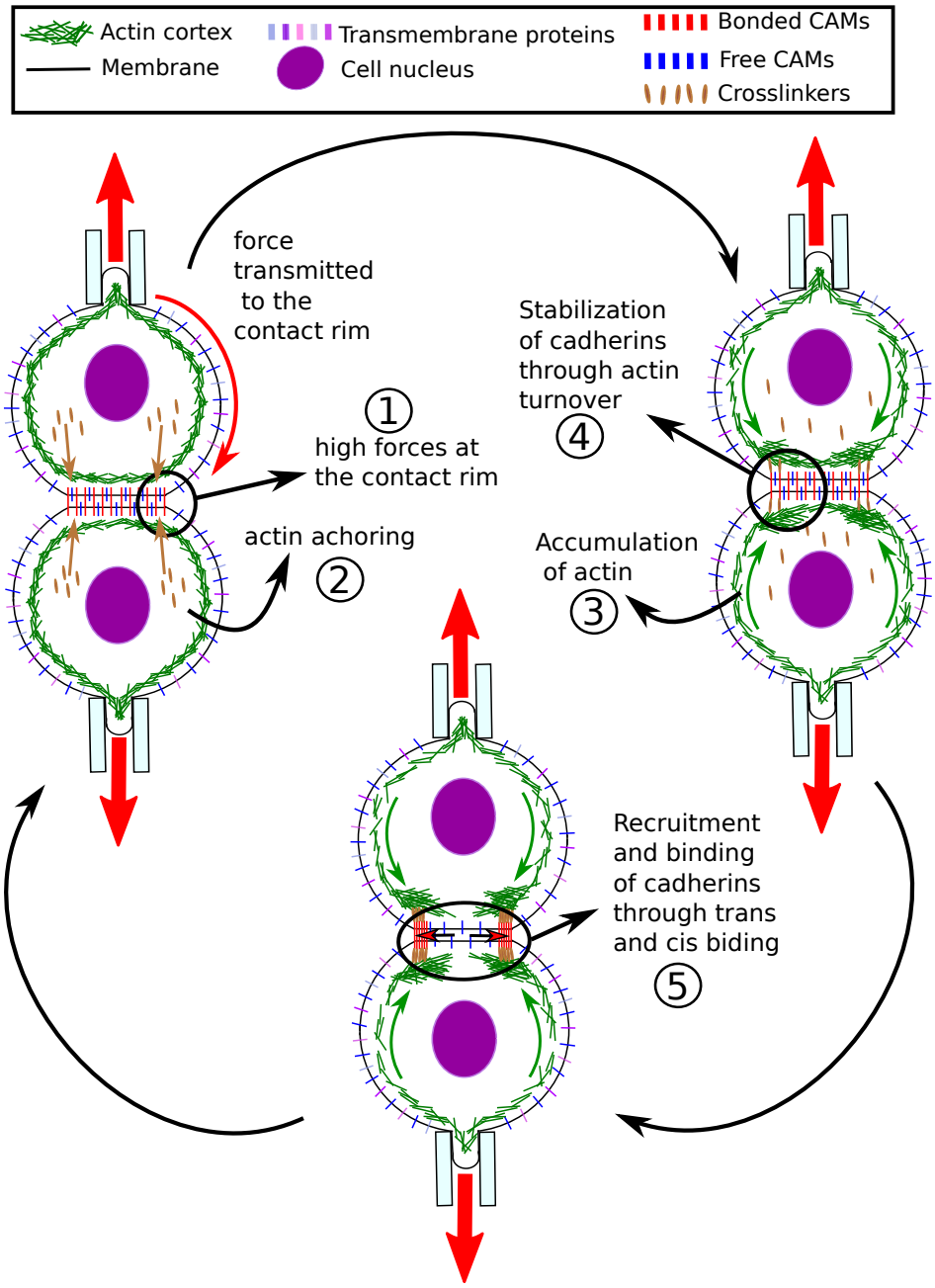

Figure 14.1: Simplified scenario for rim clustering of cadherins as a feedback loop. The different subprocesses are specified by numbers.

- The unbinding of vesicles has been studied in the past from a continuous point of view [Boulbitch et al., 2001, Brochard-Wyart and de Gennes, 2002a, de Gennes et al., 2003, Brochard-Wyart and de Gennes, 2003], but few modeling attempts have been made during the last decade to provide a general framework to study the dynamics. Since then, the experimental tools have improved a whole new range of experimental set-up are available to study the problem of soft adhesion and the above problem is a particular example.

- A first natural improvement of the model would be to extend it to axisymetry by appropriately introducing geometrical factors. The conceptual extension to 3D is straightforward, although the numerical implementation becomes more complex. The advantage here, is that for such extension of the model, the general variational framework we used to derive the governing equations would still be valid. This would allow us to access to more information on the dynamics and explore some more complex problems. It would also provide more consistent results to be compared with experimental data.

- A feature which is not captured by the actual model is the tight coupling between cytoskeleton mechanics and cell adhesion [Gumbiner, 1996, Vasioukhin et al., 2000] which is thought to drive many important processes like cell sorting [Maître et al., 2012b]. Such a coupling is the basis of mechanotransduction between cells. Some experimental studies [Engl et al., 2014a] have used new methods to unveil the relation between the actin dynamics and cell adhesion. Such experimental methods could be used, with a proper set-up, to test our model. Thinking about the problem in another way, including actin dynamics in our model, in particular the actin anchoring, accumulation and the stabilization of the cadherins (subprocesses ②,③ and ④ in Fig. 14.1) in the form of a time-dependent friction between the bound molecules and the membrane

for example (similar to section 9.7), could help us to understand more deeply these experimental observations.

- The lateral cis-interaction between the bonds is also thought to play a critical role in cell adhesion [Fenz et al., 2017] (subprocess ⑤ in Fig. 14.1). Such an effect could be modeled through a lateral affinity of the cadherins with a dependence on the actin activity. The size of the adhesion molecules has also be proven to be a key factor for pattern formations, by segregating the different populations of adhesion molecules [Schmid et al., 2016a]. Using the ability of the variational framework to be enriched with other physical processes, our model could be able to question these observations and propose some physical interpretations.

- Finally, a thermodynamic definition of the change of the nature of the bonds, either slip or catch, should be provided in order to integrate this feature in the model without breaking the thermodynamic consistency of the model. Indeed, the slip and catch bond behavior is thought to participate to the mechanosensing [Buckley et al., 2014]. Including these different force-dependent unbinding behaviors into our variational modeling framework will require further theoretical developments.

Appendix A

Modeling biased mobility

We saw that for fast mobility of the molecules, the crack tends to be invisible for the bonds as they can easily jump from the crack to the patch during the average time of the binding/unbinding of bonds. However, a closed bond at the edge of the patch, which bears most of the force exerted by the overpressure, experiences a lateral force F_{lat}, which is due to its proximity with the crack and that will oppose to the movement towards the center of the crack and that will prevent the bonds to migrate in this direction: the lateral force biases the diffusion of the closed bonds. This observation is illustrated in Fig. A.1.

To take this effect into account in our capillary-stochastic model, we update the 1D Fokker-Planck detailed in the previous section. When a constant force F is applied along the axis x , the 1D Fokker-Planck is modified such as the probability $p(x,t)$ of finding the molecule at a position x after a time t obeys:

$$\frac{\partial p}{\partial t} = \mu \frac{\partial}{\partial x}(\phi'(x)p) + D\frac{\partial^2 p}{\partial x^2} = -\mu F \frac{\partial p}{\partial x} + D\frac{\partial^2 p}{\partial x^2} \tag{A.1}$$

where μ is the mobility given by the Stokes drag of the molecule and ϕ a potential such that F derives from ϕ as $\phi'(x) = -F$.

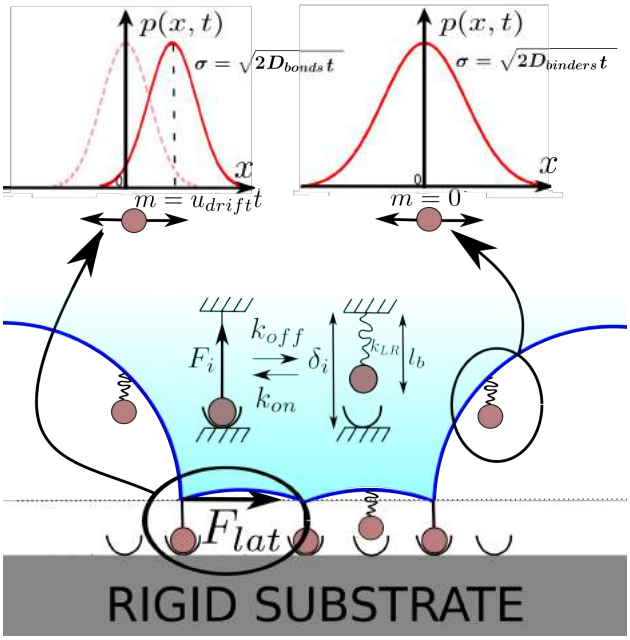

Figure A.1: Schematic representation of the diffusion of the bonds/binders and the corresponding probability distribution for the mobility of the open and closed bonds.

A solution $p(x,t)$ to this equation is:

$$p(x,t) = \frac{1}{\sqrt{4\pi Dt}} e^{-\frac{(x - x_0 - u_{drift}t)^2}{4Dt}} = \frac{1}{\sqrt{2\pi\sigma(t)^2}} e^{-\frac{(x - m(t))^2}{2\sigma(t)^2}}, \qquad \text{(A.2)}$$

with $m(t) = x0 - u_{drift}t$ the mean of the distribution and $\sigma(t) = \sqrt{2Dt}$ its standard deviation, which stays unchanged by the application of a constant force. The so-called Einstein relation gives $u_{drift} = DF/k_bT$. We can now update our Monte-Carlo scheme to take into account the effect of lateral forces on bonds diffusion. In this case bonds experiencing a lateral force $F = F_{lat}$ will move according to Eq.(A.2).

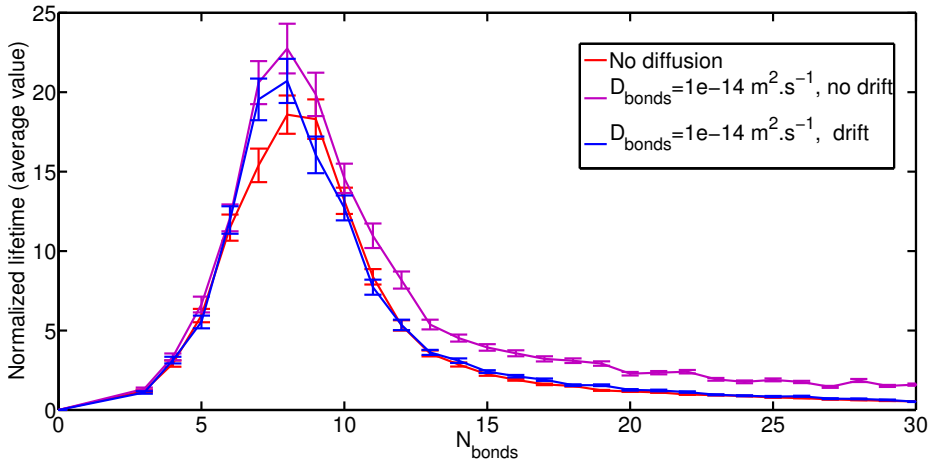

Figure A.2: Average lifetime of clusters as a function of N_{bonds} for different diffusion constant D_{bonds}. ΔP = 300 Pa. The case of immobile bonds (red curve) is given as a comparison. Lifetime and error bars are obtained from 2000 trajectories.

Influence on the lifetime

We now update the Fig. 5.10 to take into account this bias in the diffusion of the closed bonds. To do so we consider the case of $D_{bonds} = 10^{-14}$ m^2·s^{-1}. The result is given in Fig. A.2: the effect on the lifetime of large clusters of the mobility of the bonds disappears and the curve for biased diffusion almost coincides with the curve corresponding to the absence of the diffusion. Thus the mobility of the closed bonds has compensated the bias to the forces exerted by the cracks.

Appendix B

Spatial discretization of the system of coupled equations

B.1 Ideal rigid bonds

Considering the staggered problem detailed by the system of equations given in section 9.6, where we replace $(v^{n+1})^2$ by $v^n v^{n+1}$. Knowing $\hat{s}$,$\hat{v}$,δ^n,θ^n,β^n,P^n,u^n,v^n,w^n, we can solve for u^{n+1}, v^{n+1} and w^{n+1} using:

$$
\begin{aligned}
\frac{u^{n+1}-u^n}{\Delta t} &= \frac{D_1}{(\hat{s}^n)^2} u^{n+1\prime\prime} + \eta \frac{\hat{v}^n}{\hat{s}^n} u^{n+1\prime} + k_{\text{on}}(v^{n+1})^2 - k^0_{\text{off}}\, u^{n+1} \\
\frac{v^{n+1}-v^n}{\Delta t} &= \frac{D_2}{(\hat{s}^n)^2} v^{n+1\prime\prime} + \eta \frac{\hat{v}^n}{\hat{s}^n} v^{n+1\prime} - k_{\text{on}}(v^{n+1})^2 + k^0_{\text{off}}\, u^{n+1}, \\
\frac{w^{n+1}-w^n}{\Delta t} &= \frac{D_2}{(L_0-\hat{s}^n)^2} w^{n+1\prime\prime} + (1-\eta)\frac{\hat{v}^n}{L_0-\hat{s}^n} w^{n+1\prime},
\end{aligned}
$$

subject to

$$
\left[u^{n+1\prime}\right]_{\eta=0} = 0, \quad u^{n+1}(1) = \frac{2T}{k_B T}(1-\cos\theta^n)
$$

$$
v^{n+1\prime}(0) = 0, \quad v^{n+1}(1) = w^{n+1}(0), \quad \frac{D_2}{\hat{s}^n} v^{n+1\prime}(1) = \frac{D_2}{L_0-\hat{s}^n} w^{n+1\prime}(0), \quad w^{n+1\prime}(1) = 0.
$$

The above system of PDE can be made linear by replacing $(v^{n+1})^2$ by $v^n v^{n+1}$. Update the interface velocity and position

$$\hat{v}^{n+1} = -\frac{D_1}{\hat{s}^n u^{n+1}(1)} \left[+u^{n+1\prime} \right]_{\eta=1}, \qquad \hat{s}^{n+1} = \hat{s}^n + \Delta t \hat{v}^{n+1}.$$

Then we can solve the mechanical part of the problem to compute θ^{n+1},β^{n+1} and P^{n+1} and the mini model to compute δ^{n+1}
Then we can set $n+1 \longrightarrow n$ and start again the procedure.

Separating the terms in n+1 et the terms in n, multiplying by tests functions and integrating between 0 and 1 we obtain;

$$\frac{1}{\Delta t}\int_0^1 u^{n+1}\Phi_u d\eta - \frac{D_1}{(\hat{s}^n)^2}\int_0^1 u^{n+1\prime\prime}\Phi_u d\eta - \frac{\hat{v}^n}{\hat{s}^n}\int_0^1 \eta u^{n+1\prime}\Phi_u d\eta \tag{B.1}$$
$$- k_{\text{on}}\int_0^1 v^n v^{n+1}\Phi_u d\eta + k^0_{\text{off}}\int_0^1 u^{n+1}\Phi_u d\eta = \frac{1}{\Delta t}\int_0^1 u^n \Phi_u d\eta$$

$$\frac{1}{\Delta t}\int_0^1 v^{n+1}\Phi_v d\eta - \frac{D_2}{(\hat{s}^n)^2}\int_0^1 v^{n+1\prime\prime}\Phi_v d\eta + \frac{\hat{v}^n}{\hat{s}^n}\int_0^1 \eta v^{n+1\prime}\Phi_v d\eta \tag{B.2}$$
$$+ k_{\text{on}}\int_0^1 v^n v^{n+1}\Phi_v d\eta - k^0_{\text{off}}\int_0^1 u^{n+1}\Phi_v d\eta = \frac{1}{\Delta t}\int_0^1 v^n \Phi_v d\eta$$

$$\frac{1}{\Delta t}\int_0^1 w^{n+1}\Phi_w d\eta - \frac{D_2}{(L_0-\hat{s}^n)^2}\int_0^1 w^{n+1\prime\prime}\Phi_w d\eta \tag{B.3}$$
$$+ \frac{\hat{v}^n}{L_0-\hat{s}^n}\int_0^1 (1-\eta) w^{n+1\prime}\Phi_w d\eta = \frac{1}{\Delta t}\int_0^1 w^n \Phi_w d\eta$$

$$\tag{B.4}$$

For the second term (and the last term of the left hand side for the first equation), we perform an integration by parts using the given boundary conditions and choosing the good set of B-splines test functions. $\Phi_u(1) = 0$ because a Dirichlet boundary condition is enforced at $\eta = 1$.

The integration by parts gives:

$$
\begin{aligned}
\int_0^1 u^{n+1\prime\prime}\Phi_u d\eta &= \left[u^{n+1\prime}\Phi_u\right]_0^1 - \int_0^1 u^{n+1\prime}\Phi_u' d\eta \\
&= -\left[u^{n+1\prime}\right]_{\eta=0} - \int_0^1 u^{n+1\prime}\Phi_u' d\eta \quad \Phi_u(1) = 0 \\
\int_0^1 v^{n+1\prime\prime}\Phi_v d\eta &= \left[v^{n+1\prime}\Phi_v\right]_0^1 - \int_0^1 v^{n+1\prime}\Phi_v' d\eta \\
&= v^{n+1\prime}(1) - v^{n+1\prime}(0) - \int_0^1 v^{n+1\prime}\Phi_v' d\eta \\
\int_0^1 w^{n+1\prime\prime}\Phi_w d\eta &= \left[w^{n+1\prime}\Phi_w\right]_0^1 - \int_0^1 w^{n+1\prime}\Phi_w' d\eta \\
&= -w^{n+1\prime}(1) - w^{n+1\prime}(0) - \int_0^1 w^{n+1\prime}\Phi_w' d\eta \\
\int_0^1 \left(\delta^{n\prime}u^{n+1}\right)'\Phi_u d\eta &= \left[\delta^{n\prime}u^{n+1}\Phi_u\right]_0^1 - \int_0^1 \delta^{n\prime}u^{n+1}\Phi_u' d\eta \\
&= -\left[\delta^{n\prime}u^{n+1}\right]_{\eta=0} - \int_0^1 \delta^{n\prime}u^{n+1}\Phi_u' d\eta
\end{aligned}
\tag{B.5}
$$

The blue terms disappear with boundary conditions at $s = 0$ and $s = L_0$ and the terms in red will have to be enforced.
We choose B-splines B_i, $i = 1..N_b$, as a basis, then we can write:

$$
u^{n+1} = \sum_{j=1}^{N_b} B_j u_j^{n+1}, \qquad v^{n+1} = \sum_{j=1}^{N_b} B_j v_j^{n+1}, \qquad w^{n+1} = \sum_{j=1}^{N_u} B_j w_j^{n+1},
$$

with

$$
\mathbf{u^{n+1}} = \left[u_1^{n+1}, \ldots, u_{N_b}^{n+1}\right], \quad \mathbf{v^{n+1}} = \left[v_1^{n+1}, \ldots, v_{N_b}^{n+1}\right], \quad \mathbf{w^{n+1}} = \left[w_1^{n+1}, \ldots, w_{N_u}^{n+1}\right].
$$

In the case of u, as we enforce a Dirichlet boundary condition at $\eta = 1$ we have $\Phi_u(1) = 0$.

Applying Galerkin method, ie choosing the B-splines B_i as tests function, we obtain the the following system of equations that can be written in matricial form.

$$\underbrace{\left(\frac{1}{\Delta t}M^b + k^0_{\text{off}}M^{off} + \frac{D_1}{(\hat{s}^n)^2}K^b - \frac{\hat{v}^n}{\hat{s}^n}A^b\right)}_{C_u}\mathbf{u^{n+1}} - k_{\text{on}}M^{nl}\mathbf{v^{n+1}} = \frac{1}{\Delta t}M^b\mathbf{u^n} \tag{B.6}$$

$$\underbrace{\left(\frac{1}{\Delta t}M^b + k^0_{\text{on}}M^{nl} + \frac{D_1}{(\hat{s}^n)^2}(K^b - B_v) - \frac{\hat{v}^n}{\hat{s}^n}A^b\right)}_{C_v}\mathbf{v^{n+1}} - k_{\text{off}}M^{off}\mathbf{u^{n+1}} = \frac{1}{\Delta 1t}M^b\mathbf{v^n} \tag{B.7}$$

$$\underbrace{\left(\frac{1}{\Delta t}M^u + \frac{D_2}{(1-\hat{s}^n)^2}(K^u + B_w) - \frac{\hat{v}^n}{1-\hat{s}^n}A^u\right)}_{C_w}\mathbf{w^{n+1}} = \frac{1}{\Delta t}M^u\mathbf{w^n} \tag{B.8}$$

$$\begin{bmatrix} C_u & -k_{\text{on}}M^{nl} & 0 \\ -k_{\text{off}}M^{off} & C_v & 0 \\ 0 & 0 & C_w \end{bmatrix}\mathbf{X^{n+1}} = \begin{bmatrix} \frac{1}{\Delta t}M^b & 0 & 0 \\ 0 & \frac{1}{\Delta t}M^b & 0 \\ 0 & 0 & \frac{1}{\Delta t}M^u \end{bmatrix}\mathbf{X^n} \text{ with } \mathbf{X^n} = \begin{bmatrix} \mathbf{u^n} \\ \mathbf{v^n} \\ \mathbf{w^n} \end{bmatrix} \tag{B.9}$$

With, for $(i, j) \in [1..N_b]^2$,

$$M^b_{ij} = \int_0^1 B_iB_jd\eta, \quad K^b_{ij} = \int_0^1 B'_iB'_jd\eta, \quad A^b_{ij} = \int_0^1 \eta, B_iB'_jd\eta, \tag{B.10}$$
$$M^{nl}_{ij} = \int_0^1 v^nB_iB_jd\eta, \quad M^{off}_{ij} = \int_0^1 B_iB_jd\eta,$$

and for $(i, j) \in [1..N_u]^2$,

$$M^u_{ij} = \int_0^1 B_iB_jd\eta, \quad K^u_{ij} = \int_0^1 B'_iB'_jd\eta, \quad A^u_{ij} = \int_0^1 (1-\eta)B_iB'_jd\eta. \tag{B.11}$$

And B_v and B_w, two spare matrices, such as:

$$B_v\mathbf{v^{n+1}} = v^{n+1\prime}(1) \quad and \quad B_w\mathbf{w^{n+1}} = w^{n+1\prime}(0)$$

B.2 Ideal compliant bonds

For the case of ideal compliant bonds we need to for another vector for the separation δ^{n+1}, expressed on the basis of B-splines as:

$$\delta^{n+1} = \sum_{j=1}^{N_b} B_j \delta_j^{n+1} \quad and \quad \delta^{\mathbf{n+1}} = \left[\delta_1^{n+1}, ..., \delta_{N_b}^{n+1}\right],$$

To take into account the compliance of the bonds we need to form a new matrix $A2^b$ for the biased diffusion and update the matrix for the binding reaction M^{nl} with, for $(i, j) \in [1..N_b]^2$:

$$A2_{ij}^b = 2\int_0^1 \delta^n \delta^{n'} B_i B_j' d\eta, \quad M_{ij}^{nl} = \int_0^1 \exp\left(\frac{\delta^{n2}}{x_\gamma^2}\right) v^n B_i B_j d\eta, \tag{B.12}$$

and the system to be solved is:

$$\begin{bmatrix} C_u + \frac{D_1}{(\hat{s}^n)^2 x_\gamma^2} A2^b & -k_{\text{on}} M^{nl} & 0 \\ -k_{\text{off}} M^{off} & C_v & 0 \\ 0 & 0 & C_w \end{bmatrix} \mathbf{X^{n+1}} = \begin{bmatrix} \frac{1}{\Delta t} M^b & 0 & 0 \\ 0 & \frac{1}{\Delta t} M^b & 0 \\ 0 & 0 & \frac{1}{\Delta t} M^u \end{bmatrix} \mathbf{X^n} \tag{B.13}$$

B.3 Slip bonds

To take into account the slip bond behavior, the unbinding reaction matrix M^{off} is modified such as, for $(i, j) \in [1..N_b]^2$:

$$M_{ij}^{off} = \int_0^1 \exp\left(\frac{\delta^n}{x_\beta}\right) B_i B_j d\eta, \tag{B.14}$$

Using the previous matrix system and updating this matrix we can solve the system of equation for slip bonds.

B.4 Slip bonds on a crowded vesicle

For this last system of equations we have to form these new matrices K^{b11},K^{b12},K^{b21} and K^{b22} , for $(i, j) \in [1..N_b]^2$:

$$K^{b11}_{ij} = \int_0^1 \left(1 + 2\frac{u^n}{c_{max} - u^n - v^n}\right) B_i B'_j d\eta, \quad K^{b12}_{ij} = \int_0^1 2\frac{u^n}{c_{max} - u^n - v^n} B_i B'_j d\eta,$$
$$K^{b21}_{ij} = \int_0^1 \frac{v^n}{c_{max} - u^n - v^n} B_i B'_j d\eta, \quad K^{b22}_{ij} = \int_0^1 \left(1 + \frac{v^n}{c_{max} - u^n - v^n}\right) B_i B'_j d\eta,$$

and for $(i, j) \in [1..N_u]^2$:

$$K^{u3}_{ij} = 2\int_0^1 \frac{c_{max}}{c_{max} - w^n} B_i B'_j d\eta, \tag{B.15}$$

We can then form the following matrices:

$$C_u = \left(\frac{1}{\Delta t} M^b + k^0_{\text{off}} M^{off} + \frac{D_1}{(\hat{s}^n)^2} K^{b11} - \frac{\hat{v}^n}{\hat{s}^n} A^b\right)$$
$$C_v = \left(\frac{1}{\Delta t} M^b + k^0_{\text{on}} M^{nl} + \frac{D_1}{(\hat{s}^n)^2}(K^{b22} - (1 + \frac{u^n(N_b)}{c_{max} - u^n(N_b) - u^n(N_b)})B_v) - \frac{\hat{v}^n}{\hat{s}^n} A^b\right)$$
$$C_w = \left(\frac{1}{\Delta t} M^u + \frac{D_2}{(1 - \hat{s}^n)^2}(K^{u3} + B_w \frac{c_{max}}{c_{max} - w^n(1)}) - \frac{\hat{v}^n}{1 - \hat{s}^n} A^u\right) \tag{B.16}$$

and then solve the following system of equations:

$$\begin{bmatrix} C_u + \frac{D_1}{(\hat{s}^n)^2 x_\gamma^2} A2^b & -k_{\text{on}} M^{nl} + \frac{D_1}{(\hat{s}^n)^2} K^{b12} & 0 \\ -k_{\text{off}} M^{off} + \frac{D_1}{(\hat{s}^n)^2}(K^{b21} - B^*_v) & C_v & 0 \\ 0 & 0 & C_w \end{bmatrix} \mathbf{X^{n+1}} = \begin{bmatrix} \frac{1}{\Delta t} M^b & 0 & 0 \\ 0 & \frac{1}{\Delta t} M^b & 0 \\ 0 & 0 & \frac{1}{\Delta t} M^u \end{bmatrix} \mathbf{X^n}, \tag{B.17}$$

with $B^*_v = \frac{v^n(N_b)}{c_{max} - u^n(N_b) - u^n(N_b)} B_v$.

Appendix C

Dissipation potential capturing the slip bond behavior

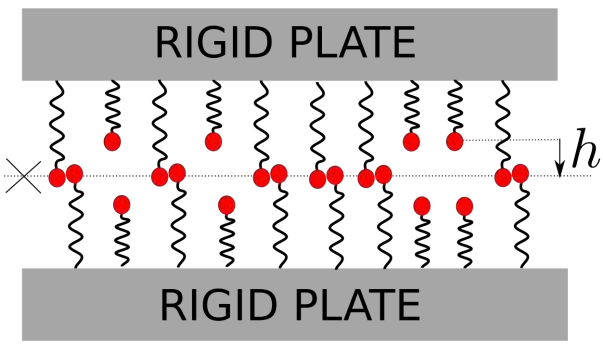

Figure C.1: Sketch of the problem. Adhesion patch made of c_1 bonds and c_2 free binders between two rigid plates. h denotes the elongation of the bonds from their rest position.

In this appendix we develop a new approach to model the slip bonds by considering a new form of the dissipation potential. To do so, let us consider the following simple model illustrated on Fig. C.1. Two rigid plates adhere

through adhesion molecules. c_1 and c_2 are the concentrations of bonds and free binders between the two rigid plates. For simplicity we consider that both species do not diffuse . The bonds are stretched between the plates from the rest position by a distance h. We will apply Onsager's variational principle to obtain the governing equations of this problem.
For this problem, the set of state variables is $Z = (c_1, c_2, h)$.
First, we need an expression for the free energy $\mathcal{F}(Z)$ of the problem:

$$\mathcal{F}(Z) = \frac{k_B T}{2} c_1 \left(\log \frac{c_1}{c_0} - 1 \right) + \frac{1}{2} \mu_1^0 c_1 + \frac{1}{2} k_0 c_1 h^2 + k_B T c_2 \left(\log \frac{c_2}{c_0} - 1 \right) + \mu_2^0 c_2 \tag{C.1}$$

We can identify the chemical potential of the bonds and the binders as:

$$\mu_1 = \mu_1^0 + k_B T \log \frac{c_1}{c_0} + k_0 h^2 \tag{C.2}$$

$$\mu_2 = \mu_2^0 + k_B T \log \frac{c_2}{c_0}. \tag{C.3}$$

The laws of balance of mass state that:

$$\dot{c_1} = -r \tag{C.4}$$

$$\dot{c_2} = r, \tag{C.5}$$

with r the net rate of binding. The set of process variables is $W = (r, \dot{h})$. We can now write the rate of the free energy as a function of Z and W as:

$$\dot{\mathcal{F}}(Z, W) = \left(\mu_2 - \frac{1}{2} \mu_1 \right) r + k_0 h \dot{h} c_1. \tag{C.6}$$

For the dissipation, we will consider the following coupled dissipation potential:

$$\mathcal{D}(Z, W) = \frac{1}{2} \begin{pmatrix} r & \dot{h} \end{pmatrix} \underbrace{\begin{pmatrix} \bar{k}^{-1} & \bar{\eta} \\ \bar{\eta} & \bar{\nu} \end{pmatrix}}_{\mathbb{M}} \begin{pmatrix} r \\ \dot{h} \end{pmatrix} \tag{C.7}$$

To ensure the problem to be dissipative, $\mathcal{D}(Z, W)$ should ensure that $\mathbb{M}$ is positive-definite :

$$\bar{k}^{-1}\nu - \eta^2 > 0 \quad \text{or} \quad \frac{\nu}{\bar{k}\eta^2} > 1 \tag{C.8}$$

Applying the Onsager's variational principle and minimizing with respect to the net rate of binding r gives:

$$r = \bar{k}(\frac{1}{2}\mu_1 - \mu_2 - \eta\dot{h}), \tag{C.9}$$

and the minimization with respect to $\dot{h}$ gives:

$$\dot{h} = -\frac{\eta}{\nu}r - \frac{k_0 h c_1}{\nu} \tag{C.10}$$

Plugging Eq. (C.10) in Eq.(C.9) we obtain the expression for r:

$$r = \frac{\bar{k}}{1 - \frac{\bar{k}\eta^2}{\nu}}\left(\frac{1}{2}\mu_1 - \mu_2 + \frac{k_0\eta h c_1}{\nu}\right), \tag{C.11}$$

Finally, plugging Eq. (C.11) in Eq. (C.10) gives the expression for $\dot{h}$:

$$\dot{h} = -\frac{\eta}{\nu}\frac{\bar{k}}{1 - \frac{\bar{k}\eta^2}{\nu}}\left(\frac{1}{2}\mu_1 - \mu_2 + \frac{k_0\eta h c_1}{\nu}\right) - \frac{k_0 h c_1}{\nu} \tag{C.12}$$

For simplicity, in the limit of $\bar{k}\eta^2/\nu \to 0$, we can write Eq. (C.11) and Eq. (C.12) as :

$$r = \bar{k}\left(\frac{1}{2}\mu_1 - \mu_2 + \frac{k_0\eta h c_1}{\nu}\right), \tag{C.13}$$

$$\dot{h} = -\frac{\eta\bar{k}}{\nu}\left(\frac{1}{2}\mu_1 - \mu_2 + \frac{k_0\eta h c_1}{\nu}\right) - \frac{k_0 h c_1}{\nu} \tag{C.14}$$

Now, we can make the following assumptions for the different terms of $\mathbb{M}$:

$$\eta = \bar{\eta}c_1 \quad \text{with } \bar{\eta} > 0 \tag{C.15}$$

$$x_\beta = \frac{\nu}{2k_B T\bar{\eta}k_0}, \tag{C.16}$$

and replacing these terms in Eq. (C.11), we have:

$$r = \bar{k}\left(\frac{1}{2}\mu_1 - \mu_2 + \frac{1}{2}k_B T\frac{h}{x_\beta}\right), \tag{C.17}$$

This way we obtain an expression for the net binding rate r with the right structure to capture the slip bond effect. Indeed, making the following choice for $\bar{k}$:

$$\bar{k} = k \frac{\exp\left(\frac{h}{x_\beta}\right) \exp\left(\frac{\mu_1^0 - 2\mu_2^0}{k_B T}\right) c_1 - c_2^2/c_0 \exp\left(\frac{-h^2}{x_\gamma^2}\right)}{\frac{1}{2}\mu_1(h) - \mu_2 + \frac{1}{2}k_B T \frac{h}{x_\beta}}, \tag{C.18}$$

where $k > 0$ is a rate constant and $x_\gamma = \sqrt{\frac{k_B T}{k_0}}$, a direct calculation shows that

$$\bar{k} = \frac{2kc_0}{k_B T} \exp\left(-\frac{2\mu_2^0}{k_B T}\right) \exp\left(-\frac{h^2}{x_\gamma^2}\right) \frac{\exp\left(\frac{\mu_1(h) + k_B T h/x_\beta}{k_B T}\right) - \exp\left(\frac{2\mu_2}{k_B T}\right)}{\frac{\mu_1(h) + k_B T h/x_\beta}{k_B T} - \frac{2\mu_2}{k_B T}}, \tag{C.19}$$

which is clearly positive as required. This way, plugging Eq. (C.18) in Eq.(C.11), we can write the net binding rate r as :

$$r = k_{\text{off}}^0 \exp\left(\frac{h}{x_\beta}\right) c_1 - k_{\text{on}}^0 \exp\left(-\frac{h^2}{x_\gamma^2}\right) c_2^2 \quad \text{in} \quad (0, \hat{s}), \tag{C.20}$$

where

$$k_{\text{on}} = \frac{k}{c_0} \exp\left(-\frac{h^2}{x_\gamma^2}\right) \quad \text{and} \quad k_{\text{off}} = k \exp\left(\frac{\mu_1^0 - 2\mu_2^0}{k_B T}\right) \exp\left(\frac{h}{x_\beta}\right). \tag{C.21}$$

We recognize the classic expression for binding/unbinding reaction equation for slip bonds. The following equation can be used to compute h through $\dot{h}$:

$$\nu \dot{h} = -k_0 h c_1 - \eta r. \tag{C.22}$$

This equation is a balance of forces between a viscous force, an elastic fore and an additional chemical force due to the change in the number of attached springs because of the chemical reaction. Thus using this coupled expression for the dissipation potential related to the chemical reaction we are able to reproduce the required Bell's law for the unbinding rate, and we obtain a corresponding mechanical force associated to the rate of the chemical reaction, which to our knowledge has not been described before.

Bibliography

A Albersdörfer, T Feder, and E Sackmann. Adhesion-induced domain formation by interplay of long-range repulsion and short-range attraction force: a model membrane study. *Biophysical journal*, 73(1):245–257, 1997.

Ricard Alert and Jaume Casademunt. Bleb Nucleation through Membrane Peeling. *Physical Review Letters*, 116(6):068101, feb 2016.

Marino Arroyo and Antonio DeSimone. Relaxation dynamics of fluid membranes. *Physical Review E*, 79(3):031915, 2009.

Marino Arroyo, Nikhil Walani, Alejandro Torres-Sánchez, and Dimitri Kaurin. OnsagerâĂŹs variational principle in soft matter: Introduction and application to the dynamics of adsorption of proteins onto fluid membranes. In *The Role of Mechanics in the Study of Lipid Bilayers*, pages 287–332. Springer, 2018.

W Baumgartner, P Hinterdorfer, W Ness, A Raab, D Vestweber, H Schindler, and D Drenckhahn. Cadherin interaction probed by atomic force microscopy. *Proceedings of the National Academy of Sciences*, 97(8):4005–4010, 2000.

G. Bell. Models for the specific adhesion of cells to cells. *Science (80-.).*, 200 (4342):618–627, may 1978a.

G. Bell, M Dembo, and P. Bongrand. Cell adhesion. Competition between nonspecific repulsion and specific bonding. *Biophys. J.*, 45(6):1051–64, 1984a.

George I Bell. Models for the specific adhesion of cells to cells. *Science*, 200 (4342):618–627, 1978b.

GEORGE I Bell, MICAH Dembo, and PIERRE Bongrand. Cell adhesion. competition between nonspecific repulsion and specific bonding. *Biophysical journal*, 45(6):1051–1064, 1984b.

D. Berk and E. Evans. Detachment of agglutinin-bonded red blood cells. III. Mechanical analysis for large contact areas. *Biophysical Journal*, 59(4):861–872, apr 1991.

A-L Bernard, M-A Guedeau-Boudeville, L Jullien, and J-M Di Meglio. Strong adhesion of giant vesicles on surfaces: dynamics and permeability. *Langmuir*, 16(17):6809–6820, 2000.

Timo Bihr, Udo Seifert, and Ana Sunčana Smith. Nucleation of ligand-receptor domains in membrane adhesion. *Physical Review Letters*, 109(25):1–5, 2012.

Timo Bihr, Udo Seifert, and Ana Suncana Smith. Multiscale approaches to protein-mediated interactions between membranes - Relating microscopic and macroscopic dynamics in radially growing adhesions. *New Journal of Physics*, 17(8), 2015.

Alexei Boulbitch, Zeno Guttenberg, and Erich Sackmann. Kinetics of membrane adhesion mediated by ligand–receptor interaction studied with a biomimetic system. *Biophysical Journal*, 81(5):2743–2751, 2001.

F Brochard-Wyart and Pierre-Gilles de Gennes. Adhesion induced by mobile binders: dynamics. *Proceedings of the National Academy of Sciences of the United States of America*, 99(12):7854–9, jun 2002a.

F Brochard-Wyart and Pierre-Gilles de Gennes. Adhesion induced by mobile binders: dynamics. *Proc. Natl. Acad. Sci. U. S. A.*, 99:7854–7859, 2002b.

Françoise Brochard-Wyart and Pierre-Gilles de Gennes. Unbinding of adhesive vesicles. *Comptes Rendus Physique*, 4(2):281–287, mar 2003.

Agustí Brugués, Ester Anon, Vito Conte, Jim H Veldhuis, Mukund Gupta, Julien Colombelli, José J Muñoz, G Wayne Brodland, Benoit Ladoux, and Xavier Trepat. Forces driving epithelial wound healing. *Nature physics*, 10 (9):683, 2014.

R Bruinsma and E Sackmann. Bioadhesion and the dewetting transition. *Comptes Rendus l'Académie des Sciences*, 2147(01):803–815, 2001.

Maria Bruna and S Jonathan Chapman. Diffusion of multiple species with excluded-volume effects. *The Journal of chemical physics*, 137(20):204116, 2012.

Craig D Buckley, Jiongyi Tan, Karen L Anderson, Dorit Hanein, Niels Volkmann, William I Weis, W James Nelson, and Alexander R Dunn. The minimal cadherin-catenin complex binds to actin filaments under force. *Science*, 346(6209):1254211, 2014.

Yu Cai, Nitesh Shashikanth, Deborah E Leckband, and Daniel K Schwartz. Cadherin diffusion in supported lipid bilayers exhibits calcium-dependent dynamic heterogeneity. *Biophysical journal*, 111(12):2658–2665, 2016.

Laura Casares, Romaric Vincent, Dobryna Zalvidea, Noelia Campillo, Daniel Navajas, Marino Arroyo, and Xavier Trepat. Hydraulic fracture during epithelial stretching. *Nat. Mater.*, 14(3):343–351, feb 2015.

Lindsay B. Case and Clare M. Waterman. Integration of actin dynamics and cell adhesion by a three-dimensional, mechanosensitive molecular clutch. *Nature Cell Biology*, 17(8):955–963, 2015.

Matthieu Cavey, Matteo Rauzi, Pierre-François Lenne, and Thomas Lecuit. A two-tiered mechanism for stabilization and immobilization of e-cadherin. *Nature*, 453(7196):751, 2008.

Nigel Chaffey. Alberts, b., johnson, a., lewis, j., raff, m., roberts, k. and walter, p. molecular biology of the cell, 2003.

Rishita Changede and Michael Sheetz. Integrin and cadherin clusters: A robust way to organize adhesions for cell mechanics. *BioEssays*, 39(1):1–12, 2017.

Q. H. Cheng, P. Liu, H. J. Gao, and Y. W. Zhang. A computational modeling for micropipette-manipulated cell detachment from a substrate mediated by receptor-ligand binding. *J. Mech. Phys. Solids*, 57(2):205–220, 2009.

Scott E Chesla, Periasamy Selvaraj, and Cheng Zhu. Measuring two-dimensional receptor-ligand binding kinetics by micropipette. *Biophysical journal*, 75(3):1553–1572, 1998.

Yeh-Shiu Chu, William a Thomas, Olivier Eder, Frederic Pincet, Eric Perez, Jean Paul Thiery, and Sylvie Dufour. Force measurements in E-cadherin-mediated cell doublets reveal rapid adhesion strengthened by actin cytoskeleton remodeling through Rac and Cdc42. *J. Cell Biol.*, 167(6):1183–94, dec 2004a.

Yeh-Shiu Chu, William A Thomas, Olivier Eder, Frederic Pincet, Eric Perez, Jean Paul Thiery, and Sylvie Dufour. Force measurements in e-cadherin–mediated cell doublets reveal rapid adhesion strengthened by actin cytoskeleton remodeling through rac and cdc42. *J Cell Biol*, 167(6):1183–1194, 2004b.

Yeh Shiu Chu, Sylvie Dufour, Jean Paul Thiery, Eric Perez, and Frederic Pincet. Johnson-Kendall-Roberts theory applied to living cells. *Phys. Rev. Lett.*, 94 (2):1–4, 2005.

Cindi Cozens-Roberts, Douglas A Lauffenburger, and John A Quinn. Receptor-mediated cell attachment and detachment kinetics. i. probabilistic model and analysis. *Biophysical journal*, 58(4):841–856, 1990.

Damien Cuvelier and Pierre Nassoy. Hidden dynamics of vesicle adhesion induced by specific stickers. *Physical Review Letters*, 93(22):1–4, 2004.

Matthew B Dalva, Andrew C McClelland, and Matthew S Kayser. Cell adhesion molecules: signalling functions at the synapse. *Nature Reviews Neuroscience*, 8(3):206, 2007.

Sabyasachi Dasgupta, Kapish Gupta, Yue Zhang, Virgile Viasnoff, and Jacques Prost. Physics of lumen growth. *Proceedings of the National Academy of Sciences*, 115(21):E4751–E4757, may 2018.

P.-G. de Gennes, P.-H. Puech, and F. Brochard-Wyart. Adhesion Induced by Mobile Stickers: A List of Scenarios. *Langmuir*, 19(17):7112–7119, aug 2003.

Pierre-Gilles de Gennes, Françoise Brochard-Wyart, and David Quéré. *Capillarity and Wetting Phenomena: drops, pearls, waves*. Springer, New York, 2004.

Masao Doi. OnsagerâĂŹs variational principle in soft matter. *Journal of Physics: Condensed Matter*, 23(28):284118, 2011.

Masao Doi. OnsagerâĂŹs variational principle in soft matter dynamics. In *Non-Equilibrium Soft Matter Physics*, pages 1–35. World Scientific, 2012.

Alberto Elosegui-Artola, Roger Oria, Yunfeng Chen, Anita Kosmalska, Carlos Pérez-González, Natalia Castro, Cheng Zhu, Xavier Trepat, and Pere Roca-Cusachs. Mechanical regulation of a molecular clutch defines force transmission and transduction in response to matrix rigidity. *Nature Cell Biology*, 18(5):540–548, may 2016.

W Engl, B Arasi, L L Yap, J P Thiery, and V Viasnoff. Actin dynamics modulate mechanosensitive immobilization of E-cadherin at adherens junctions. *Nature Cell Biology*, 16(6):584–591, jun 2014a.

W Engl, B Arasi, LL Yap, JP Thiery, and V Viasnoff. Actin dynamics modulate mechanosensitive immobilization of e-cadherin at adherens junctions. *Nature cell biology*, 16(6):584, 2014b.

Thorsten Erdmann and Ulrich S Schwarz. Stochastic dynamics of adhesion clusters under shared constant force and with rebinding. *J. Chem. Phys.*, 121 (18):8997–9017, nov 2004.

Thorsten Erdmann and Ulrich S Schwarz. Bistability of cell-matrix adhesions resulting from non-linear receptor-ligand dynamics. *BioPhys. J. E*, 91(L60), 2006.

Thorsten Erdmann and Ulrich S Schwarz. Impact of receptor-ligand distance on adhesion cluster stability. *The European Physical Journal E: Soft Matter and Biological Physics*, 22(2):123–137, 2007.

C Ross Ethier and Craig A Simmons. *Introductory biomechanics: from cells to organisms*. Cambridge University Press, 2007.

E Evans, DJ Klingenberg, W Rawicz, and F Szoka. Interactions between polymer-grafted membranes in concentrated solutions of free polymer. *Langmuir*, 12(12):3031–3037, 1996.

Evan Evans. Probing the relation between force-lifetime-and chemistry in single molecular bonds. *Annual review of biophysics and biomolecular structure*, 30(1):105–128, 2001.

Evan Evans and Ken Ritchie. Dynamic strength of molecular adhesion bonds. *Biophysical journal*, 72(4):1541–1555, 1997.

Evan Evans, Andrew Leung, Dan Hammer, and Scott Simon. Chemically distinct transition states govern rapid dissociation of single l-selectin bonds under force. *Proceedings of the National Academy of Sciences*, 98(7):3784–3789, 2001.

Evan Evans, Andrew Leung, Volkmar Heinrich, and Cheng Zhu. Mechanical switching and coupling between two dissociation pathways in a p-selectin adhesion bond. *Proceedings of the National Academy of Sciences of the United States of America*, 101(31):11281–11286, 2004.

Susanne F. Fenz and Kheya Sengupta. Giant vesicles as cell models. *Integrative Biology*, 4(9):982, 2012.

Susanne F. Fenz, Timo Bihr, Daniel Schmidt, Rudolf Merkel, Udo Seifert, Kheya Sengupta, and Ana Sunčana Smith. Membrane fluctuations mediate lateral interaction between cadherin bonds. *Nature Physics*, 13(9):906–913, 2017.

Ernst-Ludwig Florin, Vincent T Moy, and Hermann E Gaub. Adhesion forces between individual ligand-receptor pairs. *Science*, 264(5157):415–417, 1994.

Jean-Baptiste Fournier. On the hydrodynamics of bilayer membranes. *International Journal of Non-Linear Mechanics*, 75:67–76, 2015.

L. B. Freund and Yuan Lin. The role of binder mobility in spontaneous adhesive contact and implications for cell adhesion. *J. Mech. Phys. Solids*, 52 (11):2455–2472, 2004.

Jürgen Fritz, Andreas G Katopodis, Frank Kolbinger, and Dario Anselmetti. Force-mediated kinetics of single p-selectin/ligand complexes observed by atomic force microscopy. *Proceedings of the National Academy of Sciences*, 95 (21):12283–12288, 1998.

Yuan-cheng Fung. *Biomechanics: mechanical properties of living tissues*. Springer Science & Business Media, 2013.

Huajian Gao, Jin Qian, and Bin Chen. Probing mechanical principles of focal contacts in cell-matrix adhesion with a coupled stochastic-elastic modelling framework. *J. R. Soc. Interface*, 8(62):1217–32, sep 2011.

Daniel T Gillespie. A general method for numerically simulating the stochastic time evolution of coupled chemical reactions. *Journal of computational physics*, 22(4):403–434, 1976.

Daniel T Gillespie. Exact stochastic simulation of coupled chemical reactions. *The journal of physical chemistry*, 81(25):2340–2361, 1977.

Charlène Guillot and Thomas Lecuit. Mechanics of Epithelial Tissue Homeostasis and Morphogenesis. *Science*, 340(6137):1185–1189, jun 2013.

Barry M Gumbiner. Cell adhesion: the molecular basis of tissue architecture and morphogenesis. *Cell*, 84(3):345–357, 1996.

Andrew R Harris, Loic Peter, Julien Bellis, Buzz Baum, Alexandre J Kabla, and Guillaume T Charras. Characterizing the mechanics of cultured cell monolayers. *Proceedings of the National Academy of Sciences*, 109(41):16449–16454, 2012.

Shinji Hirano and Masatoshi Takeichi. Cadherins in brain morphogenesis and wiring. *Physiological Reviews*, 92(2):597–634, 2012.

Nobutaka Hirokawa and John E Heuser. Quick-freeze, deep-etch visualization of the cytoskeleton beneath surface differentiations of intestinal epithelial cells. *The Journal of cell biology*, 91(2):399–409, 1981.

Jinglei Hu, Reinhard Lipowsky, and Thomas R Weikl. Binding constants of membrane-anchored receptors and ligands depend strongly on the nanoscale roughness of membranes. *Proc. Natl. Acad. Sci. U. S. A.*, 110(38):15283–8, 2013.

Derek L. Huang, Nicolas A. Bax, Craig D. Buckley, William I. Weis, and Alexander R. Dunn. Vinculin forms a directionally asymmetric catch bond with F-actin. *Science*, 357(6352):703–706, aug 2017. ISSN 0036-8075.

Kenneth Langstreth Johnson, Kevin Kendall, and AD Roberts. Surface energy and the contact of elastic solids. *Proc. R. Soc. Lond. A*, 324(1558):301–313, 1971.

Miklós SZ Kellermayer, Steven B Smith, Henk L Granzier, and Carlos Bustamante. Folding-unfolding transitions in single titin molecules characterized with laser tweezers. *Science*, 276(5315):1112–1116, 1997.

Nargess Khalilgharibi, Jonathan Fouchard, Nina Asadipour, Amina Yonis, Andrew Harris, Payman Mosaffa, Yasuyuki Fujita, Alexandre Kabla, Buzz Baum, Jose J Munoz, et al. Stress relaxation in epithelial monolayers is controlled by actomyosin. *bioRxiv*, page 302158, 2018.

Anita Joanna Kosmalska, Laura Casares, Alberto Elosegui-Artola, Joseph Jose Thottacherry, Roberto Moreno-Vicente, Víctor González-Tarragó, Miguel Ángel del Pozo, Satyajit Mayor, Marino Arroyo, Daniel Navajas, Xavier Trepat, Nils C Gauthier, and Pere Roca-Cusachs. Physical principles of membrane remodelling during cell mechanoadaptation. *Nature Communications*, 6:7292, jun 2015.

Hendrik Anthony Kramers. Brownian motion in a field of force and the diffusion model of chemical reactions. *Physica*, 7(4):284–304, 1940.

Heinrich Krobath, Bartosz Rózycki, Reinhard Lipowsky, and Thomas R. Weikl. Line tension and stability of domains in cell-adhesion zones mediated by long and short receptor-ligand complexes. *PLoS ONE*, 6(8), 2011.

Tonya L Kuhl, Alan D Berman, Sek Wen Hui, and Jacob N Israelachvili. Part 1. direct measurement of depletion attraction and thin film viscosity between lipid bilayers in aqueous polyethylene glycol solutions. *Macromolecules*, 31 (23):8250–8257, 1998.

Aditya Kumar, K Ravi-Chandar, and Oscar Lopez-Pamies. The configurational-forces view of the nucleation and propagation of fracture and healing in elastomers as a phase transition. *International Journal of Fracture*, 213(1):1–16, 2018.

Gil U Lee, David A Kidwell, and Richard J Colton. Sensing discrete streptavidin-biotin interactions with atomic force microscopy. *Langmuir*, 10(2):354–357, 1994.

Feiya Li, Sambra D Redick, Harold P Erickson, and Vincent T Moy. Force measurements of the integrin–fibronectin interaction. *Biophysical journal*, 84 (2):1252–1262, 2003.

Yuan Lin and L. B. Freund. Forced detachment of a vesicle in adhesive contact with a substrate. *Int. J. Solids Struct.*, 44(6):1927–1938, 2007.

Allen P. Liu and Daniel A. Fletcher. Biology under construction: in vitro reconstitution of cellular function. *Nature Reviews Molecular Cell Biology*, 10 (9):644–650, sep 2009.

Baoyu Liu, Wei Chen, and Cheng Zhu. Molecular Force Spectroscopy on Cells. *Annual Review of Physical Chemistry*, 66(1):427–451, apr 2015.

Mian Long, Harry L Goldsmith, David FJ Tees, and Cheng Zhu. Probabilistic modeling of shear-induced formation and breakage of doublets cross-linked by receptor-ligand bonds. *Biophysical journal*, 76(2):1112–1128, 1999.

Jean-Léon Maître and Carl-Philipp Heisenberg. Three functions of cadherins in cell adhesion. *Curr. Biol.*, 23(14):R626–33, jul 2013.

Jean-léon Maître, Hélène Berthoumieux, Simon Frederik, and Gabriel Krens. Supplementary Materials for. 2012a.

Jean-Léon Maître, Hélène Berthoumieux, Simon Frederik Gabriel Krens, Guillaume Salbreux, Frank Jülicher, Ewa Paluch, and Carl-Philipp Heisenberg. Adhesion functions in cell sorting by mechanically coupling the cortices of adhering cells. *Science (80-.).*, 338(6104):253–6, oct 2012b.

Kristine Manibog, Hui Li, Sabyasachi Rakshit, and Sanjeevi Sivasankar. Resolving the molecular mechanism of cadherin catch bond formation. *Nat Commun*, 5:1–11, 2014.

R Merkel, P Nassoy, A Leung, K_ Ritchie, and E Evans. Energy landscapes of receptor–ligand bonds explored with dynamic force spectroscopy. *Nature*, 397(6714):50–53, 1999.

Alexander Mielke. A gradient structure for reaction–diffusion systems and for energy-drift-diffusion systems. *Nonlinearity*, 24(4):1329, 2011.

Alexander Mielke. Thermomechanical modeling of energy-reaction-diffusion systems, including bulk-interface interactions. *Discret. Contin. Dyn. Syst. - Ser. S*, 6(2):479–499, nov 2012.

Bhushan Nagar, Michael Overduin, Mitsuhiko Ikura, and James M Rini. Structural basis of calcium-induced e-cadherin rigidification and dimerization. *Nature*, 380(6572):360, 1996.

Jin Nam and Maria M. Santore. The adhesion kinetics of sticky vesicles in tension: The distinction between spreading and receptor binding. *Langmuir*, 23(21):10650–10660, 2007.

Acute Respiratory Distress Syndrome Network. Ventilation with lower tidal volumes as compared with traditional tidal volumes for acute lung injury and the acute respiratory distress syndrome. *New England Journal of Medicine*, 342(18):1301–1308, 2000.

Mark Peletier. Variational Modelling : Energies , gradient flows , and large deviations Acknowledgements. 2013.

Yuriy V Pereverzev and Oleg V Prezhdo. Dissociation of biological catch-bond by periodic perturbation. *Biophysical journal*, 91(2):L19–L21, 2006.

Yuriy V Pereverzev, Oleg V Prezhdo, Manu Forero, Evgeni V Sokurenko, and Wendy E Thomas. The two-pathway model for the catch-slip transition in biological adhesion. *Biophysical journal*, 89(3):1446–1454, 2005a.

Yuriy V Pereverzev, Oleg V Prezhdo, Wendy E Thomas, and Evgeni V Sokurenko. Distinctive features of the biological catch bond in the jump-ramp force regime predicted by the two-pathway model. *Physical Review E*, 72(1):010903, 2005b.

Yuriy V Pereverzev, Eugenia Prezhdo, and Evgeni V Sokurenko. The two-pathway model of the biological catch-bond as a limit of the allosteric model. *Biophysical journal*, 101(8):2026–2036, 2011.

Sébastien Pierrat, Françoise Brochard-Wyart, and Pierre Nassoy. Enforced detachment of red blood cells adhering to surfaces: statics and dynamics. *Biophys. J.*, 87(4):2855–69, 2004a.

Sébastien Pierrat, Françoise Brochard-Wyart, and Pierre Nassoy. Enforced detachment of red blood cells adhering to surfaces: statics and dynamics. *Biophysical journal*, 87(4):2855–2869, 2004b.

Sabine Pokutta, Kurt Herrenknecht, Rolf Kemler, and Jürgen ENGEL. Conformational changes of the recombinant extracellular domain of e-cadherin upon calcium binding. *The FEBS Journal*, 223(3):1019–1026, 1994.

Lea-Laetitia Pontani, Ivane Jorjadze, and Jasna Brujic. Cis and trans cooperativity of e-cadherin mediates adhesion in biomimetic lipid droplets. *Biophysical journal*, 110(2):391–399, 2016.

K Prechtel, AR Bausch, V Marchi-Artzner, M Kantlehner, H Kessler, and R Merkel. Dynamic force spectroscopy to probe adhesion strength of living cells. *Physical review letters*, 89(2):028101, 2002.

S. Y. Qi, J. T. Groves, and A. K. Chakraborty. Synaptic pattern formation during cellular recognition. *Proceedings of the National Academy of Sciences*, 98(12): 6548–6553, 2001.

Jin Qian, Jizeng Wang, and Huajian Gao. Lifetime and strength of adhesive molecular bond clusters between elastic media. *Langmuir*, 24(4):1262–70, feb 2008.

Jin Qian, Jizeng Wang, Yuan Lin, and Huajian Gao. Lifetime and strength of periodic bond clusters between elastic media under inclined loading. *Biophysical journal*, 97(9):2438–2445, 2009.

Mohammad Rahimi and Marino Arroyo. Shape dynamics, lipid hydrodynamics, and the complex viscoelasticity of bilayer membranes. *Physical Review E*, 86(1):011932, 2012.

S. Rakshit, Y. Zhang, K. Manibog, O. Shafraz, and S. Sivasankar. Ideal, catch, and slip bonds in cadherin adhesion. *Proc. Natl. Acad. Sci.*, 109(46): 18815–18820, 2012.

Erich Sackmann and Ana-Sunčana Smith. Physics of cell adhesion: some lessons from cell-mimetic systems. *Soft Matter*, 10(11):1644, 2014.

PG Saffman and M Delbrück. Brownian motion in biological membranes. *Proceedings of the National Academy of Sciences*, 72(8):3111–3113, 1975.

Guillaume Salbreux, Guillaume Charras, and Ewa Paluch. Actin cortex mechanics and cellular morphogenesis. *Trends in cell biology*, 22(10):536–45, oct 2012a.

Guillaume Salbreux, Guillaume Charras, and Ewa Paluch. Actin cortex mechanics and cellular morphogenesis. *Trends in cell biology*, 22(10):536–545, 2012b.

Roger A Sauer. A survey of computational models for adhesion. *The Journal of Adhesion*, 92(2):81–120, 2016.

Thuan Beng Saw, Amin Doostmohammadi, Vincent Nier, Leyla Kocgozlu, Sumesh Thampi, Yusuke Toyama, Philippe Marcq, Chwee Teck Lim, Julia M. Yeomans, and Benoit Ladoux. Topological defects in epithelia govern cell death and extrusion. *Nature*, 544(7649):212–216, 2017.

Eva M. Schmid, Matthew H. Bakalar, Kaushik Choudhuri, Julian Weichsel, Hyoung Sook Ann, Phillip L. Geissler, Michael L. Dustin, and Daniel A. Fletcher. Size-dependent protein segregation at membrane interfaces. *Nat. Phys.*, 12(7):704–711, 2016a.

Eva M Schmid, Matthew H Bakalar, Kaushik Choudhuri, Julian Weichsel, Hyoung Sook Ann, Phillip L Geissler, Michael L Dustin, and Daniel A Fletcher. Size-dependent protein segregation at membrane interfaces. *Nature physics*, 12(7):704, 2016b.

U Seifert. Rupture of multiple parallel molecular bonds under dynamic loading. *Phys. Rev. Lett.*, 84(12):2750–3, mar 2000.

Lifu Sheng, Iryna LeshchynsâĂŹka, and Vladimir Sytnyk. Cell adhesion and intracellular calcium signaling in neurons. *Cell Communication and Signaling*, 11(1):94, 2013.

V B Shenoy and L B Freund. Growth and shape stability of a biological membrane adhesion complex in the diffusion-mediated regime. *Proceedings of the National Academy of Sciences of the United States of America*, 102(9):3213–8, mar 2005.

Sara Sigurbjörnsdóttir, Renjith Mathew, and Maria Leptin. Molecular mechanisms of de novo lumen formation. *Nature Reviews Molecular Cell Biology*, 15 (10):665, 2014.

Sanjeevi Sivasankar. Tuning the kinetics of cadherin adhesion. *Journal of Investigative Dermatology*, 133(10):2318–2323, 2013.

Ana-Suncana Smith, Kheya Sengupta, Stefanie Goennenwein, Udo Seifert, and Erich Sackmann. Force-induced growth of adhesion domains is controlled by receptor mobility. *Proc. Natl. Acad. Sci. U. S. A.*, 105(19):6906–11, may 2008a.

Ana-Sunčana Smith, Kheya Sengupta, Stefanie Goennenwein, Udo Seifert, and Erich Sackmann. Force-induced growth of adhesion domains is controlled by receptor mobility. *Proceedings of the National Academy of Sciences*, 105(19): 6906–6911, 2008b.

Marcos Sotomayor and Klaus Schulten. The allosteric role of the ca2+ switch in adhesion and elasticity of c-cadherin. *Biophysical Journal*, 94(12):4621–4633, 2008.

Malcolm S Steinberg and Masatoshi Takeichi. Experimental specification of cell sorting, tissue spreading, and specific spatial patterning by quantitative

differences in cadherin expression. *Proceedings of the National Academy of Sciences*, 91(1):206–209, 1994.

Béla Suki and Rolf Hubmayr. Epithelial and endothelial damage induced by mechanical ventilation modes. *Current opinion in critical care*, 20(1):17–24, 2014.

MASATOSHI Takeichi. The cadherins: cell-cell adhesion molecules controlling animal morphogenesis. *Development*, 102(4):639–655, 1988.

DF Tees, Olivier Coenen, and Harry L Goldsmith. Interaction forces between red cells agglutinated by antibody. iv. time and force dependence of break-up. *Biophysical journal*, 65(3):1318–1334, 1993.

A. Tozeren, K. L. Sung, and S. Chien. Theoretical and experimental studies on cross-bridge migration during cell disaggregation. *Biophysical Journal*, 55(3): 479–487, 1989.

Valeri Vasioukhin, Christoph Bauer, Mei Yin, and Elaine Fuchs. Directed actin polymerization is the driving force for epithelial cell–cell adhesion. *Cell*, 100 (2):209–219, 2000.

Selwin K Wu, Anne K Lagendijk, Benjamin M Hogan, Guillermo A Gomez, and Alpha S Yap. Active contractility at e-cadherin junctions and its implications for cell extrusion in cancer. *Cell Cycle*, 14(3):315–322, 2015.

Alpha S. Yap, Guillermo A. Gomez, and Robert G. Parton. Adherens Junctions Revisualized: Organizing Cadherins as Nanoassemblies. *Developmental Cell*, 35(1):12–20, 2015.

Alpha S. Yap, Kinga Duszyc, and Virgile Viasnoff. Mechanosensing and Mechanotransduction at CellâĂŞCell Junctions. *Cold Spring Harbor Perspectives in Biology*, page a028761, 2017.

M.; Addadi L.; Geiger Zaidel-Bar, R.; Cohen. Exact stochastic simulation of coupled chemical reactions. *B. Biochem.*, 32(416), 2004.

Xiaohui Zhang, Ewa Wojcikiewicz, and Vincent T Moy. Force spectroscopy of the leukocyte function-associated antigen-1/intercellular adhesion molecule-1 interaction. *Biophysical journal*, 83(4):2270–2279, 2002.

Cheng Zhu. A thermodynamic and biomechanical theory of cell adhesion Part I: General formulism. *Journal of Theoretical Biology*, 150(1):27–50, 1991.

Cheng Zhu. Kinetics and mechanics of cell adhesion. *Journal of Biomechanics*, 33(1):23–33, 2000.